Cyclic Voltammetry to Monitor Total Antioxidant Capacity of In-Vitro Biological Models Exposed to Nanomaterials

Ole-Bendik Hofshagen

MSc Nanoscience

University of Bergen

October 2022

Acknowledgements

This master thesis is integrated in ongoing research at the Nanotoxicology group, Dept. of Biomaterials at the Faculty of Medicine and Dentistry, within the NANO2021 NFR-funded project “NanoBioReal: Towards a reliable assessment of nanomaterial health effects using advanced biological models and assays” (Grant nr.: 288768) and the RiskGone HORIZON2020 project (Grant nr.: 814425).

I would like to thank the following people for supporting me during my research, as this would not have been possible without them.

First and foremost, I would like to express my immense gratitude towards my thesis supervisors, Mihaela Roxana Cimpan and Ivan Rios Mondragon, for your support and guidance throughout this project.

Secondly, I would like to thank Emil Cimpan for your support, CV data analysis, and for our many talks on voltammetry.

Furthermore, I would like to express my appreciation of the staff at IKO, Hisham Saghayroon Abdalla, Kaia Lindstrøm Berstad, Siren Hammer Østvold and Ying Xue for the training they provided, and for always being helpful during my stay.

Finally, I would like to say a huge thanks to my mother, my siblings, my partner Emma, and my good friend and colleague, Håkon, for proofreading my thesis and providing me with emotional support during this stressful period.

Table of contents

Abbreviations

2-P-AA	2-phospho-L-ascorbic acid
Ag	Silver
AgNW	Silver nanowire
BSA	Bovine serum albumin
C	Carbon
CE	Counter electrode
CeO_2	Cerium dioxide
CI	Cell index
CO_2	Carbon dioxide
CV	Cyclic voltammetry
DLS	Dynamic light scattering
DMEM	Dulbecco's modified eagle medium
DPPH	2,2 Diphenyl-1-picrylhydrazyl
E-plate	Electrode-plate
FBS	Fetal bovine serum
FC	Fold change vs. control
h	hours
HBSS	Hank's Balanced Salt Solution
HDD	Hydrodynamic diameter
LMWA	Low-molecular-weight antioxidants
L-AA	L-ascorbic acid
min	minutes
NCI	Normalized cell index
NM	Nanomaterial
NP	Nanoparticle
PBS	Phosphate buffered saline
PCB	Printed circuit board
PdI	Polydispersity index
Pen/strep	Penicillin/streptomycin

PET	Polyethylene terephthalate
RE	Reference electrode
ROS	Reactive oxygen species
RTCA	Real-time cell analysis
SD	Standard deviation
SE	Standard error
SP	Screen-printed
SPE	Screen-printed electrode
TAC	Total antioxidant capacity
TEM	Transmission electron microscopy
TiO_2	Titanium dioxide
TMAOH	Tetranethylammonium hydroxide
UA	Uric acid
WE	Working electrode

1 Abstract

The expanding field of nanotechnology has provided novel applications in many different areas including medicine and dentistry due to the unique properties exhibited by nanoparticles (NPs). However, various types of NPs have been shown to generate excessive amounts of reactive oxygen species (ROS), a known cause of oxidative stress, and consequently of toxicity. The increasing number of NPs in consumer products has led to an urgent need to assess their potential toxic effects. Traditional colorimetric and fluorescent-based methods used to evaluate oxidative stress have been shown to suffer from NP-induced interferences. Therefore, there is need for label-free methods to determine toxicity of NPs.

The purpose of this study was to implement cyclic voltammetry (CV) as a label-free method to assess the oxidative properties of NPs using screen-printed electrodes (SPEs). Additionally, A549 adenocarcinoma human alveolar basal epithelial cells were exposed to TiO_2-, CeO_2- and Ag-based NPs at concentrations of 10, 20, 50 and 100 µg/ml to evaluate the viability of cells supplemented with ascorbic acid (L-AA) and 2-phospho-L-ascorbic acid (2-P-AA) using label-free impedance-based monitoring (xCELLigence). Additionally, the NPs' ability to induce ROS was assessed using a fluorescent-based method. Furthermore, images of exposed cells were captured using transmission electron microscopy (TEM) to make a qualitative assessment of NP uptake and internalization. Finally, steps were taken to fabricate cost-effective electrodes for CV by printing conductive inks on polyethylene terephthalate (PET) films.

The results of the studies showed that several NPs have the potential to lower the total antioxidant capacity (TAC), especially AgNW, 3.5 nm CeO_2, 8 nm TiO_2 and TiO_2 nanorods. However, the difference was not statistically significant at the timepoints used but may show significance over longer time periods. At the highest concentration, only AgNW and 8 nm TiO_2 induced a significant difference in viability between samples containing L-AA and samples without L-AA, while for 8nm TiO_2 this was also seen at 50 µg/ml.

Among the particles tested using fluorometry, only 3.5 nm CeO_2 had a significantly increased ROS production compared to control. The 50 nm AgNPs displayed a quenching effect of the fluorescence signal and thus no results could be obtained for these particles.

TEM images revealed a significant cytosolic uptake of all NPs, especially for 3.5nm CeO_2 and CeO_2 stamps. Furthermore, fabrication of cost-effective electrodes gave promising results, but will need further optimization. These methods seem to provide a reasonable estimation of oxidative properties of NPs. However, more testing is required to solidify its validity.

In conclusion, CV emerged as a promising label-free method for assessing oxidative stress caused by NPs, with little to no interference from the NPs, whereas NP interference with a fluorescence-based method was observed. The AgNWs, TiO_2 nanorods and 3.5 nm CeO_2 NPs exhibited the highest intrinsic oxidative potential. All Ag-, TiO_2-, and CeO_2-based NPs used in this project possessed size- and shape-dependent oxidative effect and toxicity.

2 Introduction

2.1 Nanotechnology and nanomaterials

The European Union defines nanomaterials (NMs) as materials where at least 50% of the particles in the size distribution have at least one dimension that is between 1 and 100 nm. Nanoparticles (NPs), are generally defined as particles with at least one dimension in the range 1-100 nm [1, 2]. Their properties are largely determined by their size, shape, composition, charge, etc. Based on their origin, the NPs can be either natural, incidental, or manufactured [3]. Natural NPs can form as a result of atmospheric processes or as volcanic ash from erupting volcanoes. Nanoparticles are also formed as a result of human activities such as mining and industrial processes. However, manufactured NPs are the most frequently researched, and are at the forefront of the field's exponential growth [4].

The interest in this technology is due to the unique optical, magnetic, thermal and electrical properties exhibited by NMs and NPs which sets them apart from bulk materials [5]. The growing field of nanotechnology has provided novel applications in many different areas, including medicine, biotechnology, renewable energy, cosmetics, food packaging and electronics. For instance, titanium dioxide (TiO_2) NPs are used in a variety of products, including cosmetics, semiconductors, paint and food colouring and solar energy conversion [6]. Silver (Ag) NPs are increasingly used in consumer products because of their antifungal, antibacterial, antiviral, and antimicrobial properties. These properties have made the use of NPs attractive in products such as clothing, bottles, pacifiers and cleaning products [7].

Surface-modified metallic NPs with therapeutic agents bound to their surfaces can be used for customised applications, including nanomedicines. NPs have been employed as effective drug-delivery agents that can pass the blood-brain barrier due to their small size and can deliver drugs at specific sites due to their surface modifications [8]. Nanoparticles with specialised ligands, for example, can target and enter cancer cells, releasing therapeutic drugs. This action may assist reduce the drug dose needed to treat diseases, as well as the drug's undesired side effects [9]. However, the very same properties that make NPs so interesting can also make them more toxic.

Since NPs are so small, they can pass through cell membranes and end up in different subcellular compartments, typically endosomes and endo-lysosomes, where they can suffer modifications, which can make it difficult to both monitor and inhibit their off-target effects [10]. Additionally, the commercial and medical applications of NPs are growing at an exponential rate, resulting in increased exposure and, ultimately, a higher degree of human health risk [6].

2.2 Nanotoxicology

A 2008 study on rats exposed to silver (Ag) NPs showed that prolonged inhalation exposure lead to lung-function changes and inflammation at much lower mass dose concentrations compared to larger particles [11]. This exemplifies the duality of nanotechnology. Huge technological advancements can be made, but these may be followed by high risks. Alongside these risks there is a need for extensive evaluation of potentially toxic effects to protect workers, end-users and the environment.

These concerns lead to the establishment of the discipline of nanotoxicology as a branch of the field of toxicology. Toxicology itself is the field of research involved in assessing risks to humans and nature of man-made and natural substances [12]. Nanotoxicology is focused on evaluating and understanding the harmful effects that NMs may portent to provide solutions in order to minimize risks while potentiating the benefits of the technology. Since NPs are frequently difficult to detect, toxicity assessment using conventional analytical approaches may be problematic. Additionally, because of their small size and high surface to volume ratio, NPs may interact in unexpected and varied ways with analytical methods, producing erroneous results regarding their level of toxicity. This is very common for graphene-based NPs, but has also been seen for other types of NPs [13]. Following this, an essential part of nanotoxicology is to develop methods for a reliable assessment of the toxic effects of NPs.

The possibility of developing generic toxicity protocols to address NP risk assessment is strongly constrained by the heterogeneity of NPs. However, for the assessment of human and environmental risk, dependable and verified techniques for assessing NP toxicity are critical [14]. There are in-vivo and in-vitro toxicity assays, each having their own benefits and

drawbacks. In vitro assays typically have lower costs, higher throughput and tighter control over the chemical and physical environment. The major disadvantage of employing in-vitro assays is that they cannot accurately mimic the conditions of cells in an organism [15].

Analytical methods for nanotoxicity assessment can be either label-based or label-free. Label-based methods uses one or several labels which are foreign molecules chemically attached to the molecule of interest, usually covalently, to detect presence or activity [16]. These methods are also limited to discrete measurements, often an end-point measurement. Nanoparticles have been shown to interfere with several label molecules, which limits the predicting-power of the assays [17]. This finding contributes to the assumption that label-free methods may provide more reliable alternatives. One such label-free method is electrical impedance-based monitoring, which monitors the intrinsic electrical properties of cells [18, 19].

2.3 Toxicity of Nanoparticles

Studies suggest that NPs < 10 nm can act similarly to gasses, and can easily pass-through skin and lung tissue, eventually ending up inside cells [20]. Once the NPs enter the body, they can freely move through the body via blood-vessels and reach several organs, such as the brain or the liver. It has been shown that Ag NPs exhibit a size-dependent toxicity, with smaller NPs having a greater ability to trigger cell death [21].

Nanoparticles come in a variety of shapes, including nanospheres, nanorods, nano-needles/wires, nanotubes, and nanocubes. The optical properties of NPs have been demonstrated to be considerably influenced by their shape. High aspect-ratio nanoparticles (nanorods, nanowires, and nanotubes) have been shown to exhibit improved optical response and long-term photostability, which can aid in medical diagnosis and treatment [22]. However, the shapes of NPs have been demonstrated to have a significant impact on cellular internalization as well as toxicity. High aspect-ratio nanotubes, for example, have been found to promote lung inflammation when inhaled, similarly to asbestos [23].

The toxicity of NPs has also been demonstrated to be depending on both their aggregation state and their charge. Positively charged NPs have been linked to higher toxicity since the

extracellular side of cell membranes is negatively charged. The increased electrostatic attraction between the cells and the positively charged NPs is largely responsible for this effect [24, 25].

There are many ways in which NPs can be harmful, including, but not limited to, damaging DNA, altering cell cycle regulation, protein denaturation, and oxidative stress. Oxidative stress is defined as a state in which the production of reactive oxygen species (ROS) is so high that antioxidant defence pathways are not able to maintain equilibrium in the cell [26]. ROS are highly reactive chemicals formed from oxygen and include molecules like peroxides and the hydroxyl radical. They are needed for normal metabolism, but when overproduced they can oxidize different parts of cells, hindering their function or rendering them unfunctional.

Uncontrolled oxidative stress can lead to diseases, both chronic and degenerative and can speed up the aging process [27]. There are several ways in which NPs can induce oxidative stress, both directly and indirectly. The most direct way is by a photocatalytic activity of NPs on the outside of the cell, which leads to ROS generation. In photocatalysis, a catalyst (usually a semiconductor) modifies the rate of a photoreaction, where light is used to produce radicals. Indirectly, ROS generation can be caused by mitochondrial dysfunction due to NP exposure, which can lead to overproduction of hydroxyl radicals [28]. This overproduction of ROS can in turn lead to dysfunction of other organelles, cascading the damage done by ROS.

To evaluate the toxic effects of NPs, biomarkers of oxidative stress can be used. There are several biomarkers available, such as biological molecules that directly react with ROS, negating their effects and thus consumed in the process. Our natural defence system is the sacrifice of antioxidants, which neutralizes ROS by being oxidized themselves, hence protecting the body. There are many different antioxidants, including antioxidant enzymes, and low-molecular-weight antioxidants (LMWA), such as glutathione, ascorbic acid (AA), and uric acid (UA). With these antioxidants comes a very useful variable, i.e., the total antioxidant capacity (TAC). The TAC comprises the total cumulative effect of all antioxidants in body fluids or cells and summarizes the overall activity of antioxidants [29]. Given the diversity of antioxidants found in cells and body fluids, monitoring the consumption of only one particular

antioxidant to assess the oxidative potential of NPs can be insufficient. The TAC can be used instead by assessing the reductive impact of LMWA in a sample.

Plasma is frequently used to assess ROS-induced damage because it contains various oxidative damage targets such as lipoproteins and antioxidants such as ascorbic acid (AA) and uric acid. Methods based on plasma parameter characterization can thus represent the antioxidant state of the entire body. Most approaches for evaluating the overall antioxidant capacity of biological samples are related to the samples' ability to scavenge a specific ROS. These provide critical, albeit insufficient, information on a sample's overall antioxidant profile [30].

2.4 Cyclic Voltammetry

Cyclic Voltammetry (CV) is a common tool to analyse electrochemical reactions, but can also be used in fields outside chemistry, such as neuroscience and cell biology [31]. Cyclic voltammetry is a label-free method that can be used to assess the redox-properties of biofluids by applying an electrical potential in a cyclic manner and measuring the resulting current as electrons are transferred in a redox reaction. Being label-free means that no labels, such as dyes, are required to do measurements. Instead, it uses the biological markers' inherent chemical and physical characteristics. Because most LMWAs are reducing agents that scavenge ROS and quench them by electron donation, measuring a sample's total reducing power by CV can reveal LMWA activity in the sample. In theory, this approach might be used to track the activity of LMWA in various body fluids [30].

The oxidative scan is crucial for evaluating TAC because it gives critical details about the antioxidant content of the sample. According to figure 2.4.1, the anodic peak current, $i_{pa,}$ describes the antioxidant's reducing power, and the anodic peak potential, E_{pa}, characterizes the specific antioxidant measured. Together, they provide information on what antioxidants are present, their inherent capacity of reducing other substances, and their concentrations. i_{pa} increases linearly with concentration, and can thus be used to estimate antioxidant concentration [32]. The resulting micro-scale currents make it possible to track even minute changes in antioxidant capacity. When a voltage is applied to the working electrode, it becomes sufficiently positive or negative to oxidise or reduce the molecule of interest. In the

case of an oxidative scan, the current increases until it reaches the i_{pa}, then decreases as the reduced state of the molecule of interest depletes at the anodic surface.

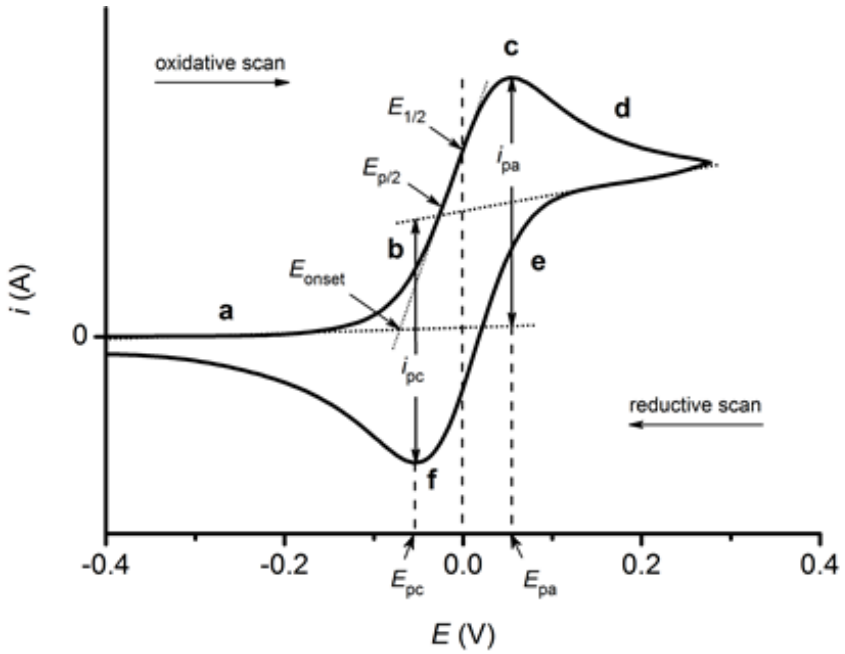

Figure 2.4.1: Typical cyclic voltammogram where i_{pc} and i_{pa} shows the cathodic and anodic peak current, respectively. E_{pc} and E_{pa} shows the cathodic and anodic peak potential, respectively.

A cyclic voltammogram's oxidative scan is heavily reliant on the antioxidants present in the sample, as they donate electrons at their oxidation potential. As a result, the integrated value of the oxidative scan can be presented as the sample's total antioxidant capacity. This method of evaluating antioxidant capacity, however, does not determine which specific antioxidants are present. As previously stated, various antioxidants can be distinguished by the anodic peak potential at which they are oxidised. The potency of the antioxidants determines the potential for oxidation. For example, AA is a more effective antioxidant than UA and is oxidised at around 40 mV lower potential than UA [33]. In more complex biological samples where several antioxidants may contribute to the overall current, it has been proposed that the TAC may prove more useful when monitoring changes in antioxidant content than I_{pa} [34]. Because antioxidants are depleted during oxidative stress and CV is very sensitive to changes in antioxidant concentration, this approach has been demonstrated to be capable of tracking oxidative stress [33].

For electrochemically reversible couples (when both the oxidized and reduced form is stable in solution and does not readily react with other species and can therefore be oxidized/reduced to its original state), the formal redox potential (E°) for the couple is the midpoint between E_{pc} and E_{pa}.

Figure 2.4.2 shows a schematic representation of a traditional electrochemical cell and a commercial screen-printed electrode (SPE). CV typically employs a three-electrode configuration; the working, counter and reference electrodes. The oxidation/reduction reaction takes place at the working electrode. A potentiostat is used to apply a working electrode potential that is a function of the reference electrode potential. The working electrode's most significant properties are that it is inert to redox reactions and that it has a clean surface. The purpose of the reference electrode is to have a stable and well-defined equilibrium potential. This is extremely valuable since it serves as a reference against which the other electrodes are measured. Silver wires fed into a glass tube filled with electrolyte solution are commonly used as a reference electrode. Current begins to flow when a voltage is provided to the working electrode and a redox reaction occurs. The counter electrode completes the circuit, allowing the current to be measured [35].

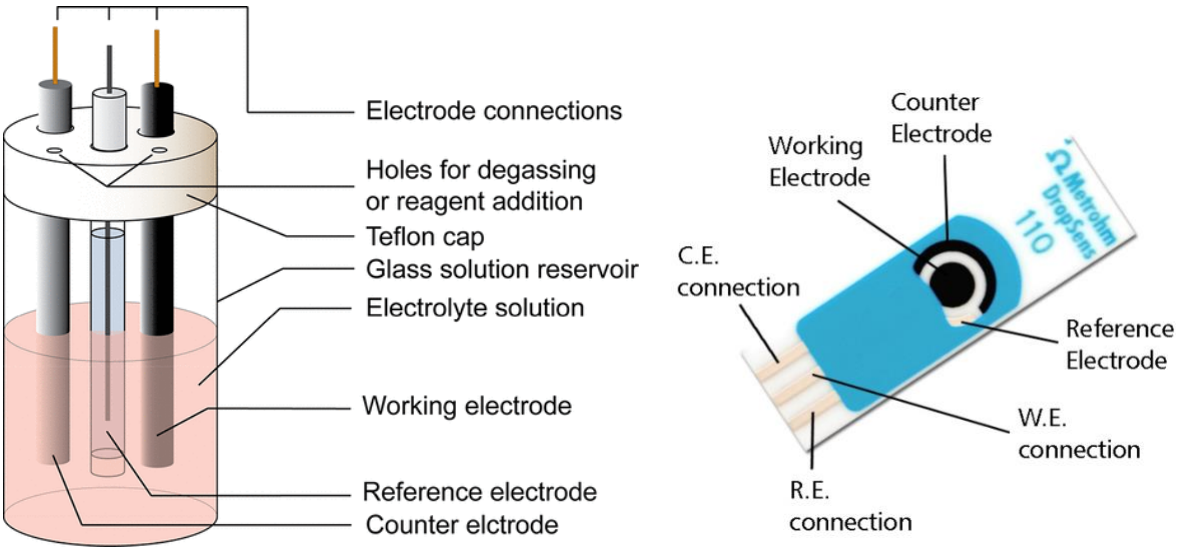

Figure 2.4.2: Traditional electrochemical cell (left) and commerical screen printed electrode (right)

2.5 Impedance-based monitoring of cells

Impedance-based methods rely on the structural properties and composition of cells to impede current flow. Impedance is a total measure of both resistance and reactance measured collectively. Resistance is the opposition to flow inside the internal structure of a conductor, whereas reactance is the resistance to the movement of electrical charge that results from changing magnetic and electric fields in circuits carrying alternating currents (AC) [36].

Cell size and shape, the integrity of the cell membrane, cell-cell or cell-substrate junctions, among other factors affect how successfully cells impede the flow of current applied by an electrical field. The two layers of phospholipids and the embedded proteins that make up the cell membrane makes it a semipermeable membrane that allows only certain molecules to pass through. Especially difficult is the free movement of polar species, like ions, across the phospholipid bilayer. Thus, the electrolytic solutions inside and outside of the cell become conductors, separated by an insulator. As a result, the cell can be viewed as a capacitor, because the conductivity of the cell membrane is substantially lower than that of the cytoplasm inside and the extracellular fluid outside the cell [37].

The ions in the intra- and extracellular fluid will move with the flow of the current when an AC is applied to the cells, polarizing the cells. This effect is frequency dependent. The cell will be strongly polarized and have a high capacitance when operating at low frequencies (kHz to MHz) since ions have the time to rearrange as the polarity of the current changes (figure 2.5.1). Thus, the measured impedance will be high because the cells will act as insulators. It is then feasible to evaluate the impedance of the extracellular space in order to study cell junctions, adhesion/detachment and membrane integrity caused by, for instance, cell death. As the cell is depolarized at higher frequencies (MHz to GHz), the capacitance will decrease, enabling examination of the integrity of the cell membrane and cytoplasm [37-39].

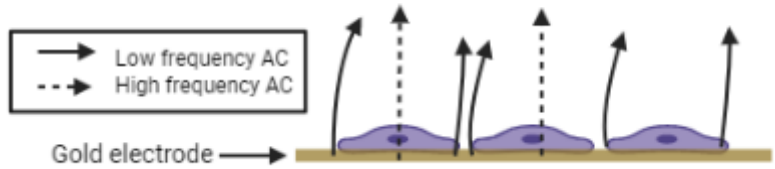

Figure 2.5.1: Impedance measurement of cells adherent on gold microelectrodes. At low frequencies (full arrows), the cells will be strongly polarized, and cells act as insulators. The current will therefore pass through the intercellular space, and not through cell membranes. At high frequencies (dashed arrows), the cells are depolarized, and the current can pass through cell membranes. Image created with biorender.com

Based on this, electrical impedance-based methods are fast approaching as a reliable label-free, non-invasive method for determining NP toxicity in real-time.

3 Aims of the study

The aim of this thesis was to implement and investigate the efficacy of employing cyclic voltammetry as a label-free method to detect NP-induced oxidative stress in biological systems. Because of the increased risk of inhalation exposure to NPs portent, NPs may end up in the lungs. Therefore, epithelial lung cancer cells were chosen, as they are located at the interface between the environment and the organism. The viability of epithelial cells was assessed under static conditions.

3.1 Specific Aims

- To implement and assess the applicability of label-free CV for the detection of NP-induced oxidative stress in biological systems.
- To implement the use of disposable electrodes to monitor ascorbic acid oxidation by NPs.
- To analyse the effect of supplementation with ascorbic acid in cells exposed to NPs
- To monitor ROS production in cells exposed to NPs.
- To fabricate cost-effective electrodes for CV by printing conductive inks.

3.2 Hypotheses

NPs may have concentration-, size and shape-dependent oxidative potential. When in contact with biological systems, oxidative stress may be caused directly by NP-generated ROS as they react with the extracellular milieu and/or indirectly as NPs induce cellular damage that leads to cell-mediated ROS production. Antioxidants present in biological systems will tend to counteract ROS by donating electrons causing oxidation of the antioxidant. The remaining pool of reduced antioxidants can be quantified to assess the impact of NPs in ROS generation. In this regard, cyclic voltammetry is a label-free analytical method used to study redox reactions and could be implemented to quantify the pool of reduced antioxidants. Therefore, we expect CV to be a sensitive and reliable alternative, i.e., not prone to NP-induced interference, for screening of NPs' oxidative effect.

4 Materials and Methods

4.1 Physicochemical characterization of nanoparticles used in the study

All the nine NPs used in this project were bought from Applied Nanoparticles (Barcelona, Spain): 8 nm TiO_2, 50 nm TiO_2 aggregates, 140 x 40 nm TiO2 nanorods, 3.5 nm CeO2, 50 nm CeO2 aggregates and 10 x 10 nm CeO2 stamps were all dispersed in 10 mM tetramethylammonium hydroxide (TMAOH) in 2 mM sodium citrate. The 20 nm AgNP, 50 nm AgNP and 5-10 um x 50 nm Ag nanowires (AgNW) were dispersed in 5 mM sodium citrate (SC) + 1 mg/ml 10k polyvinylpyrrolidone (PVP). The NPs were diluted in full cell culture medium at four different concentrations: 10, 20, 50 and 100 µg/ml, before being applied to the cells. The hydrodynamic diameter (HDD) and polydispersity index (PdI) of the particles suspensions were measured by dynamic light scattering (DLS) shortly after exposure and 24 h after exposure, using a Zetasizer Nano ZSP (Malvern Panalytical, UK). Applied Nanoparticles provided DLS measurements of the nine NPs in ultra-pure Milli-Q water (Millipore, MA, USA). Table 4.1 has a detailed list of all the particles utilized, their dimensions, and stock concentrations. TEM images of the Ag-based NPs, TiO_2 NPs and CeO_2 NPs are depicted in Figures 4.1 - 4.3.

Table 4.1: List of nanoparticles tested for cytotoxicity

Abbreviation	Description	Stock concentration (mg/ml)
AgNW	5-10 µm x 50 nm Ag nanowires in 5 mM SC + 1 mg/ml 10k PVP	0.94
AgNP-1	20 nm Ag in 5 mM SC + 1 mg/ml 10k PVP	0.84
AgNP-2	50 nm Ag in 5 mM SC + 1 mg/ml 10k PVP	1.80
3.5 nm CeO_2	3.5 nm CeO_2 in 10 mM TMAOH	1.75
50 nm CeO_2	50 nm CeO_2 aggregates in 10 mM TMAOH	2.65
CeO_2 stamps	10 x 10 nm CeO_2 in 10 mM TMAOH	2.59
8 nm TiO_2	8 nm TiO_2 in 10 mM TMAOH	2.46
50 nm TiO_2	50 nm TiO_2 aggregates in 10 mM TMAOH	2.38
TiO_2 nanorods	140 x 40 nm TiO_2 nanorods in 10 mM TMAOH	2.56

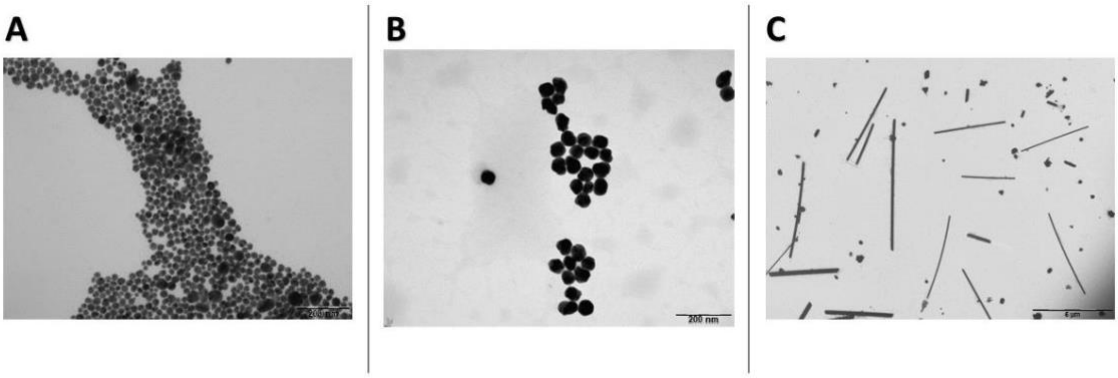

Figure 4.1: Transmission electron microscopy (TEM) images of **A)** 20 nm AgNPs (AgNP-1), **B)** 50 nm AgNPs (AgNP-2) and **C)** Ag nanowires (AgNW). The scale bar' length in **A)** and **B)** is 200 nm, while 5 µm in **C)**. Images were provided by Applied Nanoparticles (Barcelona, Spain)

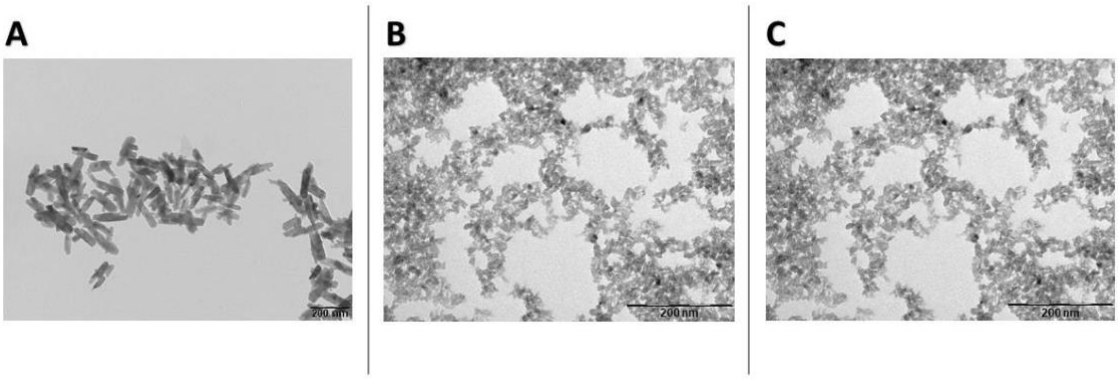

Figure 4.2: Transmission electron microscopy (TEM) images of **A)** TiO_2 nanorods, **B)** 50 nm TiO_2 aggregates and **C)** 8 nm TiO_2 NPs. The scale bars' length is 200 nm. Images were provided by Applied Nanoparticles (Barcelona, Spain)

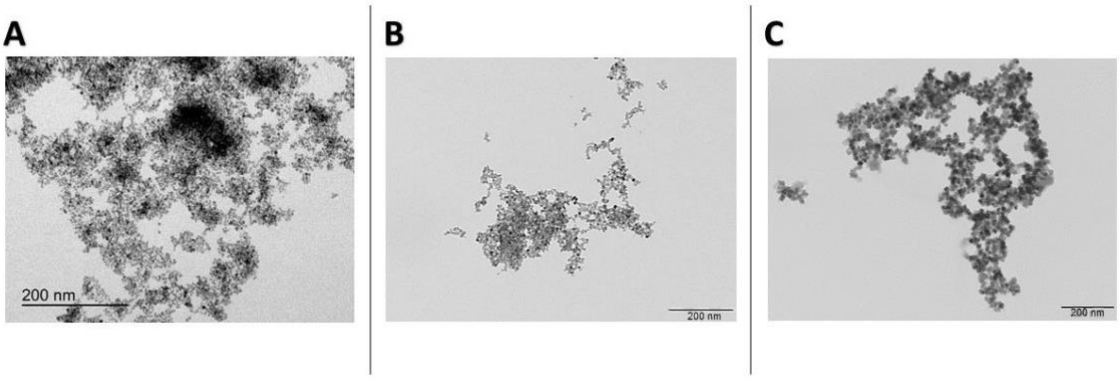

Figure 4.3: Transmission electron microscopy (TEM) images of **A)** 3.5 nm CeO_2, **B)** 50 nm CeO_2 aggregates and **C)** 10x10 nm CeO_2 NPs. The scale bars' length is 200 nm. Images were provided by Applied Nanoparticles (Barcelona, Spain)

4.2 Cell culture

A549 adenocarcinoma human alveolar basal epithelial cells (A549, ATCC, VA, USA) kept in liquid nitrogen at -196°C were thawed in a water bath for one min at 37°C, before being suspended in 3 mL of fresh complete cell culture medium and subsequently centrifuged at 900 rpm for 3 min. The cells were then resuspended in complete cell culture medium after the supernatant was removed and seeded at roughly 5000 cells/cm^2 in cell culture flasks (T-175, ThermoFisher, MA, USA). The entire cell culture medium was changed every 3-4 days while the cells were allowed to continue growing in an incubator at 37°C with 5 % CO_2. After reaching a confluency of 80-90%, the cells were split by first washing them two times with 10 mL Dulbecco's phosphate buffered saline (PBS, ThermoFisher, MA, USA) before being exposed to 4 mL trypsin-EDTA (Trypsin, Gibco, ThermoFisher, MA, USA) for 5 min in the incubator. The next step involved deactivating the trypsin by adding an equal amount of complete growth medium, centrifuging the cell suspension for 3 min at 900 rpm, discarding the supernatant and then diluting the cell suspension in complete cell culture medium. An automatic cell counter (Countess II, ThermoFisher, MA, USA) was used along with 0,4 % Trypan Blue staining (ThermoFisher, MA, USA) (1:1 mixture with cell suspension) to count the cells and determine their viability, then the suspension was diluted to the wanted cell density. Only cell batches with viability over 95 % were selected.

Two different types of cell growth media were used. For impedance and cyclic voltammetry-based measurements Dulbecco's Modified Eagle Medium (DMEM, Gibco, ThermoFisher, MA, USA) supplemented with 10% fetal bovine serum (FBS, Sigma-Aldrich, MO, USA) and 1% Penicillin/streptomycin (pen/strep, Sigma-Aldrich, MO, USA) was used. For fluorescence-based assays, DMEM with no phenol red and no glutamine was used, supplemented with 10% FBS, 1 % pen/strep and 1 % Glutamax (Gibco, ThermoFisher, MA, USA).

4.3 Impedance-based assessment of cell viability and proliferation

The A549 cells were cultured in the presence of NPs and 250 µM L-ascorbic acid (L-AA) and 1.0 mM 2-Phospho-L-ascorbic acid (2-P-AA) while monitoring cell viability and proliferation in real-time using the xCELLigence system (Agilent, US). This system can monitor cells under static exposure conditions in real-time without the use of labels. 2-P-AA was used as it is a

long-lasting vitamin C derivative precursor that is metabolised by living cells to L-AA. There are three electrode-plate (E-plate) stations on the Real-Time Cell Analysis (RTCA) system. To evaluate the impedance, an alternate current is applied through the microelectrodes at the bottom of the E-plates at three different frequencies (10, 25 and 50kHz), and the voltage drop across the electrodes is measured. Subsequently, the impedance obtained is the quotient Voltage/Current. The E-plates are single-use plates with 16 wells, each 5 mm in diameter (surface area 0.2cm^2) where 80 % of the bottom is filled with microelectrodes. Our research group had already defined a suitable seeding density of A549 for use with the impedance-based assay in 24-h exposure assays [40]. Therefore, the seeding density was set to 25 000 cells/cm^2 using DMEM with 10 % FBS. Long-term repetitive passaging of cancer cell lines has been shown to regularly result in changes in characteristics, including alterations in cell shape, growth rates, and the frequency of genetic abnormalities [41, 42]. Therefore, cells were only used if the passage number was designated as an early passage (<15). The plate was then placed in the RTCA station, housed inside an incubator at 37°C with 5 % CO_2 for 24 h to let cells proliferate. Afterwards, the cells were exposed to 10, 20, 50 and 100 µg/ml of NPs for 24 h. Impedance readings were taken every 15 min. For each timepoint, the software provides the measured impedance as a Cell Index (CI), which is a nondimensional quantity. In both the presence and absence of cells, the CI is a measurement of electrical impedance normalized by a frequency factor, Z_n (equation 4.1):

$$CI = \frac{Z_t - Z_0}{Z_n} \quad (4.1)$$

Where Z_t = Impedance at time t

Z_0 = Impedance at time 0 (background)

Z_n = Frequency factor

Increase of cell proliferation and attachment are indicated by a rise in the CI, whereas detachment, loss of membrane integrity, and cell death are indicated by a reduction in the CI. Each measurement condition was performed in duplicates, and the experiments were performed three times independently. A stable free radical that is known as an oxidizing

agent, i.e., 2,2 Diphenyl-1-picrylhydrazyl (DPPH), was utilized as a positive control at a concentration of 0.5 mM.

4.4 Cyclic Voltammetry

4.4.1 Electrode configuration

The choice of electrodes is essential for a thorough analysis of electrochemical phenomena. Three electrodes are utilized in the voltametric cell assembly for CV:

- **The working electrode (WE)**, which carries out the electrochemical event of interest.
- **The counter electrode (CE)**, which completes the electrical circuit so that current flows between WE and CE when potential is applied at WE.
- **The reference electrode (RE)**, which has a well-defined and stable potential and therefore is used as a reference point against which the other potentials are measured.

Three different electrode setups were used to track the oxidation of AA at concentrations varying from 50-500 μM in cell culture medium without cells:

1) Traditional glassy carbon WE / Pt CE / Ag RE (PalmSens, The Netherlands)
2) Screen printed (SP) electrodes with the configuration C / Pt / Ag (Metrohm Autolab, The Netherlands)
3) SP electrodes with the configuration C / C / Ag (Metrohm Autolab, The Netherlands)

Using a scan rate of 100 mV/s, the CV was performed in the range of -0.5 V to 1.2 V.

4.4.2 Scan rate testing

To find the optimal scan rates for measuring small changes in the availability of ascorbic acid, cyclic voltammetry was performed between -0.5 and 1.2 V using either PBS with 250 μM L-AA or DMEM with 10% FBS and 4 concentrations of L-AA: 0, 100, 250 and 500 μM. Five different scan-rates were tested: 100, 150, 200, 300 and 400 mV/s. Initial measurements were performed using a traditional Glassy Carbon/Pt/Ag electrode, before moving on to using screen-printed C/Pt/Ag electrodes.

4.4.3 Oxidative potential of NPs in Hank's balanced salt solution

The NP's intrinsic redox characteristics and their oxidative abilities were evaluated using a multiplexed potentiostat (PalmSens) and disposable screen-printed Carbon/Carbon/Ag electrodes. The CV for the NPs was performed in Hank's Balanced Salt Solution with Ca^{2+} and Mg^{2+} (HBSS) at 0, 10 and 30 min after addition of NPs with and without 250 µM L-AA, by applying an electrical voltage sweep from -1 V to 1.2 V and measuring the resulting current as electrons are transferred in a redox reaction. Experiments were performed using either pure L-AA or L-AA from dissolved over-the-counter Vitamin-C tablets. 150 µL of each prepared sample was pipetted directly on top of each of the C/C/Ag SP electrodes. To prevent light-induced degradation of L-AA, a cover was placed on top of the system shortly after the samples were pipetted on top of the electrodes. For the resulting voltammograms, the peak height and area under the curve were measured. The area under the curves were found by integrating the CV voltammograms using MATLAB (Mathworks) with the help of Assoc. Prof. Emil Cimpan (Western Norway University of Applied Sciences)

4.5 Fluorometry

Cells exposed to NPs in the presence or absence of L-AA and 2-P-AA were monitored for ROS generation using label-based fluorescence (CellROX reagent, ThermoFisher). In a 96-well plate (half area, black, Greiner) A549 cells were seeded at 3750 cells/well for 24 h. A total of 100 µL were added to the wells. After 24 h, 75 µL were removed and 25 µL of prestaining solution containing 10 mM CellROX Orange fluorescent dye was added. The dye is nonfluorescent in a reduced state and fluoresce bright orange upon oxidation by ROS. After 30 min of prestaining, the cells were exposed to 50 µL solutions of NPs containing 5 mM dye and a Varioscan LUX multimode microplate reader (ThermoFisher) was used to measure the fluorescence intensity at the exposure times 0, 0.5, 1, 2, 6, 24 and 48 h. The maximum excitation and emission wavelengths of the dye are at 545 and 565 nm, respectively. Each well was measured for 500 ms from the bottom of the wells moving in a bilateral direction while the instrument's excitation bandwidth was 5 nm. As a positive control, 200 µM Menadione (Vitamin K_3) was used as it generates ROS through redox cycling.

4.6 Transmission Electron Microscopy

Prior to fixation, A549 cells were treated with 10 and 50 µg/ml NPs for 24 h in 6-well plates. Cells were fixed with 1.5 % glutaraldehyde in 0.1 M Na-cacodylate buffer (pH 7.4) to fix the cells in their current state. Post fixation was done in 1 % osmium tetraoxide in 0.1 M Na-cacodylate buffer for 60 min. After washing with 0.1 M Na-cacodylate buffer twice, the samples were dehydrated in ethanol (30-100%) before embedding in Agar resin. Subsequently, the samples were hardened by adding gelatine capsules into the thin resin layer and stored in an incubator at 60°C over-night. After hardening, the capsules were filled with resin and put back into an incubator at 60°C over-night. Finally, the samples were sectioned and analysed by TEM (JEOL-JEM-1230) at 60 kV. Images were taken to evaluate the cellular uptake of NPs in A549 cells. A qualitative assessment was made regarding cellular uptake and fate.

4.7 Printing of electrodes

The delivery of screen-printed electrodes from the producer Metrohm had been considerably delayed because of Covid-related issues. Thus, procedures for in-house printing of electrodes have been done. A desktop Printed Circuit Board (PCB) printer (Voltera, ON, Canada) has been modified to print electrodes on top of polyethylene terephthalate (PET)-based Mylar films. Silver ink (Conductor-2, Voltera) and two carbon inks, as well as an UV-cured solder insulator have been tested to find the optimal formulation to provide printed electrodes of optimal quality. The carbon inks tested had a carbon content (by weight) of 16 % (DZP Technologies, UK) and 40 % (Dycotec Materials, UK) and sheet resistance of 100 and 15 Ohm/cm^2, respectively. Figure 4.7.1 depicts the layout of the three layers from the Voltera software. The layouts were made using LayoutEditor (Juspertor GmbH, Germany). To prepare for printing, blank PCB boards (Voltera) and 0.25 mm thick Mylar films (RS Components, UK) were rinsed with distilled water before being dried with a dry cloth, after which they were wiped clean with isopropanol. They were quickly glued together, taking care not to trap air bubbles between them. After the PET film was fixed to the blank PCB board, they were placed on top of the PCB printer and secured with clamps screwed onto the printer to prevent the board from moving.

Following fixation, a probe was installed on the printer, and the board was probed to obtain a height map of the board's surface. While was mechanism was probing, the ink in the dispenser was primed. Priming was performed by gently turning the dispenser's gear until the dispensing plunger made contact with the ink and a small amount of ink was pushed out of the nozzle. The dispensing unit was then attached to the printer and calibrated by printing a calibration pattern while adjusting the amount of ink with buttons in the software. Along with the desired features for printing, alignment marks were printed in the first layer to allow the second layer to be aligned.

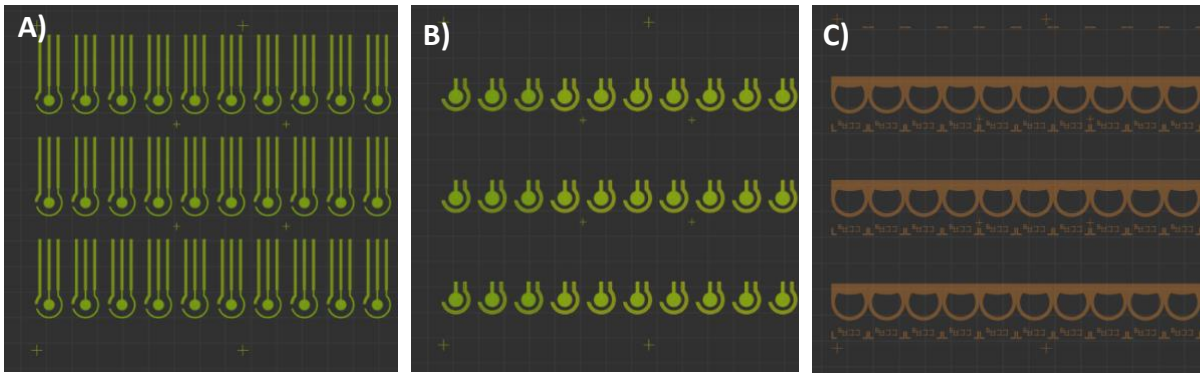

Figure 4.7.1: Layout of circuits of printed layers using the PCB printer and conductive inks. The layers were printed on top of each other on a PET film. **A)** The first layer: a silver layer. B) The second layer: a carbon layer. C) The third layer: an insulating layer.

4.8 Data Analysis

Data from the xCELLigence studies, CV and fluorometry were analysed using the IBM SPSS statistical software tool (version 26.0) [43]. For multiple sample comparisons, a One-Way ANOVA with a Tukey Post Hoc test was employed, and for paired comparisons of independent samples, the independent sample test (t-test) was performed ($p \leq 0.05$ denotes statistical significance with a 95 % confidence interval).

5 Results

5.1 Cyclic Voltammetry

The primary purpose of employing CV in this research was to evaluate the overall oxidative capacity of NPs by monitoring NP-mediated oxidation of L-AA. The antioxidants present in the sample are oxidised during a CV oxidative scan. The peak height and area of the voltammogram reveal information about the sample's antioxidant content. If NPs oxidise the antioxidant, the amount of L-AA available for oxidation during CV is reduced. As a result, we anticipate lower current heights at the oxidation potential for L-AA than in the control conditions where no NPs are added. Thus, we can infer which NPs produce oxidative stress in vitro and in vivo by monitoring this.

Furthermore, we sought to investigate the use of SP electrodes since they could reduce the time required for the experiments and can be multiplexed to allow high-throughput screening of the NP oxidative effect.

5.1.1 Electrode configuration

One downside of using traditional electrode setups is that electrodes can adsorb species on their surfaces during experiments and this may lead to increased signal in a potential range where the solvent is usually electrochemically inert. Therefore, the working electrode must be cleaned and polished after each subsequent measurement. The cleaning procedure takes time and makes time-sensitive measurements more challenging. By usings SPEs, one can avoid this issue. Therefore, preliminary tests were conducted to evaluate whether C/C/Ag or C/Pt/Ag SP-electrodes could perform at the same level or even outperform the traditional setup of Glassy Carbon/Pt/Ag. Various concentrations of L-AA in PBS and cell culture medium were utilized in these assays. Figure 5.1.1 shows the voltammograms from two of these tests, in which 50 and 250 µM L-AA in PBS were used. PBS was chosen in this exploratory testing as it is an isotonic solution, a good electrolyte and functions as a pH buffer. Therefore, cells could potentially be exposed to NPs for short periods of time in a PBS solution. Another key property of PBS used as a CV buffer is that it is stable toward oxidation and reduction in the experiment's potential range. For both tests, the highest peak current was found for the C/C/Ag setup with peak currents around 2.6 and 22.6 µA as seen in figure 5.1.1 A) and B),

respectively. This setup displayed pronounced peaks around 0,45 V for both concentrations using SPEs, and around 0.5 V for the traditional Glassy Carbon/Pt/Ag electrodes. The C/Pt/Ag also provided higher peak currents than the traditional setup and it was similar to CV profile observed the C/C/Ag electrode. Peak current values (2.0 and 21.3 µA in figure 5.1.1 A) and B), respectively), however, were not as high as for the C/C/Ag electrode configuration.

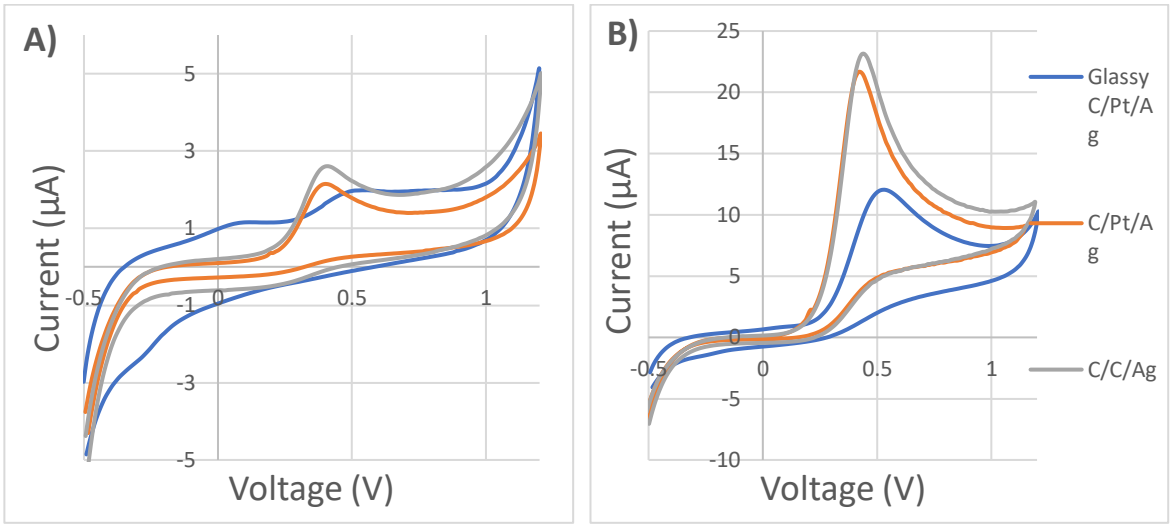

Figure 5.1.1: Cyclic voltammograms using three different electrodes: a traditional Glassy Carbon/Pt/Ag electrode (blue), C/Pt/Ag SP-electrode (orange) and C/C/Ag SP-electrode (grey) in the range of – 0,5 to 1,2 V using a scan rate of 100 mV/s. (**A**) 50 µM L-AA in PBS. (**B**) 500 µM L-AA in PBS.

Figure 5.1.2 shows the results of measuring 250 µM L-AA in DMEM with 10 % FBS; to note, the background signal of DMEM with 10 % FBS and no L-AA was subtracted. Because cell culture medium is not as stable as PBS toward oxidation and reduction in the potential range of interest, background subtraction appears to be critical when interpreting the data. The peak heights acquired are higher for the C/C/Ag (5.8 µA at 0.57 V) and C/Pt/Ag SP (5.7 µA at 0.65 V)-electrodes than for the traditional electrodes used (4.4 µA at 0.59 V). The peaks themselves are also more easily identifiable. Furthermore, using the SP-electrodes revealed additional peaks, which are most easily identified when using the C/C/Ag electrode. The three primary peaks are located at 0.57, 0.74 and 1.03 V for the C/C/Ag electrode, and two easily identifiable peaks are located around 0.65 and 1.12 V for the C/Pt/Ag electrode. Because of these findings, the C/C/Ag electrodes were used in most of the subsequent experiments. However, because the C/Pt/Ag electrodes were of comparable quality, they were chosen for scan-rate testing.

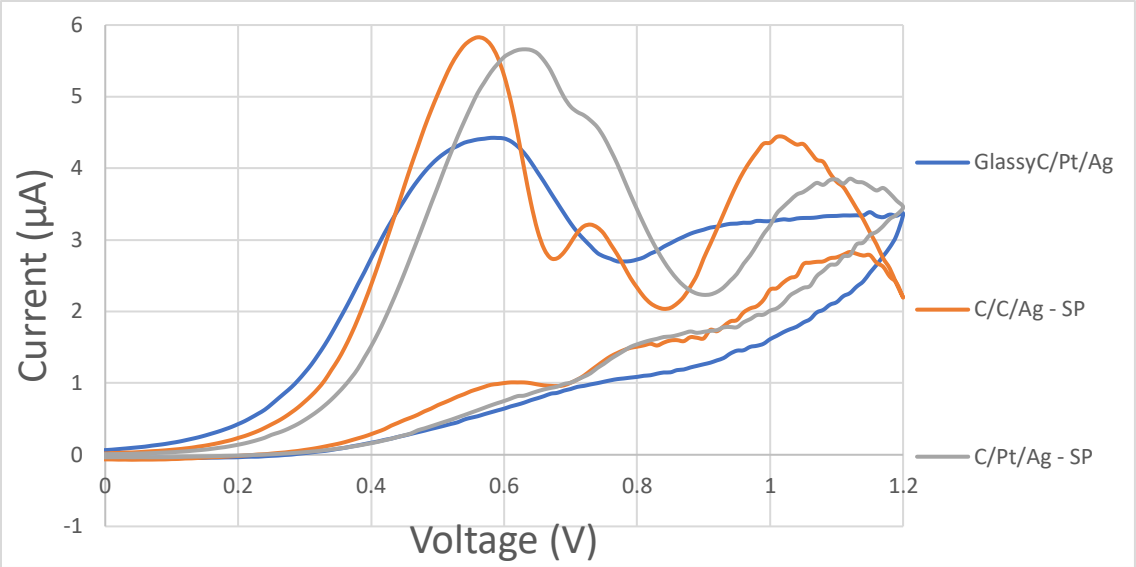

Figure 5.1.2: Partial cyclic voltammogram from 0 to 1,2 V using three different electrodes: a traditional Glassy Carbon/Pt/Ag electrode (blue), C/C/Ag SP-electrode (orange) and C/Pt/Ag SP-electrode (grey). The sample consisted of DMEM with 10 % and 250 µM L-AA. Background subtraction using DMEM with 10 % FBS was performed.

5.1.2 Scan rate testing

Initial experiments to find suitable scan rates were performed using 250 µM L-AA in PBS with a traditional Glassy Carbon / Pt / Ag electrode. Two scan rates were tested, 100 and 150 mV/s. Figure 5.1.3 displays the cyclic voltammograms from this initial test. Both voltammograms exhibit some noise. However, the higher scan rate is much noisier.

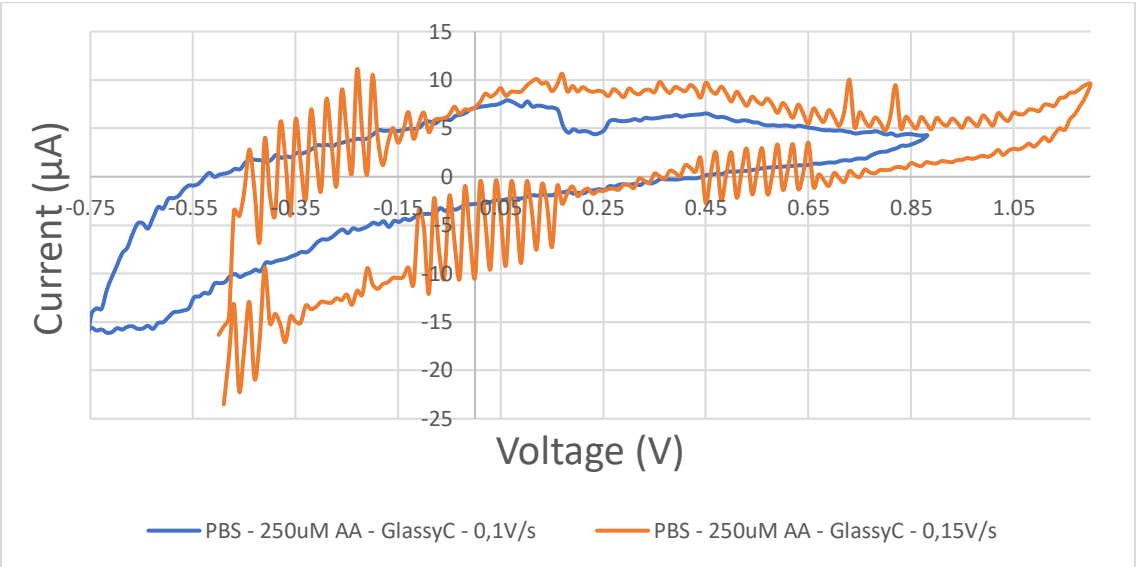

Figure 5.1.3: Cyclic Voltammogram using a traditional electrode setup (Glassy Carbon/Pt/Ag), using different scan-rates. The sample consists of 250 µM L-AA in PBS.

Scan rate testing was also performed with C/Pt/Ag SP electrodes using 150 µL of samples consisting of DMEM with 10 % FBS and varying concentrations of L-AA. Scan rates in the range of 100 – 400 mV/s were used. Figure 5.1.4 A) displays the cyclic voltammograms of these measurements, while figure 5.1.4 B) shows the peak currents for the characteristic peak of L-AA, after DMEM/FBS-background subtraction. As the scan rate increased, the overall current also increased. The peak currents for the different scan rates after background subtraction increased by 57, 118, and 126 % for scan rates 200, 300 and 400 mV/s, compared to using 100 mV/s. The peak currents were found around 0.55, 0.75, 0.78 and 0.78 V when using scan rates of 100, 200, 300 and 400 mV/s, respectively.

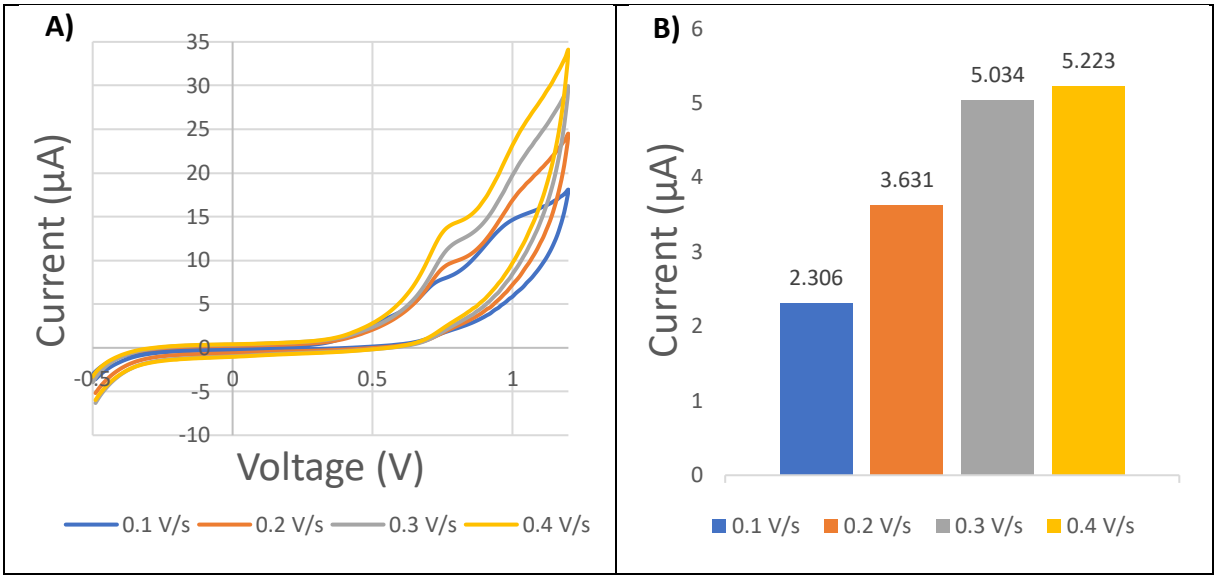

Figure 5.1.4: Results from cyclic voltammetry using C/Pt/Ag SP-electrodes in a range from -0.5 to 1.2 V. Scan rates ranged from 100 – 400 mV/s. The sample consisted of 250 µM L-AA in DMEM with 10% FBS. The figure shows **A)** Total cyclic voltammogram and **B)** Peak heights after background subtraction using DMEM/FBS.

5.1.3 NP-mediated oxidation of L-AA monitored by CV

To assess the NPs' inherent redox properties, as well as their oxidative capabilities in a label-free way, a multiplexed potentiostat and disposable SP carbon/carbon/Ag electrodes were used. The CV was performed in the range from -1.0 to 1.2 V with NPs dispersed in HBSS at 0-, 10- and 30-min incubation with and without 250 µM L-AA. This type of experiment was performed both with pure L-AA and L-AA contained in over-the-counter vitamin C tablets, containing 500 mg L-AA. Tablets were crushed to a fine powder before being dissolved in

milliQ water. HBSS was used because it is stable to oxidation and reduction in the potential range of interest, similar to PBS, and has the potential to be used as a substitute for cell culture medium when cells are exposed to NPs maintaining pH and osmotic balance, as well as to provide cells with essential inorganic ions and glucose.

Figure 5.1.5 displays the peak heights from the voltammograms at 0 and 30 min of NPs in HBSS with or without 250 µM pure L-AA. At time 0, shortly after L-AA had been added, most groups were relatively close to control, except samples containing AgNW or 8 nm TiO_2, which were both lower than control. The samples with AgNW and 8 nm TiO_2 deviated the most from the control, with values at 30 min that were 26.3 and 25.3 % lower than control, respectively. The sample containing 8 nm TiO_2 displayed the biggest diminishing effect of peak height over the 30 min. When compared to the control, the sample containing 50 nm TiO_2 were 15.1 % higher at 30 min. During the 30 min of exposure, the peak height of the sample containing 3.5 nm CeO_2 decreased by 8.1 %. Furthermore, samples containing NPs in HBSS without L-AA were evaluated in parallel to identify any possible interferences of the NPs with the analytical method. We observed that current heights at 0.5 V were low at all timepoints, indicating that the detected signal of samples containing L-AA is related to the influence NPs have on L-AA rather than a contribution from the NPs themselves. There was no peak at the oxidising potential of L-AA in samples without L-AA. The values in figure 5.1.5 from samples devoid of L-AA are thus simply the current at the oxidising potential of L-AA. No note, this experiment was carried out once due to difficulties in obtaining pure L-AA from different producers during the Covid-19 outbreak. Because of this, we decided to use L-AA from over-the-counter vitamin C tablets to continue with the studies.

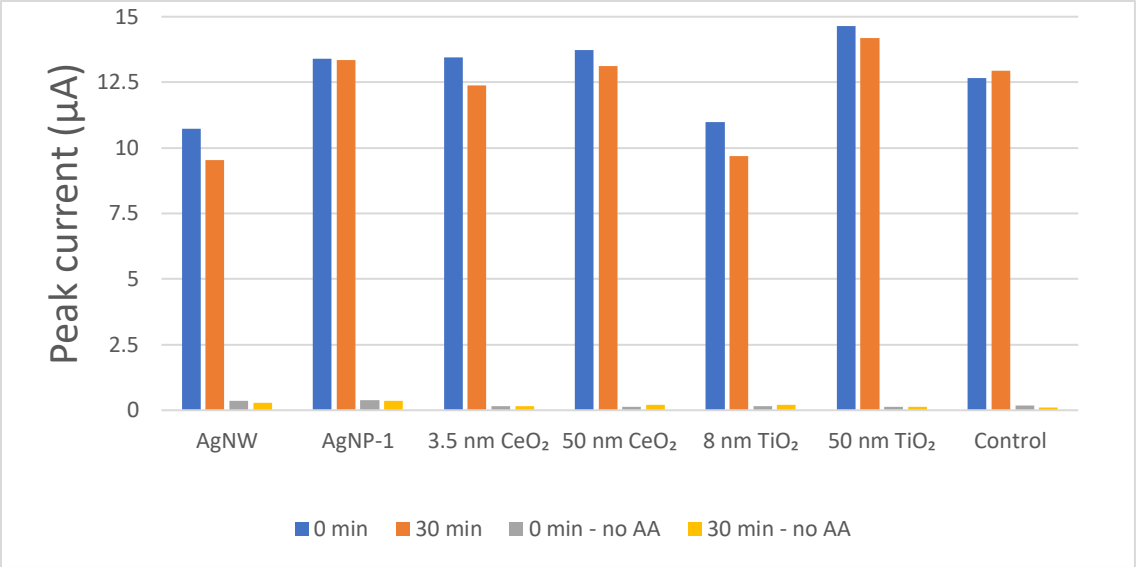

Figure 5.1.5: Peak heights at 0,5 V from CV measurements performed at 0 and 30 min at 100 mV/s. Samples consisted of HBSS containing 250 µM AA and 100 µg/ml of the indicated NP, or samples containing HBSS and 100 µg/ml of the indicated NP.

Figures 5.1.6 – 5.1.8shows the cyclic voltammograms of NPs in HBSS after 30 minutes. This figure shows that without L-AA, the NPs have no potential to be oxidised at the current potential where L-AA is oxidized (around 0.5 V). The AgNWs and 8 nm TiO_2 appear to be oxidised toward a more positive potential, and this impact appears to be minimised by the addition of AA.

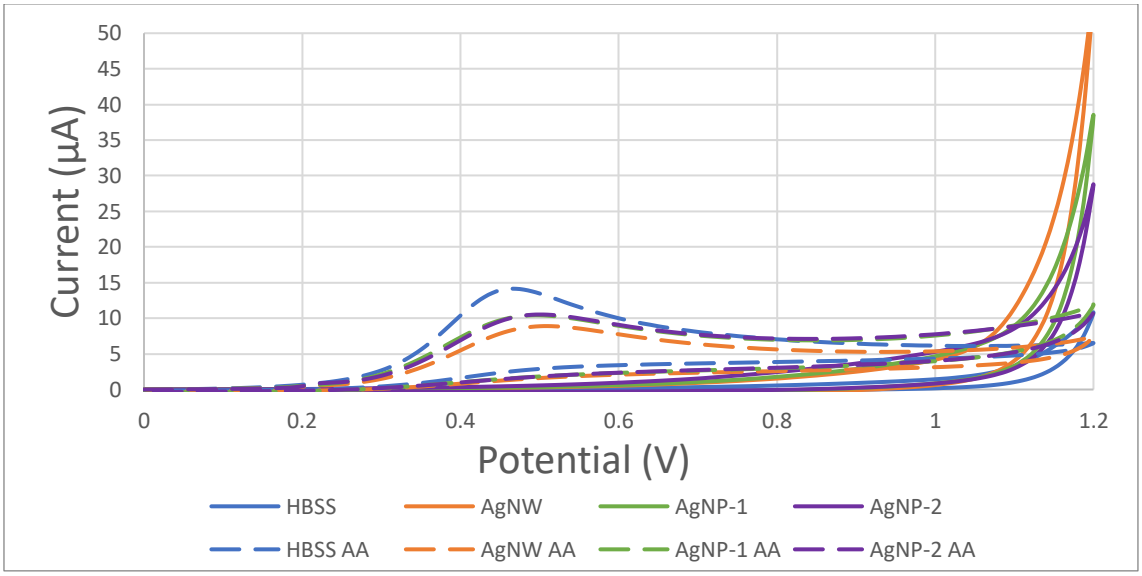

Figure 5.1.6: Cyclic voltammograms of measurements performed at 30 min. CV was performed at 100 mV/s in HBSS with or without 250 µM AA and 100 µg/ml of the indicated Ag-based NP.

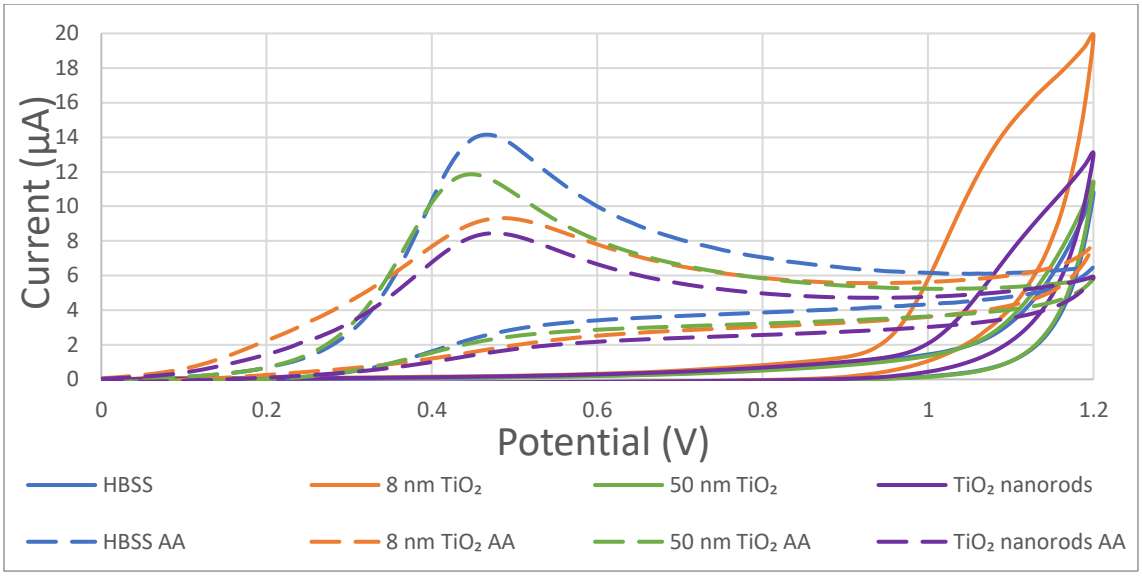

Figure 5.1.7: Cyclic voltammograms of measurements performed at 30 min. CV was performed at 100 mV/s in HBSS with or without 250 µM AA and 100 µg/ml of the indicated TiO_2-based NP.

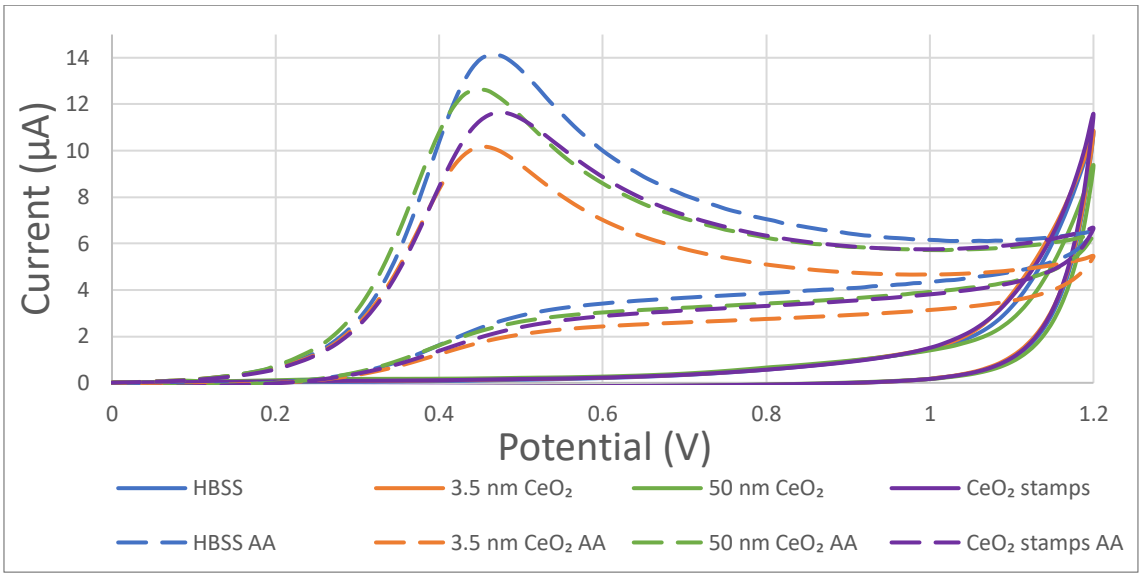

Figure 5.1.8: Cyclic voltammograms of measurements performed at 30 min. CV was performed at 100 mV/s in HBSS with or without 250 µM AA and 100 µg/ml of the indicated CeO_2-based NP.

The CV of NPs in HBSS performed at 0, 10, and 30 min provides a clearer picture of the time dependency of peak height reduction, as shown in figure 5.1.9. Although the difference between time points of the sample containing AgNW is negligible, it is significant in comparison to the control. Indeed, when compared to control, the peak heights of AgNW in HBSS are 27.6, 30.4, and 32.5 % lower at times 0, 10 and 30 min. The positive control with DPPH had higher initial values than AgNW but decreased significantly faster. At 30 min, the positive control has fallen by 30.2 % from its initial value, a difference of 36.6 % from the

negative control. The peak height of the sample containing 50 nm CeO_2 increased by 6.6, similar to the negative control, which increased by 3.6 % over the course of 30 min. Furthermore, peak heights at 30 min using 3.5 nm CeO_2 and TiO_2 nanorods were reduced by 8.0 and 10.0 % from their initial values, respectively, and by 25.5 and 32.6 % from the control after 30 min.

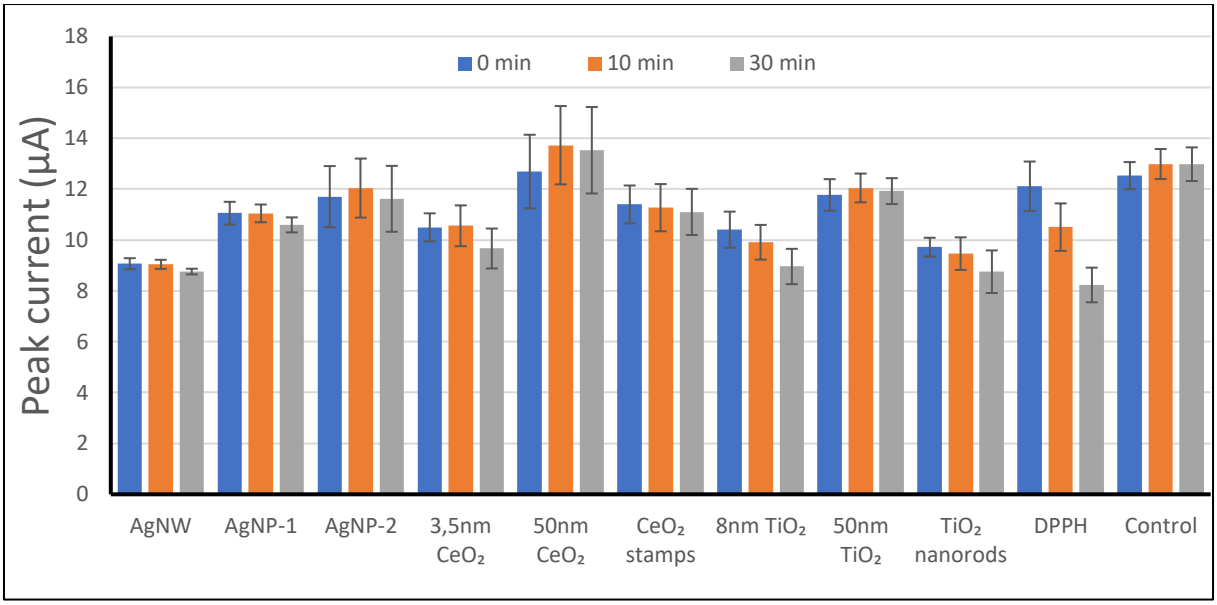

Figure 5.1.9: Peak heights at 0,5 V from CV measurements performed at 0-, 10-, and 30-min. CV was performed at 100 mV/s in HBSS containing 250 µM AA and 100 µg/ml of the indicated NP. DPPH is a stable free radical and was used as a reference control. The values listed are means of three experimental repetitions. Error bars indicate standard error of the mean.

With minor differences, experiment performed with pure L-AA or from vitamin C tablets revealed similar findings. Both demonstrated that the most oxidative NPs are AgNW, 8 nm TiO_2, and 3.5 nm CeO_2, followed by NPs with values closer to the control. One notable distinction is that AgNP-1 demonstrated higher oxidative effects with pure L-AA than from tablets.

The TAC, or the area of the voltammogram in the oxidative section (0 – 1.2 V), is another approach to understand the voltammograms. Figure 5.1.10 shows how the NPs are sorted in descending order based on how much the TAC had changed during the period of 30 minutes. This was only performed for one experimental repetition using NPs in HBSS with L-AA from tablets and must be repeated to validate the results. Analysing the NPs in this way lead to some variations in the ranking of the NPs' oxidative effect. The most notable difference being

the 8 nm TiO_2, which is ranged as the 7th most oxidative NP when monitoring TAC, while it was 3rd when examining current peak heights.

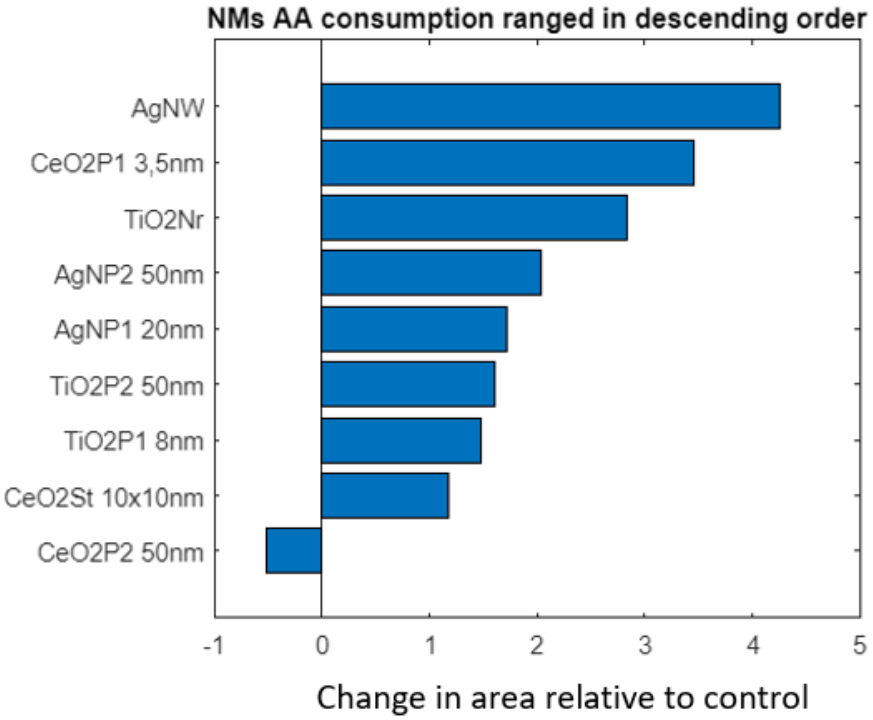

Figure 5.1.10: The NPs were ranged in descending order of total AA consumption at 30 min relative to control. The relative AA consumption in each of the CV tests was performed by integrating the CV voltammogram (provided by Emil Cimpan, with permission).

Only one experimental repetition was performed with pure L-AA, with results varying slightly from the ones performed with L-AA from tablets. Samples containing AgNP-1 and 3.5 nm CeO_2 varied the most between the two variations of the experiment. However, this experiment will need to be repeated to validate the results.

Overall, the use of CV of NPs in HBSS with L-AA demonstrated promise as a method for screening for NPs' intrinsic oxidative potential. Several NPs showed an oxidative effect at 100 µg/ml. Among the NPs with the highest intrinsic oxidative effect were AgNWs, TiO_2 nanorods, 8 nm TiO_2 and 3.5 nm CeO_2.

5.2 Dynamic light scattering

Next, we performed real-time viability/proliferation as well as ROS generation experiments with cells exposed to the different NPs to validate the CV findings. First, we carried out size-

distribution analysis of NPs in cell culture medium to characterize the stability of NPs in dispersion. Shortly after the beginning of NP exposure (time 0 h), DLS was performed using 100 µL of the highest concentration of NPs (100µg/ml). For each sample, the system measures the HDD and PdI of the NP suspension three times. The PdI is a measure of the heterogeneity of a sample based on the HDD of the NPs in solution. International standards organizations have established PdI values < 0.05 for monodisperse solutions, while values > 0.7 for polydisperse solutions [44]. The DLS was also performed at 24 h (end of exposure). Table 5.1 displays DLS measurements for all the nine NPs used in this project in milliQ water, performed by Applied Nanoparticles. Table 5.2 displays the HDD and PdI of all NP dispersions, as well as standard deviation of the mean HDD 0 and 24 h in cell culture medium supplemented with 10 % FBS. The listed values are the means of three experiment repetitions. For all particles except AgNW, the measured HDD is larger in full cell culture medium than in milliQ water. Most NPs did not show considerable differences from 0 to 24 h in cell culture medium. However, the HDD of AgNP-1, 50 nm TiO_2 and 50 nm CeO_2 all increased greatly during the time of exposure. This will be further discussed in section 6.2. The HDD of the NPs varied across repeats, being 50 nm CeO_2, 8 nm TiO_2, 50 nm TiO_2 and the TiO_2 nanorods the particle dispersions with the highest standard deviation.

Table 5.1: DLS of NPs in 1:50 dilution in mQ water at pH: 6,60. Data provided by Applied Nanoparticles, Barcelona, Spain.

NP	HDD (nm)	SD* of the mean (nm)	PdI
AgNW	1st peak(97%) : 422,8 2nd peak (3%): 5170	1st peak: 17,0 2nd peak: 219	0,226
AgNP-1	50,7	4,0	0,282
AgNP-2	63,4	1,0	0,236
8 nm TiO_2	69,7	7,3	0,362
50 nm TiO_2	197,9	6,1	0,201
TiO2 nanorods	143,4	2,8	0,118
3.5 nm CeO_2	5,48	0,6	0,25
50 nm CeO_2	197,9	6,1	0,201
CeO_2 stamps	102,4	5,0	0,129

*SD of the mean within 3 replicates.

Table 5.2: DLS measurements of 100µg/ml NPs in DMEM with 10% FBS, 0 and 24 h after exposure.

Time**	NP	HDD (nm)	SD* of the mean (nm)	PdI
0	AgNW	276,43	1,9	0,083
24	AgNW	290,96	35,2	0,192
0	AgNP-1	57,51	0,6	0,246
24	AgNP-1	136,5	30,58	0,774
0	AgNP-2	98,36	24,18	0,190
24	AgNP-2	82,75	5,11	0,149
0	8 nm TiO_2	271,5	72,57	0,240
24	8 nm TiO_2	271,83	68,83	0,227
0	50 nm TiO_2	244,8	33,69	0,193
24	50 nm TiO_2	300,37	69,7	0,182
0	TiO_2 nanorods	215,73	44,12	0,135
24	TiO_2 nanorods	220,3	53,4	0,132
0	3.5 nm CeO_2	110,42	35,77	0,330
24	3.5 nm CeO_2	106,56	18,63	0,303
0	50 nm CeO_2	511,6	164,07	0,477
24	50 nm CeO_2	606,23	220,36	0,472
0	CeO_2 stamps	306,39	5,82	0,190
24	CeO_2 stamps	298,9	8,81	0,172

*SD of the mean within 3 replicates.
** hours after cells are exposed

5.3 Impedance-based monitoring of cells exposed to NPs

To see if the intrinsic oxidative effects of NPs (section 5.1.3) directly translate to causing cytotoxic effects, we wanted to monitor the cell viability when cells were exposed to NPs and supplemented with antioxidants. To do this, we used impedance-based tests. Our research group has extensive experience with this method, and there were already data from A549 cells exposed to the nine NPs without supplementation with antioxidants. Impedance-based measurements were carried out using the xCELLigence system to assess the effect of adding L-AA on A549 cell growth and viability while the cells were exposed to various NPs. Cells were seeded and let proliferate for 24 h to reach the growth phase. After this initial growth phase, NPs were added at different concentrations (10, 20, 50 and 100 µg/ml) and cultured for a further 24 h. The CIs were normalized at time t=24 h just prior to exposure, by using equation 5.1:

$$Normalized\ Cell\ Index\ (NCI) = \frac{CI_t - CI_{background}}{CI_{t=24}} \quad (5.1)$$

Where CI_t = Average cell index of duplicate wells at time t

$CI_{background}$ = Average cell index of duplicate reference wells without cells

$CI_{t=24}$ = Average cell index of duplicate well at time 24 h, just before exposure

In order to ensure that the starting point of exposure is the same, NCIs were utilized to adjust for small variations in cell density between the wells. All experiments were performed in duplicate and repeated a total of three times. The negative control was treated with 10 mM TMAOH in 2,2 mM Sodium Citrate (Dispersion medium). The volume used was equal to the volume of NP suspension used for the treatment with the highest concentration of NPs. The stable free radical DPPH was used as a positive control at a concentration of 0,5mM.

The NCIs from the A549 exposed to AgNWs are depicted in figure 5.3.1 A). This experiment was performed in three independent experimental repetitions, and the results are presented as the mean of these repetitions. The first 2-3 h of any xCELLigence measurement show a sharper increase in CI than in the following hours, due to the cells adhering to the surface of the electrodes and starting to proliferate. A depression in NCI is observed at the beginning of exposure. At this time, the E-plate was taken out of the incubator to add medium containing NPs. The temperature and pH at this time changed as new medium and NP suspensions were added to the wells, which usually causes slight cell loosening and shrinkage. Thus, the drop in NCI.

During the initial hours after exposure, the NCI of negative control and all concentrations of AgNW kept increasing. However, at roughly 5 h after exposure, the cells exposed to 50 and 100 μg/ml AgNW reached a plateau. This plateau is at a higher NCI than the negative control. This effect may be due to a stress response by the cells that may lead to increased cell expansion, cell-cell contact, cell-subtrate contact or a combination of these. This response tried to counteract the toxic effect of the NP, but over time, the cell fails to deal with it if the NP is highly or moderately toxic. Thus, shortly after the NCI decreased rapidly. The two lowest

concentrations of AgNW diverged from the control at 9 h after exposure. The NCI of both conditions keep increasing, but not as much as the control. Figure 5.3.1 B) and C) shows the NCI of A549 cells exposed to 20 and 50 nm AgNPs, respectively. In these experiments, only the positive controls caused a decrease in NCI during exposure. The rate of increase in NCI varies with concentration of NPs. In both experiments, the highest concentration of NPs displays the smallest rate of increase in NCI, followed by the second highest concentration. The two smallest concentrations showed growth profiles relatively close to the negative control.

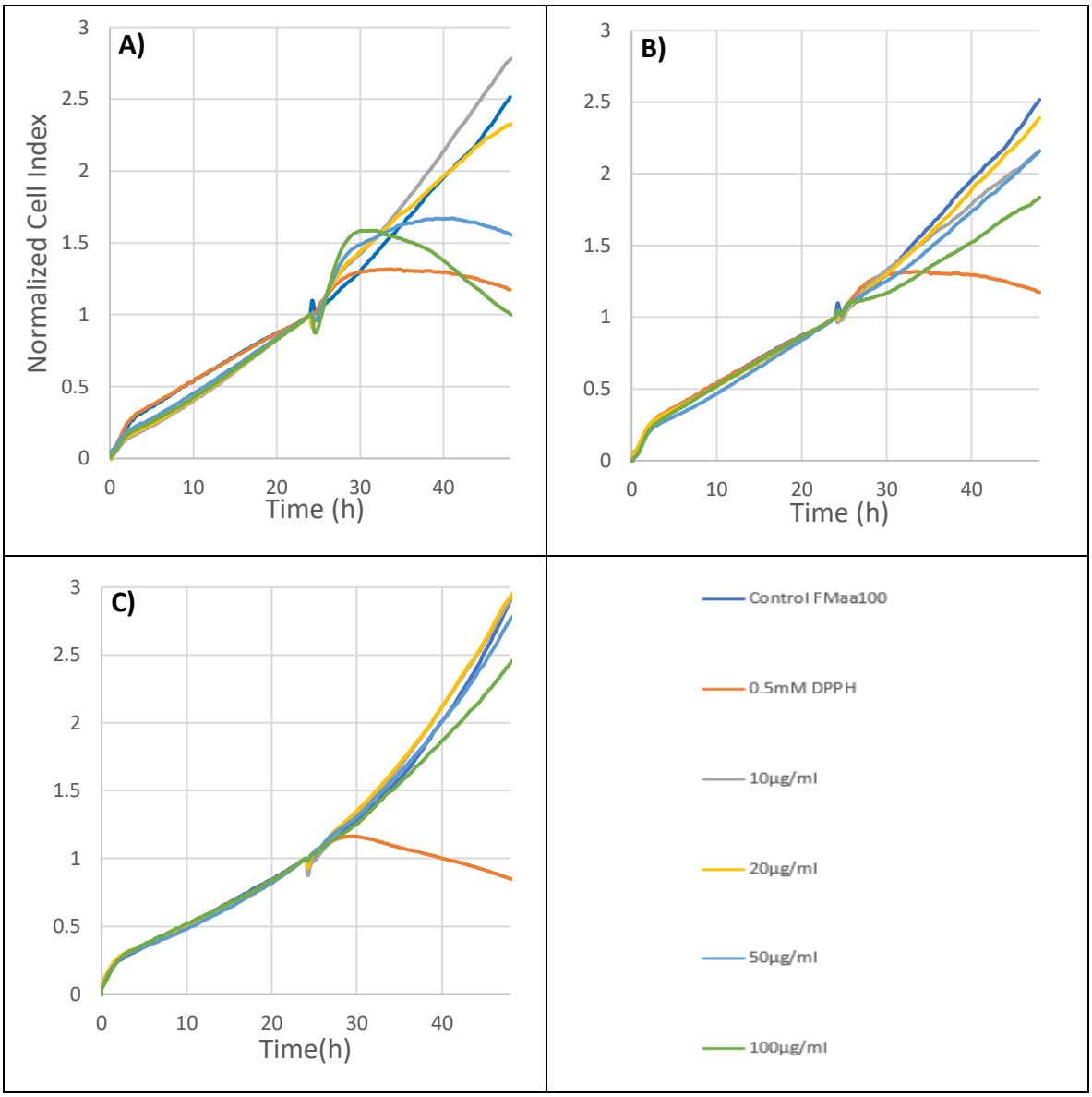

Figure 5.3.1: Normalized Cell Index of A549 cells cultured in xCELLigence E-plates with DMEM + 10% FBS. A cell density of 5,000 cells per well was used to seed the cells. The cells were treated to four different concentrations of **A)** Ag nanowires (AgNW), **B)** 20 nm Ag nanoparticles (AgNP-1), and **C)** 50 nm Ag nanoparticles (AgNP-2), 250µM AA and 1mM 2-P-AA at timepoint 24 h. Each measurement condition was performed in duplicate, and the experiments was repeated three times. The mean of the repeats is depicted in the graphs.

At the end of exposure, i.e., 24 h after addition of NPs, the fold-change (FC) vs control was calculated for each well, by using equation 5.2:

$$Fold\ change\ vs. control\ (FC) = \frac{NCI_{t=48}}{NCI_{ctrl,t=48}} \quad (5.2)$$

Where $NCI_{t=48}$ = Average normalized cell index for duplicate well at time 48 h (at the end of exposure)

$NCI_{ctrl,t=48}$ = Average normalized cell index for duplicate control wells at time 48 h

The FC represents the ratio between the NCIs of the treatment groups and the NCI for the control group and can be used to describe viability. Thus, the FC vs control for the control group is always 1. Figure 5.3.2 shows the FC for the three Ag-based NPs. For all Ag-based NPs, the FC decreased with increasing concentration. AgNWs at 20, 50 and 100 μg/ml are statistically significant compared to control (p<0,001 for all three). AgNP-1 at 100 μg/ml shows statistical significance (p<0,001). AgNP-2 also display a slight decrease with increasing concentration. However, no FC values for cells exposed to AgNP-2 are significantly different from control.

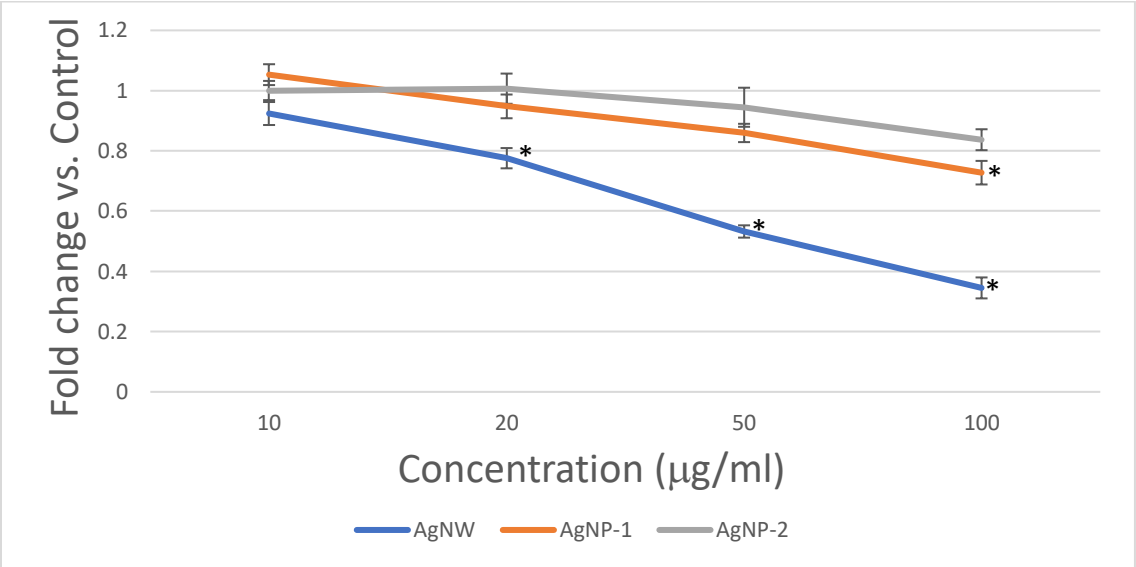

Figure 5.3.2: Fold change vs. control of A549 cells exposed to three Ag nanoparticles and subjected to impedance measurements. Four concentrations of each particle were used. The figure depicts the

mean of three experimental repeats, while the error bars depict the standard error (SE) between the three repetitions. Statistical significance ($p<0.05$) compared to control is denoted by *.

Table 5.3. presents a comparison of the FC vs control from xCELLigence studies conducted in the absence and presence of 250μM AA and 1mM 2-P-AA. The concentration 20 μg/ml had not been tested without AA and is therefore not included in the table. For cells exposed to AgNW, the addition of L-AA and 2-P-AA drastically increases the FC at 24 h exposure-time. For cells exposed to the highest concentration, the FC was increased by 359 %, while for 10 and 50 μg/ml it increased by 5 and 43 %, respectively. When adding antioxidants to AgNP-1 exposure experiments, the FC of 10, 50 and 100 μg/ml AgNP-1 increased by 18, 4 and 4 %, respectively. However, the effect of adding L-AA to AgNP-2 is more ambiguous. At the lowest and highest concentration, the FC is lowered, while it is increased for the middle concentration.

Table 5.3: Comparison of fold change vs. control from xCELLigence at 24 h exposure-time of Ag NPs with and without the presence of 250μM AA and 1mM 2-P-AA. The % change of FC-values upon addition of L-AA and 2-P-AA, and p-values comparing supplemented and not-supplemented groups are also listed. (* denotes statistical significance, $p<0.05$)

NP		**AgNW**			**AgNP-1**			**AgNP-2**		
Concentration (μg/ml)		*FC*	*change w/wo AA (%)*	*p*	*FC*	*change w/wo AA (%)*	*p*	*FC*	*change w/wo AA (%)*	*p*
10	+ AA	0.92	5.2	0.961	1.05	17.9	0.248	1.00	-1.7	1.000
	- AA	0.88			0.89			1.02		
50	+ AA	0.53	42.7	0.067	0.86	4.3	0.998	0.94	5.7	0.978
	- AA	0.37			0.82			0.89		
100	+ AA	0.35	358.6	0.001*	0.73	3.7	1.000	0.84	-3.3	0.999
	- AA	0.08			0.70			0.87		

Next, we tested possible toxicity of TiO_2 NPs on A549 cells. The NCI growth profiles of A549 cells exposed to 8 nm TiO_2 are shown in figure 5.3.3. As expected, the positive control showed a decrease in NCI compared to negative control over time. Regarding 8 nm TiO_2 NPs, we observed an increase in NCI which was proportional to the concentration of NPs. The most prominent difference between the treatment groups and the negative control is for the highest concentrations of the NP (50 and 100 μg/ml), while the two lowest concentrations are close to the negative control.

Figure 5.3.3 B) and C) displays the NCI growth profiles of A549 cells exposed to 50 nm TiO_2 NPs and TiO_2 nanorods over a period of 24 h. During exposure, the NCI of all treatment groups closely followed the trend of the negative control, which was steadily increasing over the entire exposure time. By the end of the 24 h of exposure, all concentrations of TiO_2 nanorods tested, except the lowest (10 µg/ml), showed a slight increase in NCI when compared to the negative control. In fact, around 9 h after the beginning of exposure, the first distinguishable difference emerged, where cells treated with TiO_2 nanorods seemed to have a slight increase in proliferation/viability compared to the negative control. This difference is maintained throughout the remaining exposure duration.

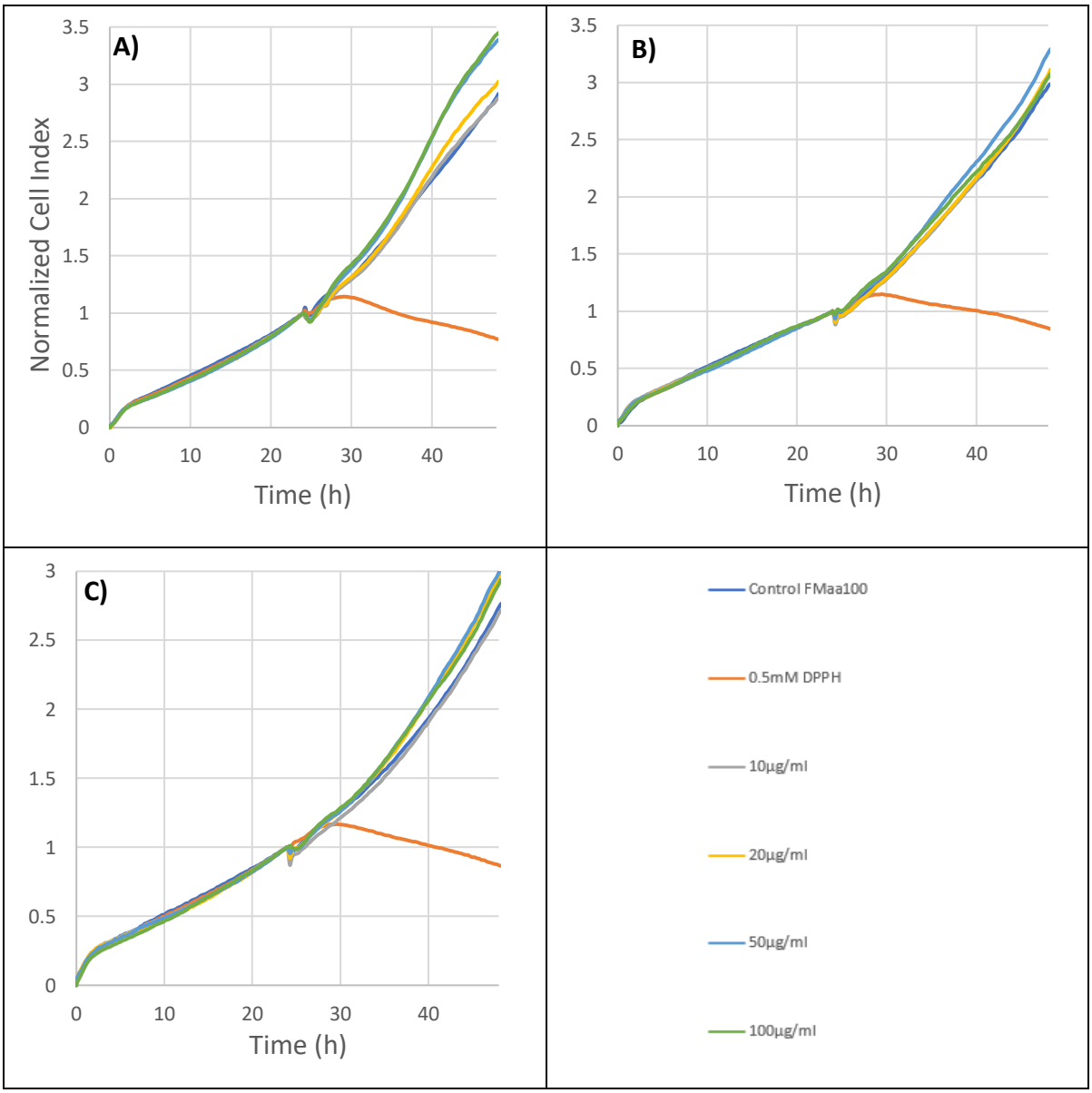

Figure 5.3.3: Normalized Cell Index of A549 cells cultured in xCELLigence E-plates with DMEM + 10% FBS. A cell density of 5000 cells per well was used to seed the cells. The cells were treated to four

different concentrations of **A)** 8 nm TiO_2 nanoparticles, **B)** 50 nm TiO_2 nanoparticles, and **C)** TiO_2 nanorods, 250μM AA and 1mM 2-P-AA at timepoint 24 h. Each condition was performed in duplicate, and the experiment was performed three times. The mean of the repeats is depicted in the graph.

The fold change vs. control of cells exposed to the three different TiO_2 NPs at the end of exposure is depicted in figure 5.3.4. No discernible cytotoxicity was obtained for any of the TiO_2 NPs at the concentrations tested. As mentioned before, A549 cells exposed to 8 nm TiO_2 showed marginal increase in viability/proliferation when compared to control and this difference augmented with increasing concentration of the NM. However, these differences were not statistically significant. In fact, no FC for any of the TiO_2 NPs was shown to be statistically significant. The biggest variation from control is for cells exposed to 100 μg/ml 8 nm TiO_2, for which the FC vs control was 19 % higher than control (p=0,086).

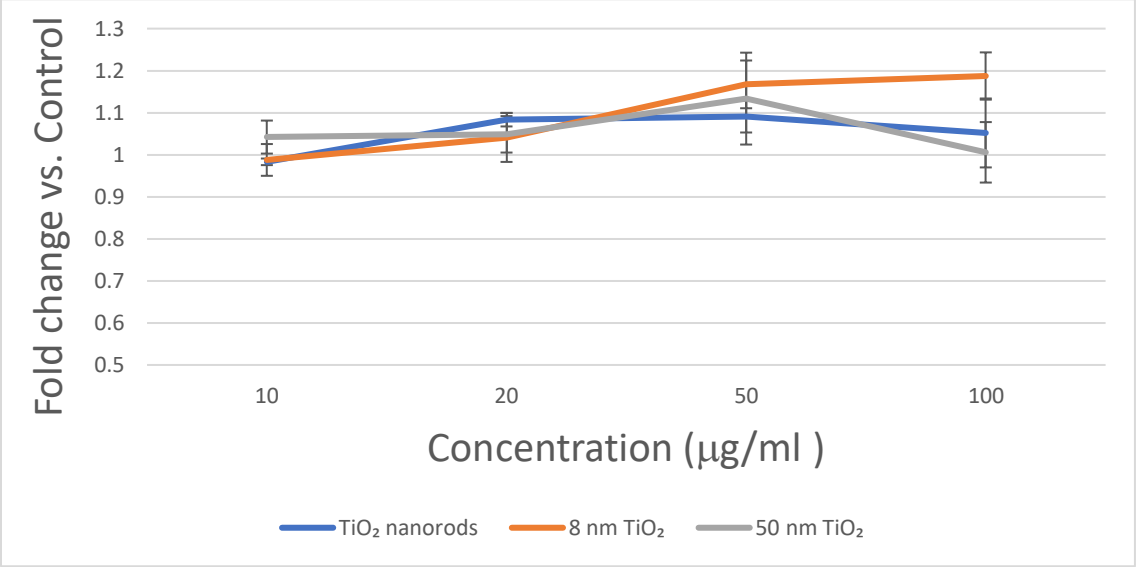

Figure 5.3.4: Fold change vs. control of A549 cells exposed to three TiO_2 nanoparticles and subjected to impedance measurements. Four concentrations of each particle were used. The figure depicts the mean of three experimental repeats, while the error bars depict the standard error (SE) between the three repetitions.

The FC vs control results from xCELLigence tests carried out with or without 250 μM L-AA and 1 mM 2-P-AA are shown in table 5.4. The table does not contain the concentration 20 μg/ml because it has not been tested without L-AA and 2-P-AA. The combination of L-AA and 2-P-AA drastically increases the FC vs control for A549 cells exposed to 8 nm TiO_2; by 69, 38 and 11 % for cells exposed to 100, 50 and 10 μg/ml of 8 nm TiO_2, respectively. Without the addition of L-AA and 2-P-AA, increasing concentrations of 8 nm TiO_2 lead to decreasing values in FC vs control. However, when L-AA and 2-P-AA were added, this trend was reversed. For the case of exposure to 50 nm TiO_2 with and without antioxidants, the FC of the cells increased by 19,

44 and 38 % for the concentrations 10, 50 and 100 μg/ml, respectively, when both L-AA and 2-P-AA were added. The addition of L-AA and 2-P-AA to cells exposed to TiO_2 nanorods did also have a positive effect in terms of viability/proliferation: cells exposed to 50 and 100 μg/ml led to an increase of FC vs control of 10 and 25 %, respectively.

Table 5.4: Comparison of fold change vs. control from xCELLigence at 24 h exposure-time of TiO_2 NPs with and without the presence of 250 μM AA and 1 mM 2-P-AA. The % change of FC-values upon supplementation of L-AA and 2-P-AA, and p-values comparing supplemented and not-supplemented groups are also listed. (* denotes statistical significance, $p<0.05$)

NP		**TiO_2 nanorods**			**TiO_2 8nm**			**TiO_2 50nm**		
Concentration (μg/ml)		*FC*	*change w/wo AA (%)*	*p*	*FC*	*change w/wo AA (%)*	*p*	*FC*	*change w/wo AA (%)*	*p*
10	+ AA	0.99	-5.04	0.997	0.99	10.6	0.864	1.04	-19.43	0.682
	- AA	1.04			0.89			0.87		
50	+ AA	1.09	10.13	0.923	1.17	37.7	0.012*	1.13	44.42	0.061
	- AA	0.99			0.85			0.78		
100	+ AA	1.05	25.18	0.313	1.19	69.1	<0.001 *	1.01	38.49	0.184
	- AA	0.84			0.70			0.73		

The NCI growth profiles of cells exposed to four concentrations of CeO_2 NPs are shown in figure 5.3.5 A-C. Cells exposed to the 100 μg/ml concentration of CeO_2 3.5 nm or stamps showed moderately higher values of NCI than negative control during the first 3 h of exposure (figure 5.3.5 A) and C). However, the NCI growth rate became lower than control around 9 h after the beginning of exposure. Cells exposed to concentrations ≤ 50 μg/ml of these two types of CeO_2 NPs displayed NCI growth rates similar to the negative control. Regarding exposure to 50 nm CeO_2 (Figure 5.3.5 B)), the NCI growth profiles of cells exposed to the two lower concentrations of CeO_2 increased similar to the negative control, while the NCI profiles of cells exposed to the two highest concentrations increased at a higher rate.

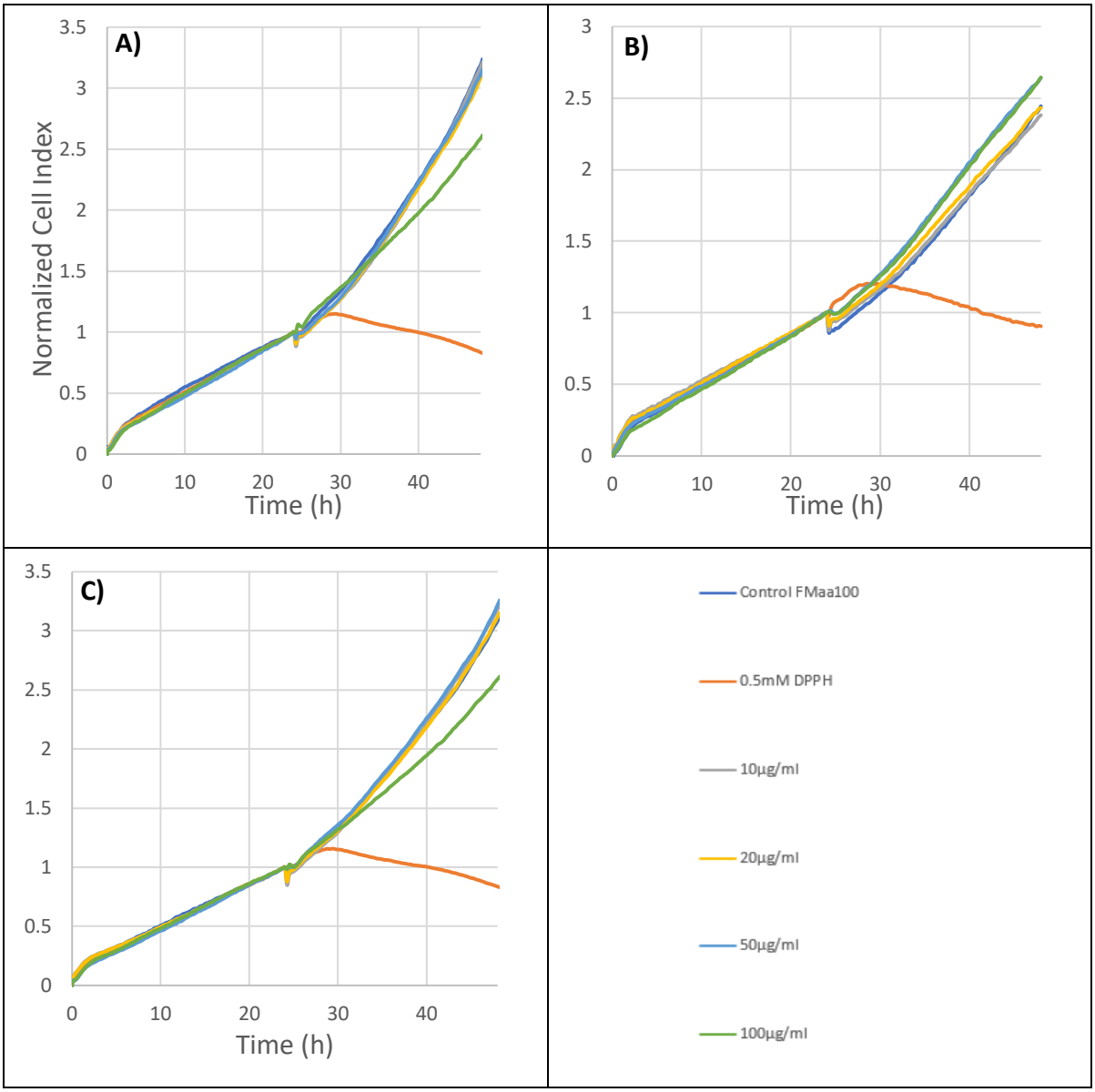

Figure 5.3.5: Normalized Cell Index of A549 cells cultured in xCELLigence E-plates with 10 % FBS. A cell density of 5000 cells per well was used to seed the cells. The cells were treated to four different concentrations of **A)** 3.5 nm CeO_2 nanoparticles, **B)** 50 nm CeO_2 nanoparticles, and **C)** CeO_2 stamps, 250µM AA and 1mM 2-P-AA at timepoint 24 h. Each condition was performed in duplicate, and the experiment was performed three times. The mean of the repeats is depicted on the graph.

Figure 5.3.6 shows the fold change vs control of cells exposed to the three varieties of CeO_2 NPs for four different concentrations at 24 h exposure-time. Cells exposed to 50 and 100 µg/ml 50 nm CeO_2 have FC higher than 1, although the differences were not statistically significant. For cells exposed to concentrations ≤ 50 µg/ml of either 3.5 nm CeO_2 or CeO_2 stamps, viability/proliferation is similar to control. However, viability/proliferation of cells exposed to either 100 µg/ml 3.5 nm CeO_2 or 100 µg/ml CeO_2 stamps was statistically significantly lower than control (p=0,007 and p=0,024, respectively). This suggests that there is slight toxicity at concentrations ≥ 100 µg/ml.

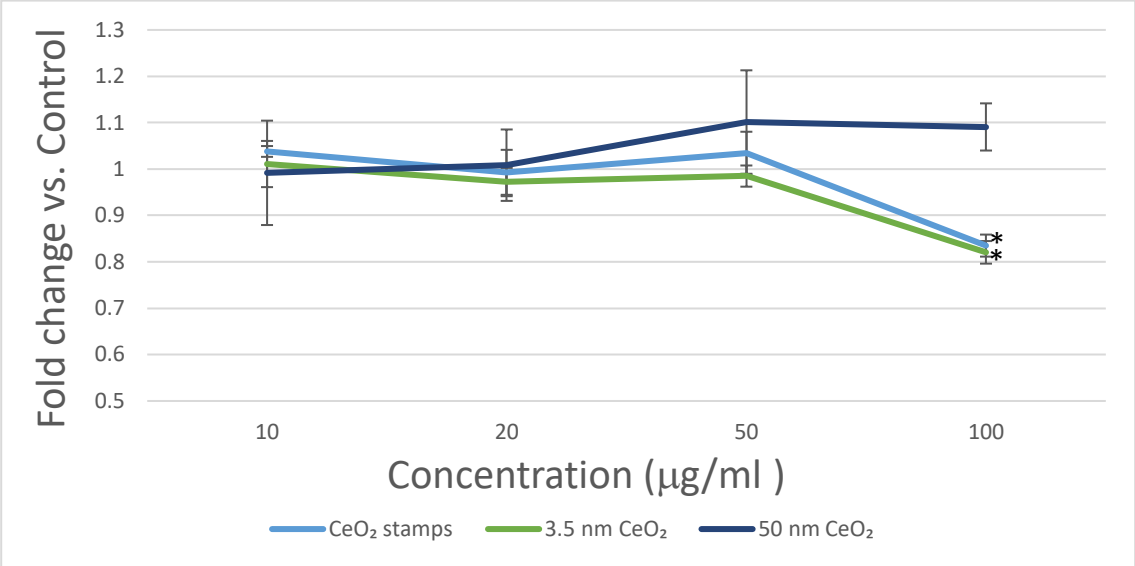

Figure 5.3.6: Fold change vs. control of A549 cells exposed to three CeO_2 NPs and subjected to impedance measurements. Four concentrations of each particle were used. The figure depicts the mean of three experimental repeats, while the error bars depict the standard error (SE) between the three repetitions. Statistical significance ($p<0,05$) is denoted by *.

Table 5.5 displays the FC vs control data from xCELLigence experiments performed with or without 250 μM L-AA and 1 mM 2-P-AA. This table does not contain the concentration 20 μg/ml as it was not tested without L-AA and 2-P-AA. For cells exposed to 3.5 nm CeO_2 the combination of L-AA and 2-P-AA does not have a clear effect on the FC in comparison to control. The differences seen for cells exposed to 3.5 nm CeO_2 with and without L-AA and 2-P-AA are marginal. Cells exposed to 50 nm CeO_2 at concentrations 50 and 100 μg/ml benefitted from the addition of L-AA and 2-P-AA, increasing by 17 and 20 %, respectively. For cells exposed to CeO_2 stamps, the FC increased by 20, 12 and 16 % for concentrations 10, 50 and 100 μg/ml, respectively. However, none of these increases were statistically significant.

Table 5.5: Comparison of fold change vs. control from xCELLigence at 24 h exposure-time of CeO_2 NPs with and without the presence of 250µM L-AA and 1mM 2-P-AA The % increase of FC-values upon addition of L-AA and 2-P-AA, and p-values comparing supplemented and not-supplemented groups are also listed. (* denotes statistical significance, p<0.05)

NP		**CeO_2 stamps**			**CeO_2 3.5 nm**			**CeO_2 50 nm**		
Concentration (µg/ml)		*FC*	*change w/wo AA (%)*	*P*	*FC*	*change w/wo AA (%)*	*P*	*FC*	*change w/wo AA (%)*	*p*
10	+ AA	1.04	20.0	0.209	1.01	7.2	0.984	0.99	-1.8	1.000
	- AA	0.86			0.94			1.01		
50	+ AA	1.03	12.4	0.633	0.98	-5.9	0.990	1.10	17.5	0.718
	- AA	0.92			1.05			0.94		
100	+ AA	0.84	15.7	0.639	0.82	-2.3	1.000	1.09	20.2	0.612
	- AA	0.72			0.84			0.91		

5.4 Fluorometry

To further assess the NPs' capabilities of causing oxidative stress in living cells, a fluorometric approach using a fluorogenic probe was attempted. The CellROX dye utilized is non-fluorescent when in the reduced form but becomes fluorescent when oxidized by ROS. As a result, the dye can serve as an indicator of ROS formation. However, due to the unique physicochemical properties of NPs, there might be factors that distort the results, which can lead to misinterpretation of data. In turn, the characterization of the oxidative capabilities of NPs is not as straightforward as for chemicals.

5.4.1 Determination of suitable positive controls

Further use of DPPH as a positive control was stopped as it showed high light absorbance in the spectral region where the CellROX dye absorbs/emits light. Figure 5.4.1 shows the DPPH concentration dependent decline in fluorescence intensity. Both concentrations of DPPH tested resulted in lower values than the untreated control. H_2O_2 was also tested as a positive control at a concentration of 200 µM. At 24 h, the fluorescence of the wells containing H_2O_2 were barely higher than the negative control, with no significant difference. Therefore, these potential positive controls were determined to be inefficient and unsuitable for use in this experiment.

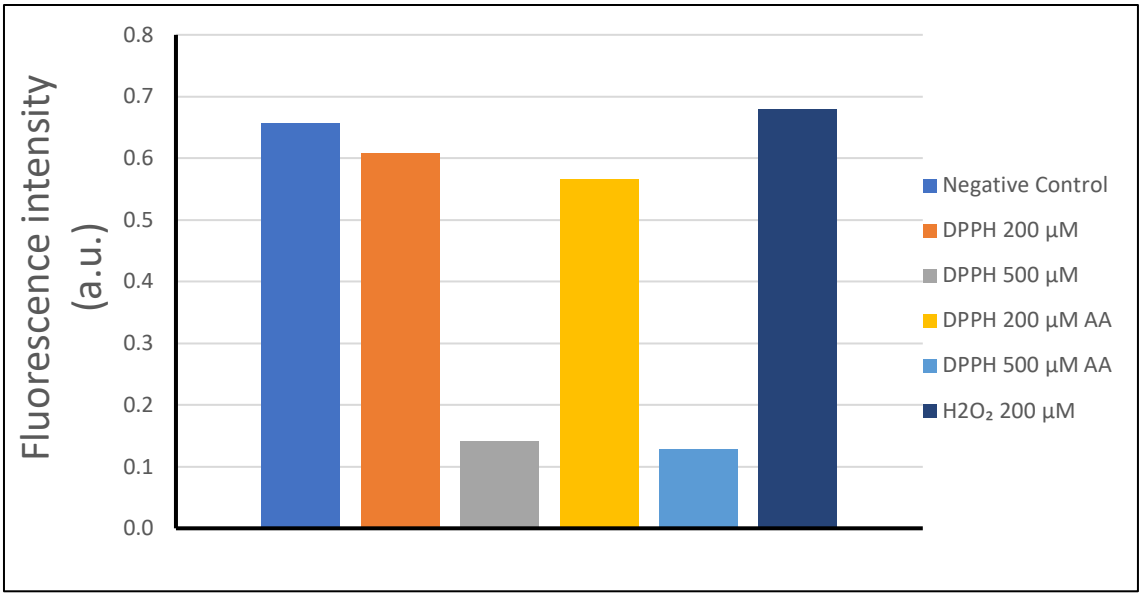

Figure 5.4.1: Fluorescence intensity at 24 h of A549 cells exposed to two different concentrations of DPPH and 200 µM H_2O_2 with 5 µM CellROX Orange fluorescent dye.

Menadione (Vitamin K_3) was also tested as a positive control at concentration 100 µM. Figure 5.4.2 displays the fluorescence intensity over time of untreated A549 cells and treated with Menadione with and without L-AA and 2-P-AA. This experiment was repeated three times and the averaged results are depicted in the figure. Background subtractions were performed using blanks with no dye. Additionally, to account for possible initial differences, the value of each well at time 0 was subtracted from the same well at each time point. Compared to the respective negative controls, menadione with and without AA shows statistical significance ($p<0,001$ for both). Therefore, menadione was utilized as a positive control in all fluorometric assays when exposing to NPs.

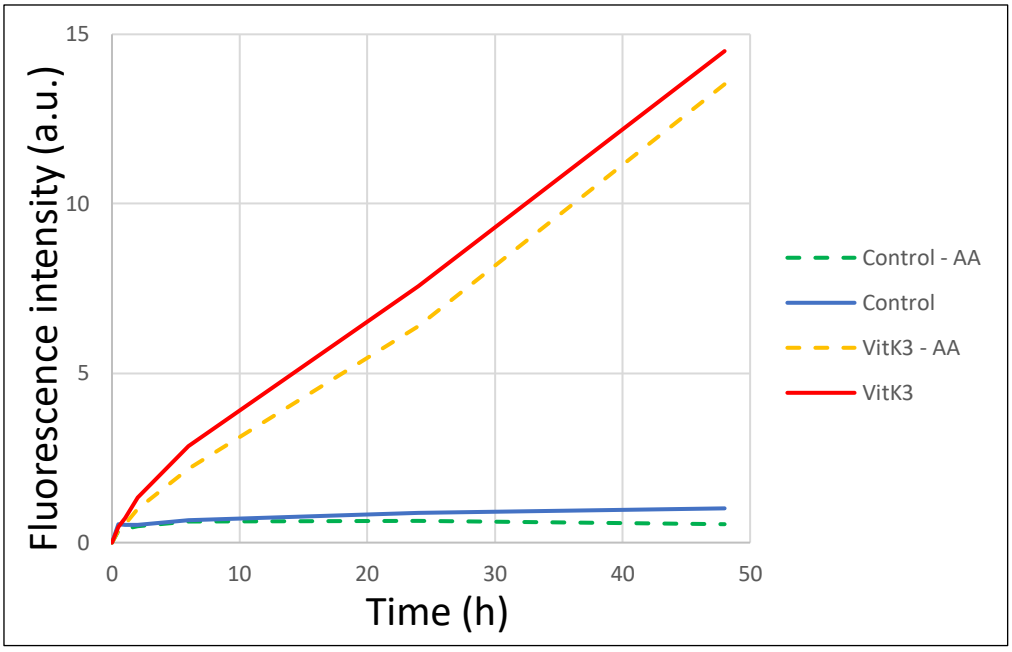

Figure 5.4.2: Evolution of fluorescence intensity of CellROX dye as measurement of ROS generation. A549 cells were seeded for 24 h before start of treatment with 100 µM Menadione ($VitK_3$). Dashed lines are for conditions containing 250 µM L-AA and 1 mM 2-P-AA and solid lines without antioxidant. Cells were stained with 5 µM CellROX Orange fluorescent dye.

5.4.2 Exposure to NPs

After finding a suitable positive control, A549 cells were exposed to the NPs under similar conditions as in the xCELLigence system. Cells were seeded at the same density (25 000 cells/cm^2) in 96-well plates and allowed to grow for 24 h before being exposed to NPs. At 30 min before exposure, the cells were subjected to pre-staining with the CellROX fluorescent dye to allow internalization of dye. At the end of the prestaining period the fluorescence was measured. Shortly after, the cells were exposed to NPs and CellROX fluorescence intensity was measured at different time points. Because AgNWs have high light absorbance in the entire UV-VIS spectrum, they were deemed unsuitable for this method, as they are likely to quench the fluorescence signal [45].

As seen in Figure 5.4.3, there was a dose-dependent decrease in fluorescence intensity of the CellROX dye with increasing concentrations of AgNP-1 or AgNP-2. This trend is similar when adding L-AA and 2-P-AA. In this instance, the 20 µg/ml concentration displays the highest fluorescence intensity among the AA treated groups at time 48 h. However, at the end of exposure, the fluorescence intensity of treatment groups containing 10 and 20 µg/ml AgNP-1 and AA is decreasing, while the intensity of the wells containing 50 and 100 µg/ml AgNP-1 and

AA is increasing. Both with and without AA, the wells containing 20 µg/ml AgNP-1 shows the highest similarity to the negative controls.

AgNP-2 exhibits similar characteristics as AgNP-1. Other effects, however, may also be observable. Figure 5.4.3 depicts the fluorescence intensity of cells exposed to AgNP-2 over time. Without AA, there is an inverse relationship between fluorescence intensity and concentration. However, the fluorescence of all conditions increased over the entire period of exposure. With AA, the fluorescence of the control condition and the two lowest concentrations of AgNP-2 developed similarly over time. The fluorescence of conditions including 50 and 100 µg/ml AgNP-2 were low throughout the period of exposure. At 48 h, cells treated with 20 µg/ml AgNP-2 had fluorescence values that were very close to the negative controls, both with and without AA.

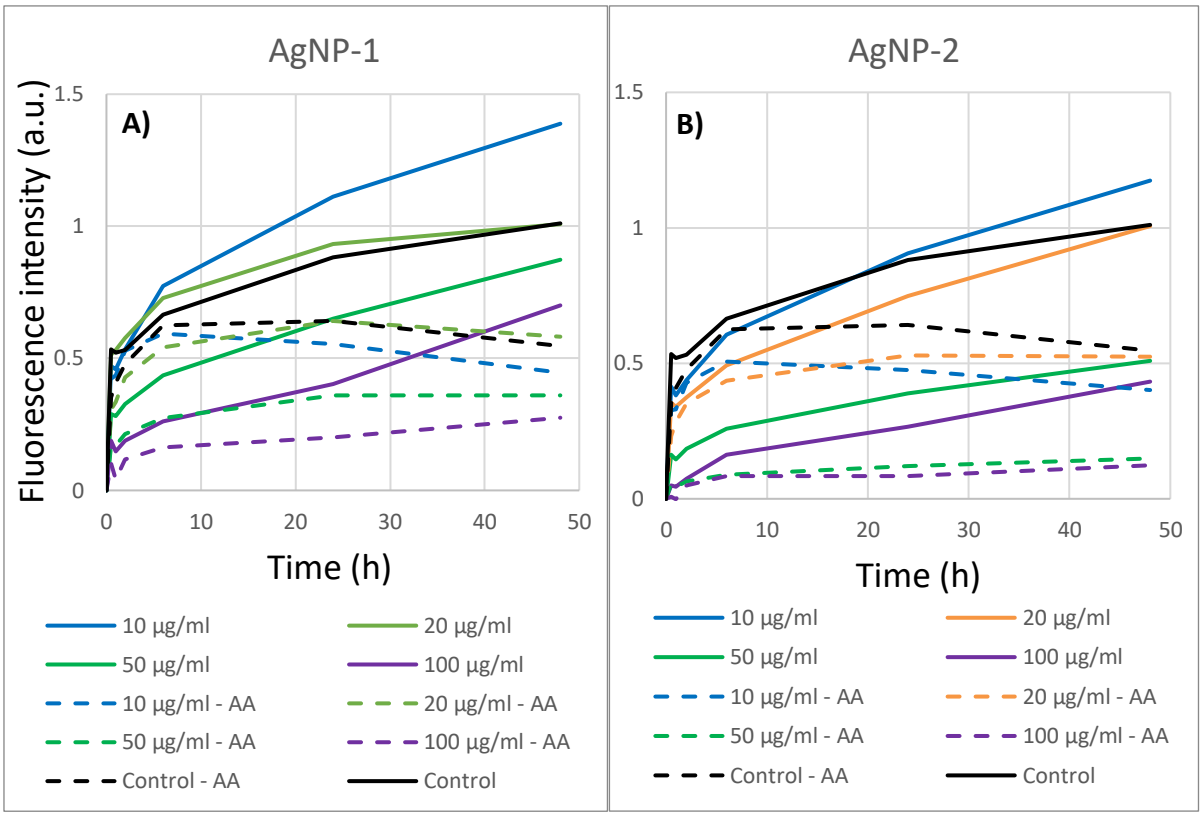

Figure 5.4.3: Evolution of fluorescence intensity of CellROX dye as measurement of ROS generation. A549 cells wereexposed to four different concentrations of **A)** AgNP-1 and **B)** AgNP-2 for a total of 48 h with 5 µM CellROX Orange fluorescent dye. Dashed lines are for conditions containing 250 µM L-AA and 1 mM 2-P-AA and solid lines without antioxidant. The data presented is the mean of three experimental repetitions.

Figure 5.4.4 displays the fluorescence intensity vs concentration graph for A549 cells exposed to AgNP-1 and AgNP-2 at 24 and 48 h after exposure with and without L-AA and 2-P-AA. For all conditions without AA, the fluorescence readings were higher at 48 h than at 24 h. When AA is added, the values for conditions of 0, 10, and 20 µg/ml are greater at 24 h than at 48 h for both NPs. Cells treated with 50 and 100 µg/ml AgNP-1 exhibited higher fluorescence intensity values at 48 h than at 24 h. The only conditions with a significant difference to control at 48 h were cells treated with 50 and 100 µg/ml AgNP-2 without AA, with p=0.023 and p=0.008, respectively.

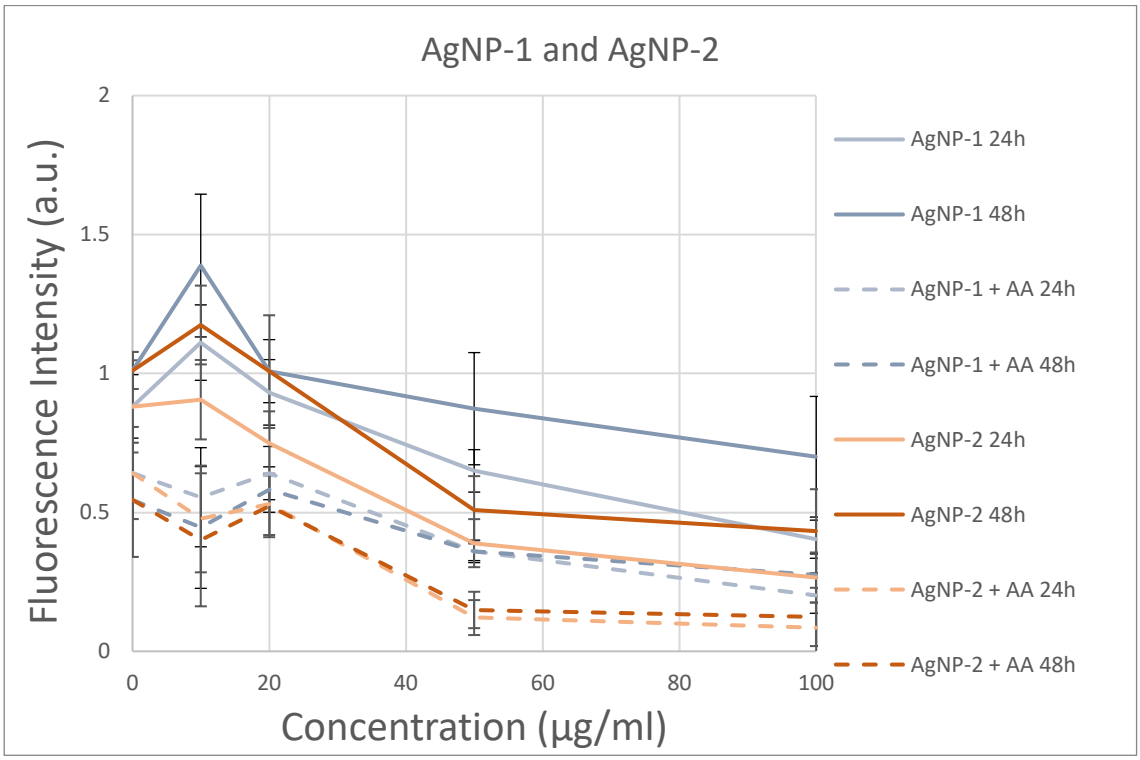

Figure 5.4.4: CellROX fluorescence intensity vs. concentration of AgNP-1 and AgNP-2 at exposure-times 24 and 48 h. AgNPs were prepared in concentrations of 0, 10, 20, 50 and 100 µg/ml in DMEM with 10% FBS. A549 cells were cultured with 5 µM CellROX Orange fluorescent dye, AgNPs and with or without 250 µM L-AA and 1 mM 2-P-AA for a total of 48 h. The data depicted is the mean of three experimental repetitions and error bars indicate standard error.

The CellROX fluorescence intensity of cells exposed to 8 and 50 nm TiO_2 NPs is shown in Figure 5.4.5. Both with and without antioxidants, the fluorescence in all conditions increased over the course of the exposure. There was an inverse relationship between concentration and fluorescence intensity with and without AA for both NPs. However, the fluorescence intensity for all conditions were lower than the negative controls at all timepoints. Without AA, the

values of cells exposed to 10 µg/ml TiO_2 are comparable to the values of cells exposed to 20 µg/ml TiO_2. The values of 50 and 100 µg/ml TiO_2 were likewise similar.

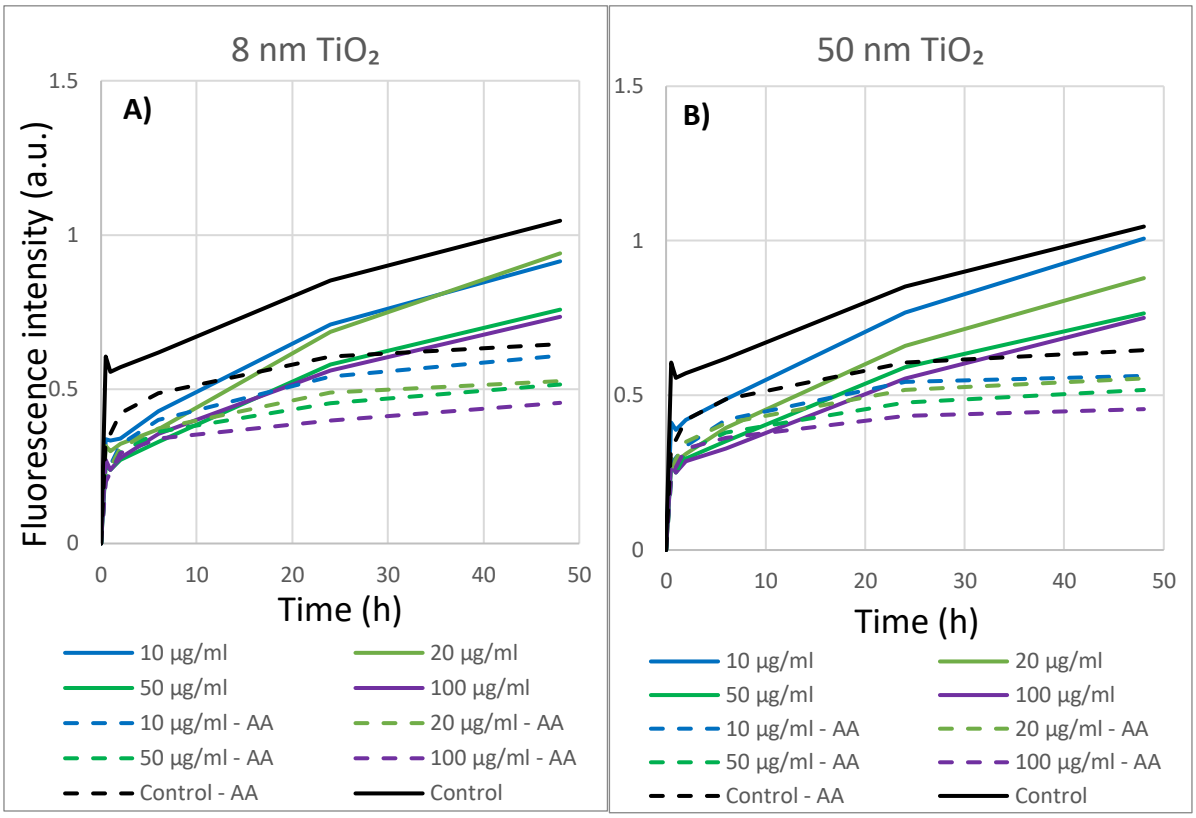

Figure 5.4.5: Evolution of fluorescence intensity of CellROX dye as measurement of ROS generation. A549 cells were exposed to four different concentrations (10, 20, 50 and 100 µg/ml) of **A)** 8 nm TiO_2 and **B)** 50 nm TiO_2 for a total of 48 h with 5 µM CellROX Orange fluorescent dye. Dashed lines are for conditions containing 250 µM L-AA and 1 mM 2-P-AA and solid lines without antioxidant. The data presented is the mean of three experimental repetitions.

Figure 5.4.6 displays the fluorescence intensity over time as A549 cells were exposed to TiO_2 nanorods for 48 h. The fluorescence of all treatment groups and controls increased for the whole time period when AA was not present. The concentration of the NP and the intensity of the fluorescence had an inverse relationship. In the absence of antioxidants, the condition containing 100 µg/ml TiO_2 nanorods had significantly ($p=0.038$) lower fluorescence intensity than the control at 48 h. Throughout the exposure period, the fluorescence of 10 µg/ml TiO_2 nanorods stayed close to the negative control. When supplemented with L-AA and 2-P-AA, the fluorescence intensities of all conditions were lower than the corresponding conditions without antioxidants. The inverse relationship between concentration and fluorescence intensity was maintained throughout the first 24 h. However, in terms of fluorescence

intensity, the 20 μg/ml concentration surpassed the 10 μg/ml concentration during the final 24 h of the experiment.

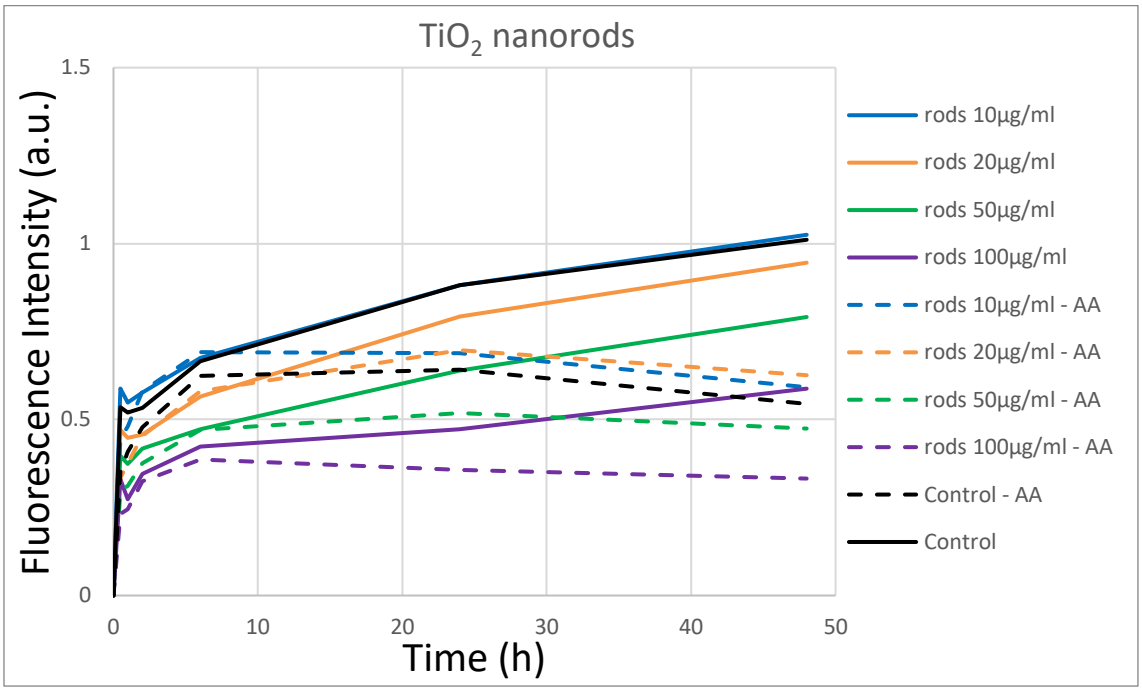

Figure 5.4.6: Evolution of fluorescence intensity of CellROX dye as measurement of ROS generation. A549 cells exposed to four different concentrations (10, 20, 50 and 100 μg/ml) of TiO_2 nanorods for a total of 48 h with 5 μM CellROX Orange fluorescent dye. Dashed lines are for conditions containing 250 μM L-AA and 1 mM 2-P-AA and solid lines without antioxidant. The data presented is the mean of three experimental repetitions.

Figure 5.4.7 depicts the CellROX fluorescence intensity versus concentration for A549 cells exposed to TiO2-based NPs. From this figure it is evident that all values at 48 h were greater than at 24 h. All values with AA were, as expected, lower than their equivalent values without AA.

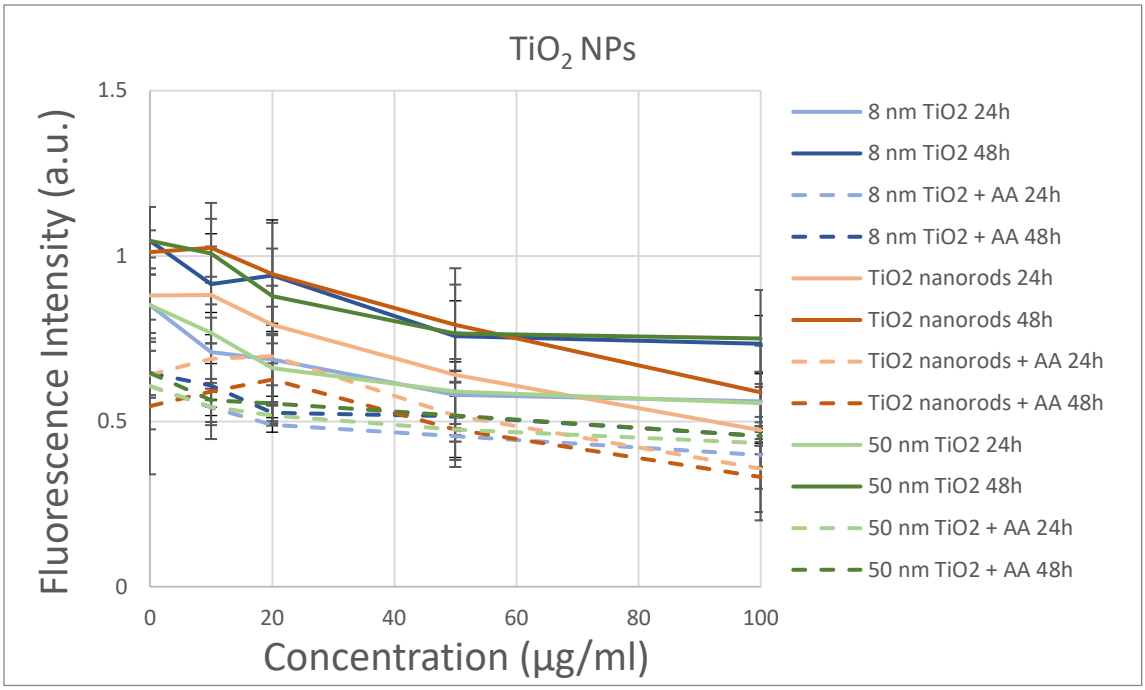

Figure 5.4.7: CellROX fluorescence intensity vs. concentration of TiO_2 NPs at exposure-times 24 and 48 h. TiO_2 NPs were prepared in concentrations of 0, 10, 20, 50 and 100 µg/ml in DMEM with 10% FBS. A549 cells were cultured with 5 µM CellROX Orange fluorescent dye, TiO_2 NPs and with or without the 250 µM L-AA and 1 mM 2-P-AA for a total of 48 h. The data depicted is the mean of three experimental repetitions and error bars indicate standard error.

Figure 5.4.8 A) depicts the CellROX fluorescence intensity over time of A549 cells exposed to four concentrations of 3.5 nm and 50 nm CeO_2 for 48 h. There is a direct relationship between NP concentration and fluorescence intensity in samples without AA. At 24 h, the fluorescence of cells exposed to the highest concentration of 3.5 nm CeO_2 was 75 % greater than that of the negative control, and 99 % higher at 48 h. The fluorescence intensities of samples containing 50 µg/ml 3.5 nm CeO_2 was 19 and 31 % higher than the negative control after 24 and 48 h, respectively. At 48 h, only the highest concentration showed a significant difference to the negative control ($p<0.001$), Throughout the exposure, the fluorescence intensities of the lowest concentrations remained lower than the negative control. Only the highest concentration of 3.5 nm CeO_2 differed greatly from the negative control when AA was added, being 26 % higher at 48 h. However, this difference was not significant. The other three concentrations of 3.5 nm CeO_2 were similar to the negative control.

The CellROX fluorescence intensity of A549 cells exposed to 50 nm CeO_2 for 48 h is shown in Figure 5.4.8 B). The highest values were obtained for the negative controls, both with and without AA, followed by the lowest concentration of CeO_2. Without AA, cells exposed to the

highest concentration of CeO_2 exhibited higher fluorescence intensity than cells exposed to the lower doses (20 and 50 µg/ml). With AA, however, the concentration and fluorescence had an inverse relationship.

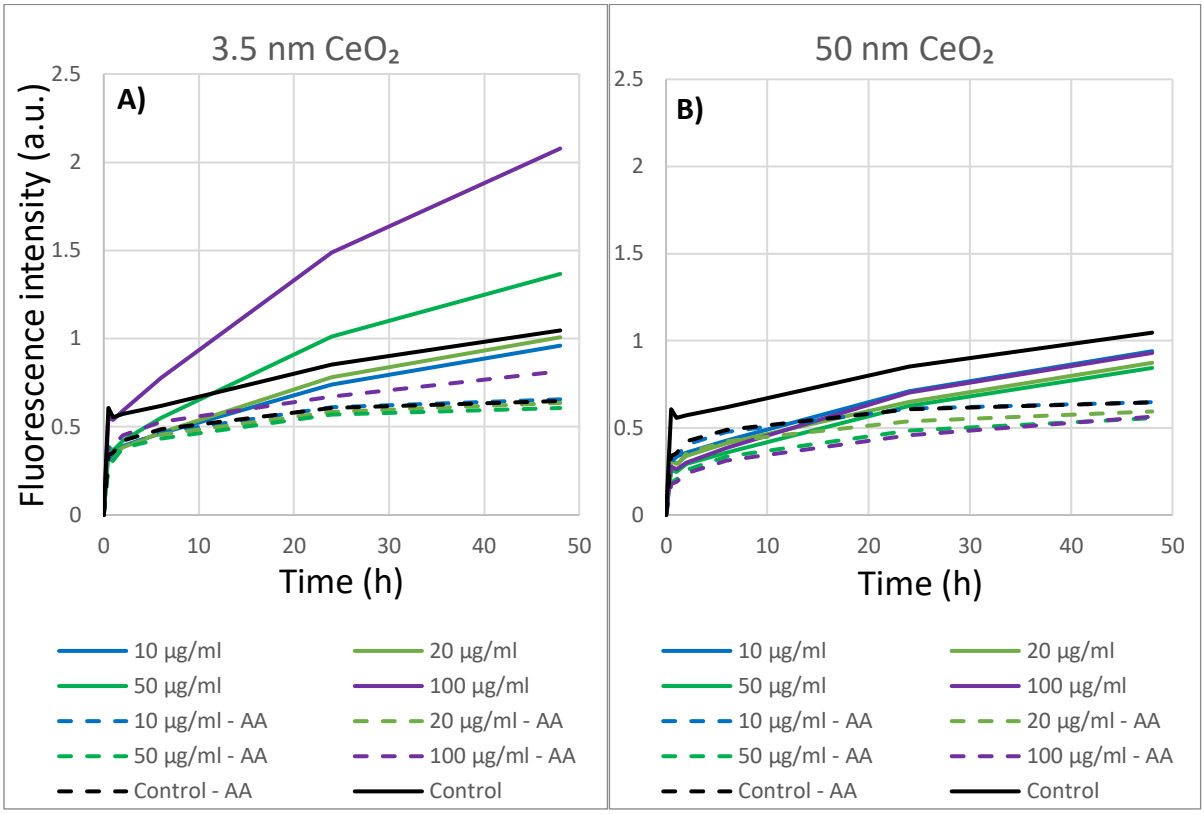

Figure 5.4.8: Evolution of fluorescence intensity of CellROX dye as measurement of ROS generation. A549 cells exposed to four different concentrations (10, 20, 50 and 100 µg/ml) of **A)** 3.5 nm CeO_2 and **B)** 50 nm CeO_2 for a total of 48 h with 5 µM CellROX Orange fluorescent dye. Dashed lines are for conditions containing 250 µM L-AA and 1 mM 2-P-AA and solid lines without antioxidant. The data presented is the mean of three experimental repetitions.

Figure 5.4.9 depicts the CellROX fluorescence intensity versus time response of A549 cells exposed to CeO_2 stamps. Without AA, the concentration of NP and fluorescence intensity had an inverse relationship. The fluorescence intensity increased during the exposure time for all conditions that did not contain AA. With AA, the intensity of all conditions rose in the first 6 h before plateauing, reaching their maximum levels either at 6 or 24 h before dropping in the following 24 h. There was no discernible trend in concentration and intensity in the presence of AA. The fluorescence intensity of conditions of cells exposed to all concentrations were higher than the negative control at 48 h. However, no conditions exhibited significantly different values than the negative controls.

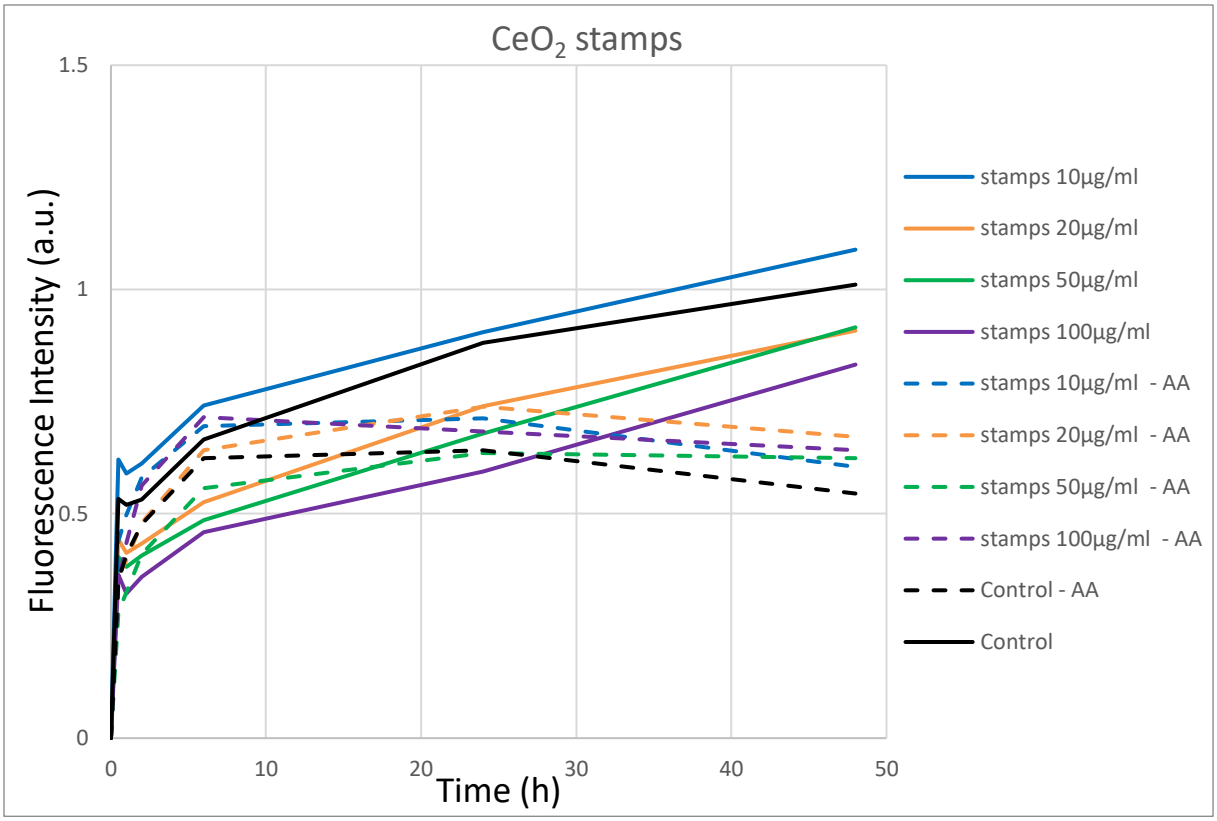

Figure 5.4.9: Evolution of fluorescence intensity of CellROX dye as measurement of ROS generation. A549 cells exposed to four different concentrations (10, 20, 50 and 100 µg/ml) of CeO_2 stamps for a total of 48 h with 5 µM CellROX Orange fluorescent dye. Dashed lines are for conditions containing 250 µM L-AA and 1 mM 2-P-AA and solid lines without antioxidant. The data presented is the mean of three experimental repetitions.

Figure 5.4.10 depicts the fluorescence intensity vs concentration for the three CeO_2 exposure experiments. Increasing concentrations of 3.5 nm CeO_2 NPs without L-AA and 2-P-AA resulted in a linear increase in fluorescence intensity. The trends become less obvious with the addition of L-AA and 2-P-AA. At 48 h, the only condition where the fluorescence intensity was significantly higher than the negative control was for 100 µg/ml of 3.5 nm CeO_2 NPs. Additionally, the greatest concentration of CeO_2 stamps resulted in lower fluorescence intensity than the other concentrations and controls. Interestingly, at 24 h, the fluorescence intensity of cells exposed to this concentration of CeO_2 stamps was lower than in the similar condition with additional L-AA and 2-P-AA.

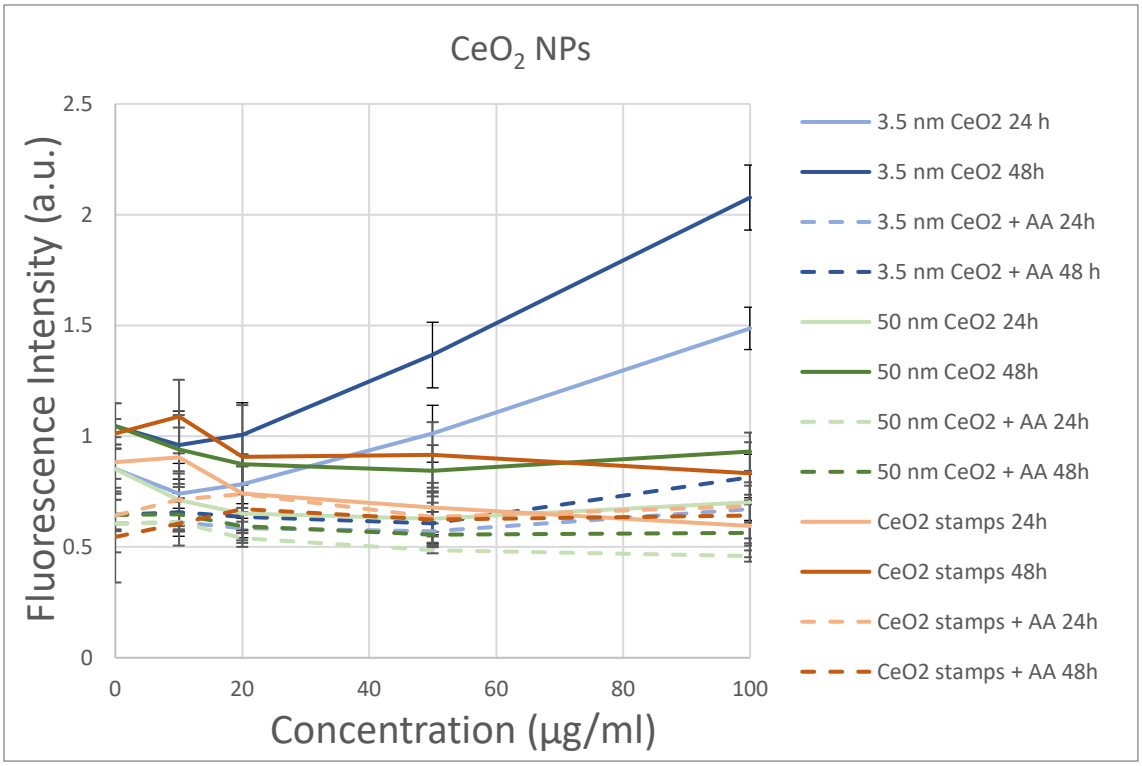

Figure 5.4.10: CellROX fluorescence intensity vs. concentration of 3.5 nm CeO_2, 50 nm CeO_2, and CeO_2 stamps at exposure-times 24 and 48 h. CeO_2 NPs were prepared in concentrations of 0, 10, 20, 50 and 100 µg/ml in DMEM with 10% FBS. A549 cells were cultured with 5 µM CellROX Orange fluorescent dye, CeO_2 NPs and with or without the 250 µM L-AA and 1 mM 2-P-AA for a total of 48 h. The data depicted is the mean of three experimental repetitions and error bars indicate standard error.

Figure 5.4.11 depicts the fluorescence intensity of CellROX fluorescent dye in NP suspensions without cells with and without L-AA and 2-P-AA. These were gathered to assess the intrinsic oxidative effects the NPs possess, as well as NP interference with the assay. The fluorescence of the dye in the sample containing 3.5 nm CeO_2 NPs in the absence of L-AA and 2-P-AA showed a much higher increase in ROS production than for any of the other NPs or the negative control. However, this effect is alleviated by the supplementation of L-AA and 2-P-AA. At 48 h, the supplementation of L-AA aided in decreasing the fluorescence intensity by 87.1 %.

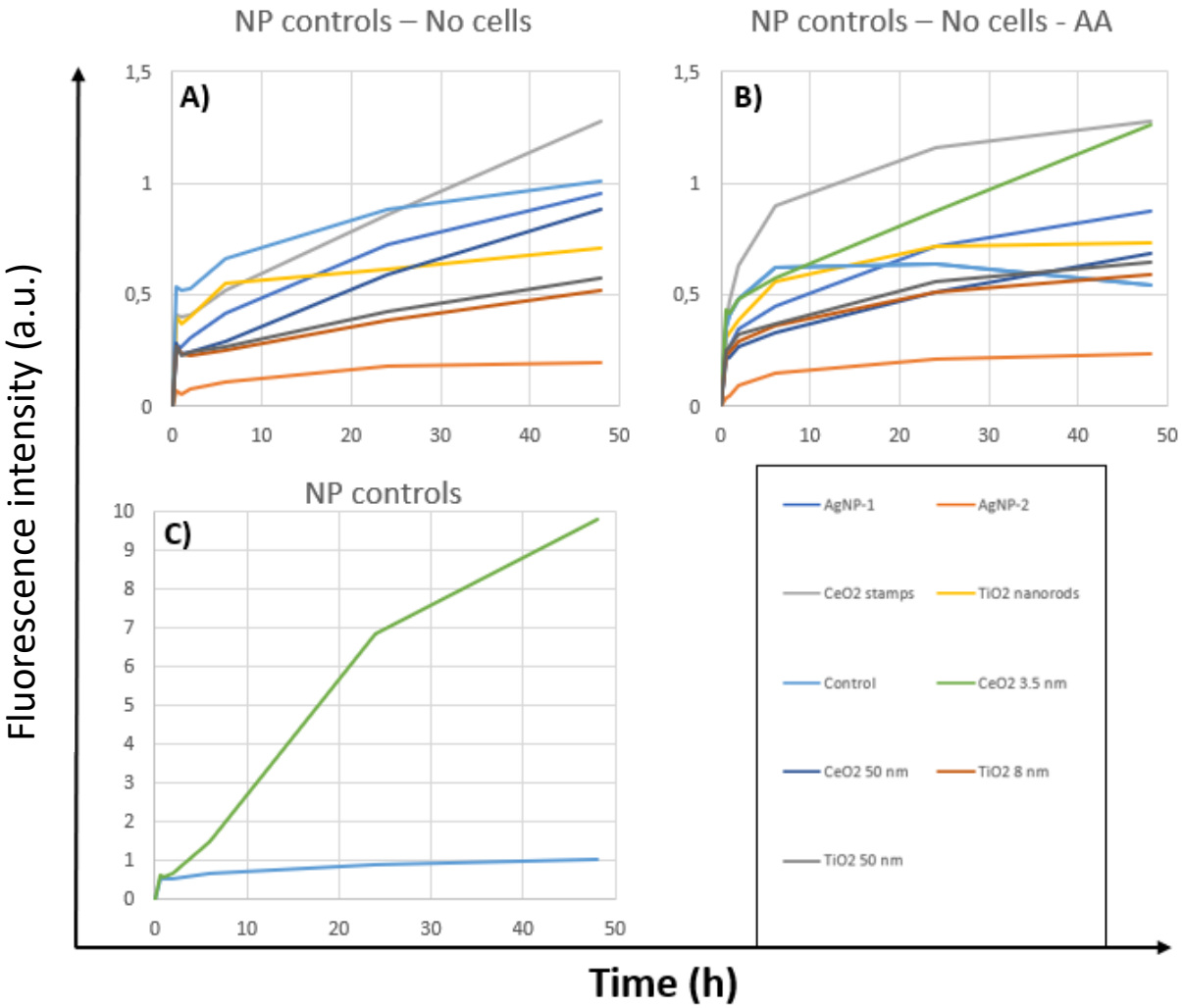

Figure 5.4.11: Evolution of fluorescence intensity of CellROX dye as measurement of ROS generation by NPs in cell culture medium without cells. NPs were prepared at 100 µg/ml in DMEM with 10% FBS. Wells were left with cell culture medium alone for 24 h before adding 5 µM CellROX Orange fluorescent dye. After the pre-treatment, NP dilutions were added either with **A)** or without **B)** 250 µM L-AA and 1 mM 2-P-AA and were incubated for a total of 48 h. **C)** CellROX fluorescence intensity vs time of 3.5 nm CeO_2 NPs incubated with CellROX for a total of 48 h without antioxidants.

5.5 Transmission electron microscopy imaging

To understand how NPs might be hazardous, it is necessary to investigate where they may affect cells. This is, if NPs act in the extracellular space, at the membrane level, intracellularly or a combination of these. In this regard, A549 cells exposed for 24 h to the nine NPs used in this study and imaged by transmission electron microscopy (TEM) to gain a better knowledge of cellular uptake and internalisation. Figure 5.5.1 depicts TEM images of A549 cells exposed to Ag NPs. Fully enveloped agglomerates were observed for all Ag NPs (Figure 5.5.1). AgNWs

appeared to cause cell structural damage to the cells. Additionally, exposure to AgNWs seems to cause autophagy, where organelles are totally engulfed in autophagosomes. The 20 and 50 nm Ag NPs were observed in both tightly agglomerated and loosely packed states within the cytoplasm and nucleus.

TEM micrographs of A549 cells exposed to TiO_2 NPs is depicted in figure 5.5.2. For all TiO_2 NPs, fully engulfed agglomerates were also observed. The TiO_2 aggregates with a diameter of 50 nm were bigger but less tightly packed than the other TiO_2 NPs. TiO_2 nanorods appear to be the least aggregated of the three TiO_2 NPs, with smaller aggregates at roughly 200 nm. The TiO_2 nanorods were incorporated into the cells at a lower level than the other TiO_2 NPs.

All the CeO_2 NPs were also discovered in agglomerates inside vesicles, as seen in figure 5.5.3. The 3.5 nm CeO_2 appeared to be more densely agglomerated than the other two CeO_2 NPs, but in smaller vesicles. The largest agglomerates were formed by 50 nm CeO_2 and were seen in less spherically shaped vesicles. CeO_2 stamps were considerably more taken up by the cells than the other NPs.

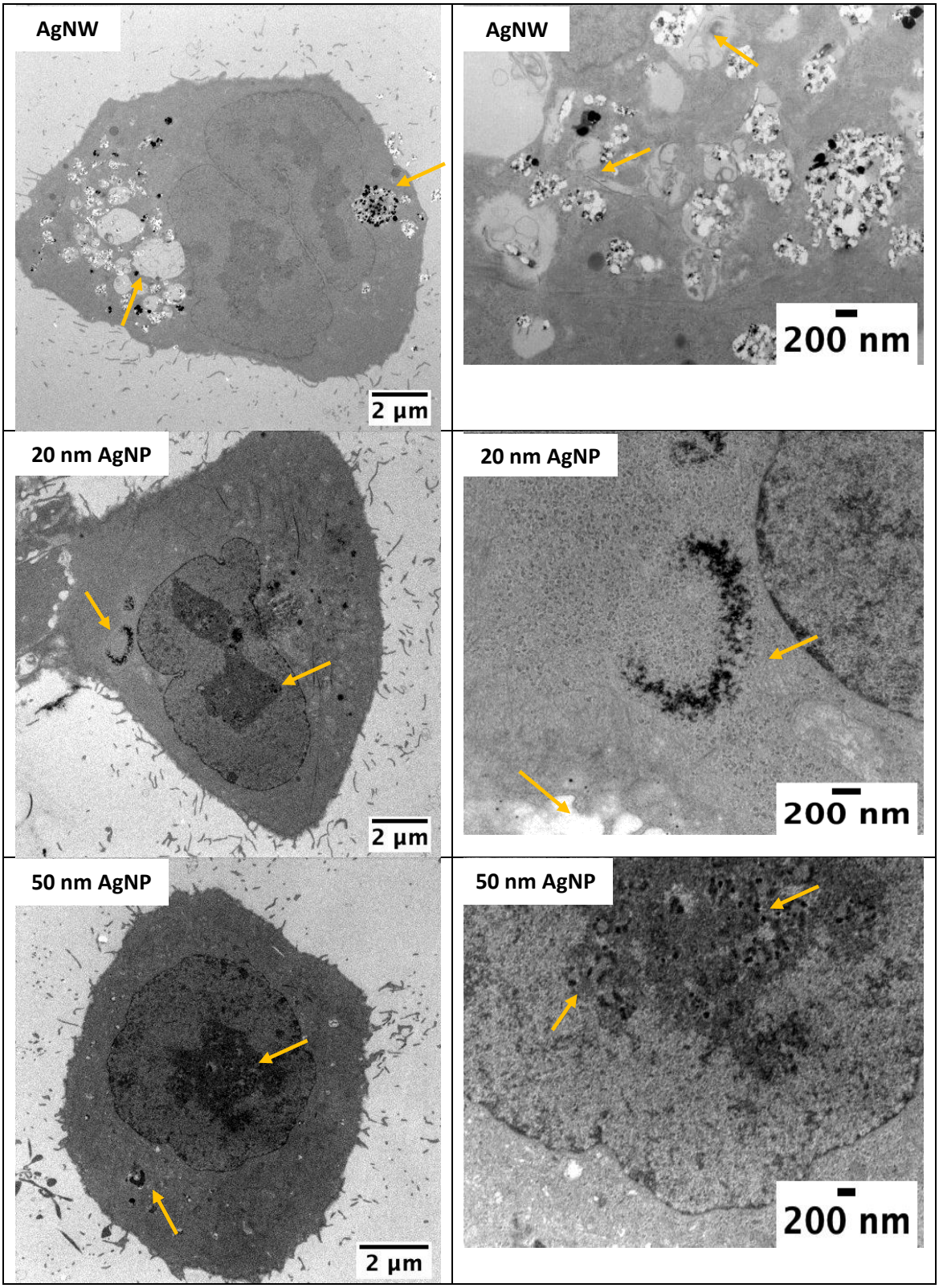

Figure 5.5.1: Transmission electron microscopy (TEM) images A549 cells treated for 24 h with 50 µg/ml of the indicated Ag NPs. Ag NPs can be observed within the nucleus and AgNWs within autophagosomes. Arrows indicate NPs inside the cell. Scale bars for images on the left represent 2 µm, while the ones on the right represent 200 nm.

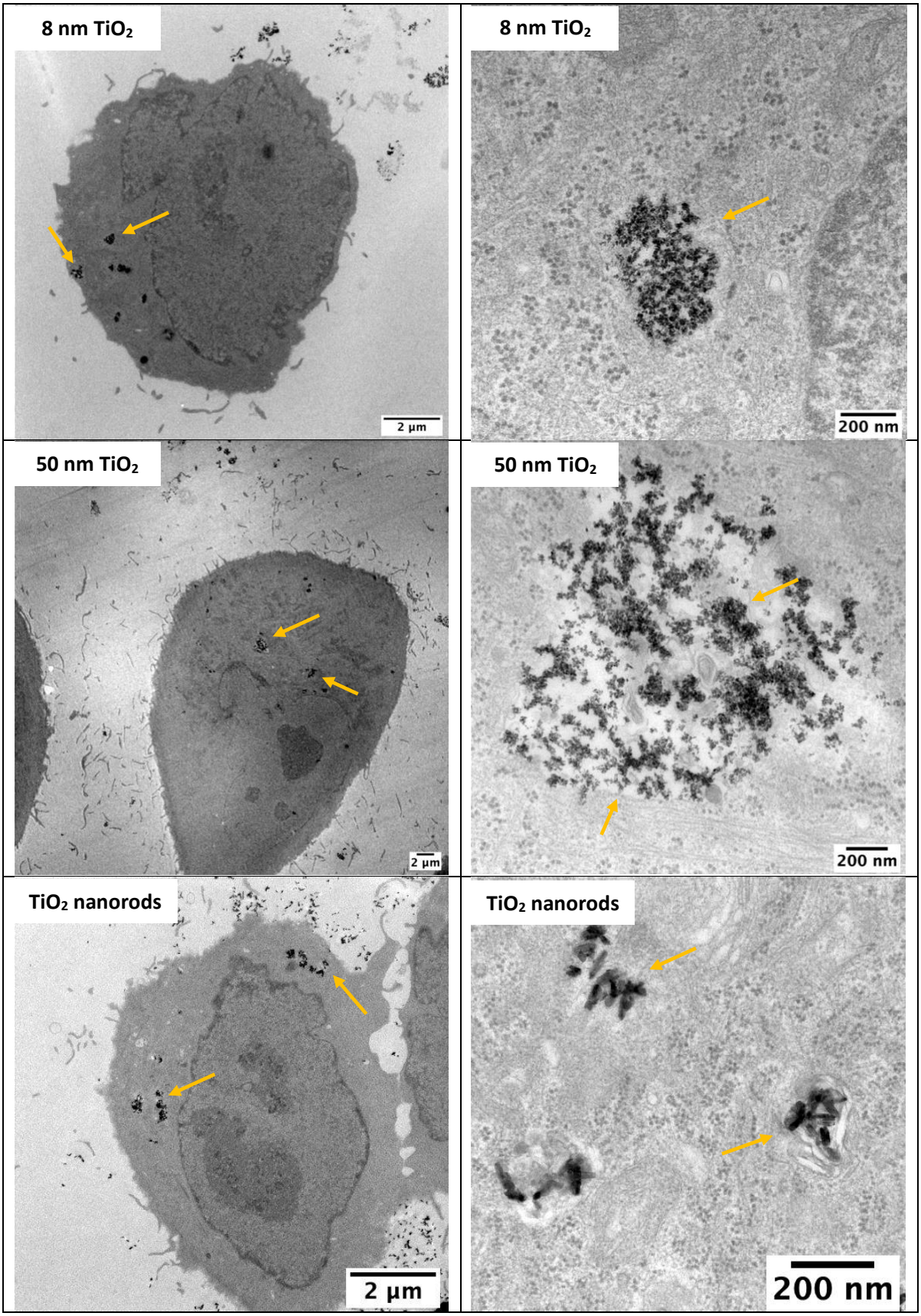

Figure 5.5.2: Transmission electron microscopy (TEM) images A549 cells treated for 24 h with 50 µg/ml of the indicated TiO_2 NPs. All TiO_2 NPs are readily taken up by the cells and accumulate in membrane-enclosed organelles (endosomes and/or lysosomes). Arrows indicate NPs inside the cell. Scale bars for images on the left represent 2 µm, while the ones on the right represent 200 nm.

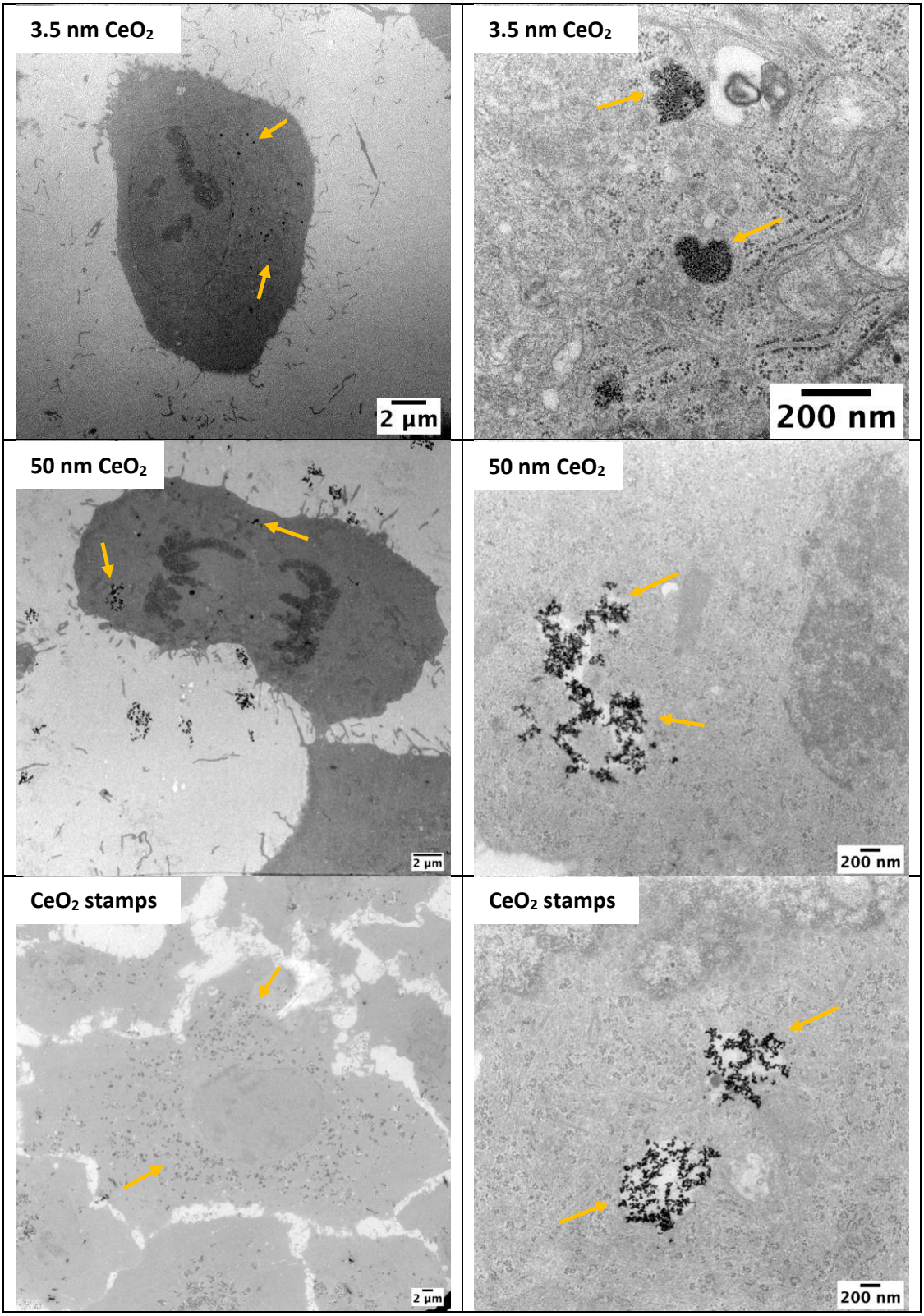

Figure 5.5.3: Transmission electron microscopy (TEM) images A549 cells treated for 24 h with 50 µg/ml of the indicated CeO_2 NPs. All CeO_2 NPs are readily taken up by the cells and accumulate in membrane-enclosed organelles (endosomes and/or lysosomes). Arrows indicate NPs inside the cell. Scale bars for images on the left represent 2 µm, while the ones on the right represent 200 nm.

5.6 Printing of electrodes

After CV had been established as a method to detect oxidation caused by NPs, we tried to fabricate cost-effective electrodes for CV by printing conductive inks on PET films. We utilised a commercially available PCB printer to produce these electrodes. Achieving high-quality, consistent printed electrodes would enable us to evaluate a broader spectrum of NPs while also allowing for high-throughput CV studies. Figure 5.6.1 displays a printed layer of the Ag component of the electrodes, as well as three electrodes: **A)** a carbon layer deposited on the silver layer, modified with picodent twinsil deposited to avoid sample spreading, **B)** a fully assembled electrode, with an insulator layer printed on top of the Ag and C, also modified with picodent twinsil, and **C)** a commercial C/C/Ag SP electrode from Metrohm.

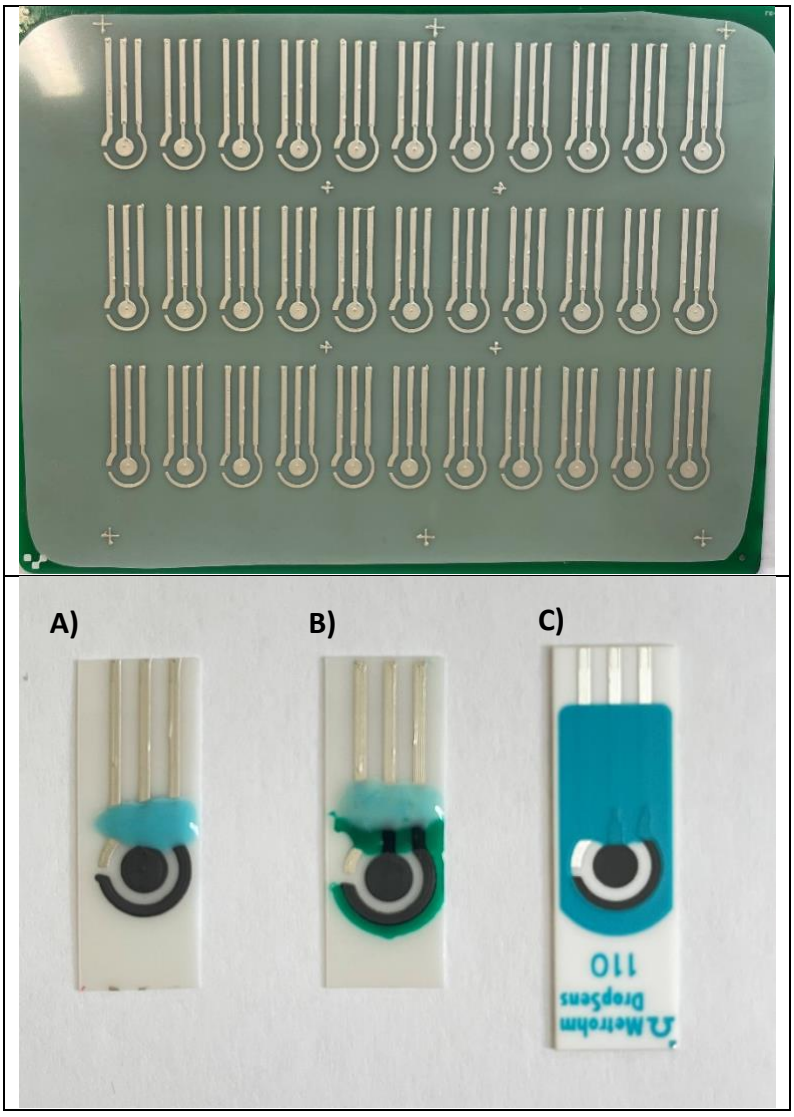

Figure 5.6.1: Top image: Ag printed on top of a PET film, with alignment markers several places around the film. Bottom image: **A)** Ag and C layers printed on a PET film, with picodent twinsil deposited to

avoid contact between samples and the silver electrode connections. **B)** Ag, C, and a resistor layer printed on top of a PET film. **C)** A commercial C/C/Ag SP-electrode. (Metrohm)

After fully printing electrodes that visually looked suitable, using silver (Conductor-2, Voltera) and carbon ink (Dycotec Materials, UK), the electrodes were tested with CV to assess their quality. Figure 5.6.2 displays the cyclic voltammograms obtained of DMEM with 250 µM L-AA using either commercial C/C/Ag Metrohm electrodes, or C/C/Ag electrodes made using the Voltera One PCB printer. The produced electrodes show higher currents than the commercial electrode. However, there was also variation between the two produced electrodes. Additionally, there was a small artefact found for one of the produced electrodes at 0.1 V, likely due to imperfections in the printed carbon layer.

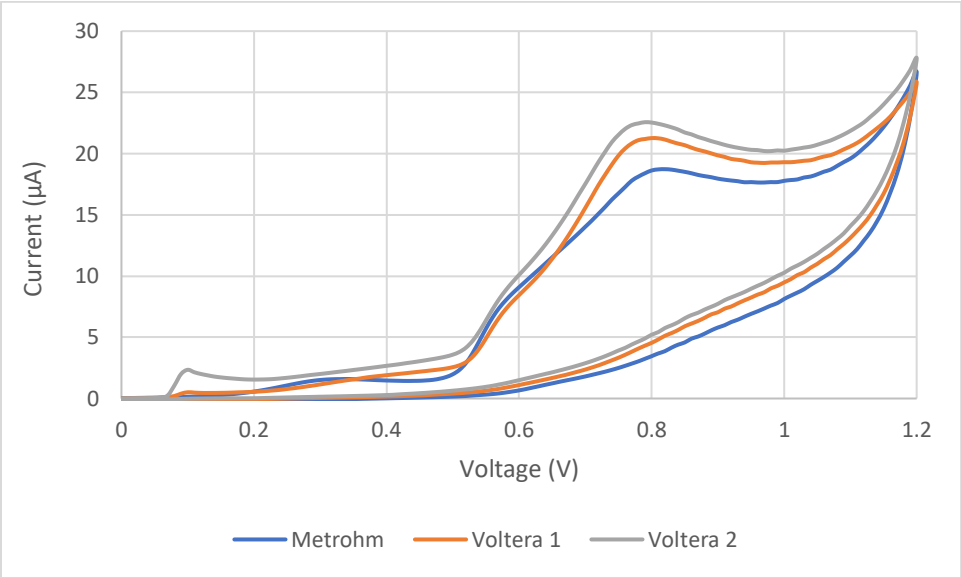

Figure 5.6.2: Cyclic voltammogram of DMEM with 250 µM L-AA using a scan rate of 100 mV/s. Three electrodes are used: a commercial Metrohm C/C/Ag electrode and two C/C/Ag electrodes produced using a Voltera One PCB printer.

The printed electrodes were comparable with the commercial electrodes and could potentially replace the more expensive commerical electrodes. However, the uniformity of the printed electrodes was an issue, and must be addressed.

6 Discussion

In this project we studied the feasibility of CV as a label-free method for analysing the oxidative potential of NPs. In order to establish this approach, adequate electrode configurations and testing conditions needed to be identified.

6.1 Electrode configuration

As mentioned in section 4.4.1, CV measurements were performed using a three-electrode system, with each electrode having its own unique set of properties. The most conventional and widely used configuration of electrodes for measuring antioxidant capacity is the combination of glassy carbon WE, platinum CE, and silver RE. Glassy carbon's properties, such as hardness, low density, low reactivity and low electrical resistance, make it suitable for a wide range of measurements [46]. However, studies have shown that bovine serum albumin (BSA), a major component of FBS, tends to adsorb to the surface of this type of electrode. Repeated use of such electrodes leads to higher variability in the voltammograms. Glassy carbon electrodes used to measure a BSA buffer solution 10 times resulted in a 43% loss in anodic response of caffeic acid [47].

The appeal of using SPEs instead of the traditional electrode configuration is clear. There are many benefits of using SPEs, including small volume of samples and quick sequential measurements of different samples. In addition, SPEs are cost effective, and as they are designed to be single use, there is no need for cleaning, which reduces the waiting time between measurements. All these advantages make SPEs ideal for high-throughput testing of NPs. Although not relevant to the results presented in this thesis, another advantage of using SPEs is that they are highly portable, and tests can be performed anywhere [48].

Figure 5.1.1 illustrates that both C/C/Ag and C/Pt/Ag SPEs show higher sensitivity at lower concentrations of L-AA than the conventional configuration. Additionally, the SPEs display higher currents for higher concentrations of L-AA. The current height value obtained with 500 μM L-AA is also higher than that reported by other researchers who used a carbon paste electrode to perform CV of L-AA at the same concentration in FBS. [49]. Figure 5.1.1 also shows

that using the C/C/Ag electrode results in increased currents at the peak for L-AA than the other electrode configurations. Additionally, the background subtraction using DMEM with 10% FBS revealed two other peaks in the voltammogram using the C/C/Ag electrodes. One of these is around 0.75 V, while the other one is around 1.05 V. However, it is not clear which components cause these peaks. Studies show that L-AA often binds to BSA found in FBS [50]. This effect might be altering the potential at which the L-AA is oxidized. These results made us choose the C/C/Ag SPEs for subsequent experiments, as they seemed better for evaluating the content of L-AA in the samples. Other concentrations of L-AA were also tested (data not shown), which gave similar results. Since the C/Pt/Ag SPE electrodes had similar sensitivity to C/C/Ag SPEs, and we had many available, they were chosen for the scan-rate testing described in section 4.4.2

6.2 Scan rate testing

Another important variable for the use of CV is the scan rate. As the redox active molecules are oxidized or reduced, a Faradic current is generated. However, the overall current is also affected by the presence of a non-Faradic current, which is a result of charge between the electrode and the analyte [46]. The non-Faradic current is often regarded as background noise. This background noise can, if large enough, limit the sensitivity of the measurement technique. The Faradic current is proportional to the square root of the scan rate, while the non-Faradic current is directly proportional to the scan rate [51]. Furthermore, the large surface of conventional electrodes, usually within 2-3 mm, can cause signal distortion when using higher scan rates (400-500 mV/s). Therefore, one study suggests that scan rates this high are only suitable when using microelectrodes [52]. The results from this thesis might strengthen those claims, as figure 5.1.3 shows considerable distortion of the voltammogram when increasing scan rate. The noise occurring at this level when increasing scan rate was only seen when using the conventional electrode setup, and not when using the SPEs.

Using higher scan rates can be used to improve sensitivity in samples containing minute concentrations of antioxidants. One study found that using scan rates of 500 mV/s and 50 mV/s made it possible to selectively detect and quantify homocysteine and glutathione. This was possible because of the different reaction rates of homocysteine and glutathione with

catechol found in the sample [53]. However, this method can be viewed as problematic, as the authors subtracted the determined homocysteine value gathered at a higher scan rate from the total peak obtained at a lower scan rate to determine the glutathione contribution to the total peak. The reason this can be viewed as problematic is that the peak from homocysteine will be higher with increasing concentration, and the determined contribution of glutathione will be lower than its actual contribution. Chevion et al. (2009), found that the CV sensitivity to L-AA was improved with higher scan rate [30]. This was complementary to our findings depicted in figures 5.1.4 A) and B), which show the increase of peak height of L-AA in DMEM with 10% FBS with increasing scan rate, ranging from 100 – 400 mV/s.

Figure 5.1.1 also displays that a scan rate of 100 mV/s is sufficient to distinguish the contribution of L-AA with concentrations of at least 50 – 500 µM. Concentrations below 50 µM should also be able to be recognized. With this in mind, this scan rate was chosen for subsequent measurements. Furthermore, it is the most commonly used scan rate when evaluating L-AA content [46].

6.3 Oxidative potential in HBSS

A common way to detect and assess the oxidative potential of NPs is the depletion of antioxidants, such as ascorbic acid, uric acid, or glutathione. Several methods that investigate the depletion of antioxidants exist, both with and without cells present in the analytical assay. The NPs can produce ROS both upon their interactions with cells, as well as in an acellular environment [54]. The ROS production upon interactions with cells is specific to the cell line treated [55]. Therefore, the evaluation of the ROS production capabilities of NPs with cells can be quite extensive. Measuring acellular ROS production can be used as a surrogate test for oxidative stress. Many different methods can be used to measure the intrinsic oxidative potential of NPs, such as methods measuring the oxidation of cytochrome c and dithiothreitol [56, 57]. However, for screening of large numbers of NPs, high-throughput assays are necessary. In this study, CV was adapted as a medium-throughput assay to screen NPs based on their intrinsic oxidative potential, but CV can be easily scaled up to 96- and even 384-well formats. The oxidative potential of nine NPs was measured in a cell-free way using CV of samples containing NPs in HBSS, at 0, 10 and 30 min after the addition of 250 µM L-AA. To

assess the depletion of L-AA, the peak heights- and area under the curve of the voltammograms were considered. This assay was selected because L-AA is oxidized in the presence of ROS causing a reduction in the pool of reduced L-AA that is available for oxidation during CV. Therefore, the L-AA content can be easily monitored using CV following parameters mentioned in section 6.3.1 and 6.3.2. Additionally, this assay is performed quickly, only requires a simple potentiostat, requires no labels, and high-throughput measurements are possible.

This method allowed us to assess the oxidative potential of Ag-, TiO_2- and CeO_2-based NPs. Based on peak heights, we observed strong (AgNW, 3.5 nm CeO_2, 8 nm TiO_2, and TiO_2 nanorods), moderate (AgNP-1 and CeO_2 stamps), and low (AgNP-2, 50 nm CeO_2, and 50 nm TiO_2) oxidation of L-AA from tablets over time. Additionally, when assessing the area under the voltammograms as a means of measuring TAC, we observed strong (AgNW, 3.5 nm CeO_2 and TiO_2 nanorods), moderate (50 nm AgNP, 20 nm AgNP, 50 nm TiO_2 and 8 nm TiO_2), and low (CeO_2 stamps and 50 nm CeO_2) oxidation of L-AA. The AgNWs are known to cause considerable oxidative stress [58]. When examining the peak heights of the voltammograms after measurements of NPs in HBSS over time, it is clear that the peak height at 30 min-incubation with AgNWs in solution is the closest to the stable free radical DPPH used as a positive control. However, the peak height of AgNWs does not change much during the 30 min; already at the first timepoint, shortly after L-AA was added to the dispersion containing AgNW, the L-AA content was much smaller than that of the negative control. This could be because the AgNWs oxidizes L-AA rapidly. These results indicate that AgNW display an intrinsic oxidative potential. This might indicate that the AgNWs have a higher potential to be toxic to cells than other NPs that do not exhibit this intrinsic oxidative potential. Although AgNWs appear to reduce the amount of L-AA in the sample rapidly, this does not necessarily mean that the same will happen when cells undergo AgNW exposure. Using TT1 cells, Sweeney et al. (2015), showed that after 1 h of exposure, AgNWs had not increased the generation of ROS [59]. However, they did observe a significant increase in ROS after 4 and 24 h. It must be noted that the concentrations used by Sweeney et al., were much lower than the ones used in this study, with their highest concentration being 25 µg/ml. Higher concentrations of AgNW would probably induce more pronounced effect in the short term. It is also worth noting that Sweeney et al., assessed the ROS generation of AgNWs in living cells, where there are many

other antioxidants present, both intracellularly and in the cell culture medium. The synergistic action of all these antioxidants may have counteracted the oxidative stress caused by the AgNWs in the short term.

Following AgNW in terms of intrinsic oxidative potential were TiO_2 nanorods and 3.5 nm CeO_2. The 8 nm TiO_2 NPs display higher oxidative capability when the peak height is assessed but does not appear to lower the total antioxidant capacity of the sample. The 8 nm TiO_2 NPs might influence the L-AA itself, which could contribute to changing the potential where it is oxidized, but this would need to be tested further. Delaval et al. (2017), reported that CeO_2 and TiO_2 NPs possess no acellular oxidative capacity, but induced moderate cellular responses [56]. For these NPs, our method seems to be a better predictor for cellular response as we observed a strong oxidative effect of these NPs, coupled with a moderate cellular response when L-AA and 2-P-AA was not supplemented. Supplementation of L-AA and 2-P-AA to cells exposed to 3.5 nm CeO_2 did not mitigate the toxic effects of the NPs when using 10 and 100 µg/ml CeO_2, but an increase in viability was seen for cells exposed to 50 µg/ml. This might indicate that the production of ROS does not play a large part in the toxicity. Additionally, we observed a positive size-dependent effect on cytotoxicity as well as oxidative potential of CeO_2 NPs. The intrinsic oxidative potential of 3.5 nm CeO_2 is further discussed in section 6.4.

The 20 nm AgNP-1 and CeO_2 stamps displayed a moderate intrinsic oxidative potential. Interestingly, as shown in section 5.2, the toxic effect of both NPs is mitigated by the supplementation of L-AA and 2-P-AA, especially at lower concentrations of the NPs. At higher concentrations, the supplementation does not appear to influence viability.

AgNP-2, 50 nm CeO_2 and 50 nm TiO_2 display virtually no intrinsic oxidative properties. The supplementation of L-AA and 2-P-AA does not appear to influence the viability of cells exposed to AgNP-2 but does appear to have an effect on cells exposed to 50 nm CeO_2 and 50 nm TiO_2. This may indicate that 50 nm CeO_2 and 50 nm TiO_2 might cause cellular responses, without displaying intrinsic oxidative properties. In all assays presented in this thesis, the 50 nm AgNP-2 does not seem to cause ROS. One study suggested that the toxicity and intracellular ROS production is highly dependent on the size of the AgNPs. The toxicity and ROS generation

appeared to be largely due to interactions with cells, and not as a result of the intrinsic oxidative properties of the NP [60].

Taken together, CV of NPs in HBSS with L-AA showed promise as a tool for screening NPs' inherent oxidative potential. Crucially, the NPs did not seem to interfere with the method, displaying very low currents at the oxidation potential of L-AA when no antioxidants were present. At 100 µg/ml, several NPs exhibited an oxidative impact. AgNWs, TiO_2 nanorods, 8 nm TiO_2, and 3.5 nm CeO_2 were among the NPs with the strongest inherent oxidative impact.

6.4 Physicochemical characterization of nanoparticles

Characterization of NPs' physicochemical properties is required before assessing their cytotoxic effects. It has been reported that the agglomeration of TiO_2 NPs influences their toxicity [61]. To assess the size-dependency of hazardous effects, it is necessary to determine whether the sizes of the NPs dispersed in the exposure medium used for exposure are stable over time. It has been reported that the addition of 10 % FBS reduces the size of TiO_2 agglomerates significantly, resulting in a stable dispersion of TiO_2 nanoparticles [62]. The electrosteric effects of the proteins in FBS stabilizes the NPs in suspension by forming a protein corona [63, 64]. The HDD of NPs is defined as the diameter of a perfect sphere with the same diffusion characteristics as the measured NP. As a result, this particle size measurement is most accurate for spherical particles [65]. The HDD is dependent among others on the surface modifications made to the NP, the pH as well as the viscosity of the liquid in which the NPs are dispersed in. Therefore, differences between the DLS measurements made by Applied Nanoparticles in ultrapure water (milliQ) and the ones performed in cell culture medium with 10 % FBS were expected. There is a high likelihood that the protein corona is the reason why the HDD was larger in cell culture medium than in milliQ water. Furthermore, according to the definition of HDD, the spherical particles used in this project should have a better approximation of true size than the non-spherical NPs. Indeed, the spherical Ag NPs (AgNP-1 and AgNP-2) display values that are closer to the reported size than the non-spherical TiO_2 and CeO_2 NPs.

The DLS measurements performed in cell culture medium reveals that the HDD of the AgNPs was slightly larger than the reported sizes. However, DLS measurements of the AgNPs in milliQ water displayed similar values, indicating that the AgNPs were not highly aggregated or agglomerated when dispersed in cell culture medium. The AgNP-1s display higher values at the end of the exposure, but this could be a result of not thoroughly shaking the vial before measuring the DLS. The high standard deviation at the 24 h timepoint also indicates high variability between repetitions.

6.5 Impedance-based monitoring of cells exposed to nanomaterials

We wanted to evaluate the contribution of the oxidative effect of NPs on the total toxicity of the NPs because several of them demonstrated an innate oxidative potential (section 5.1.3). We hypothesised that supplementing with L-AA and 2-P-AA would mitigate the toxic effect of NPs with an oxidative potential, but not of non-oxidative NPs. The A549 cell line was used in these tests as it is highly proliferative and can remain in the log phase for the duration of the exposure. Cells proliferate the most during the log phase, and the cell density grows exponentially due to the nature of cell division. At this stage, the cell population is supposed to be most sensitive to toxicants. As a result, determining cellular function is best assessed at this stage [66].

Previous research had found that concentrations of 250 μM L-AA and 1 mM 2-P-AA offer a constant concentration of L-AA in culture medium, are harmless to cells, and stimulate cell growth both in the short and long term, and is also close to the concentrations in blood of a healthy adult [67-69]. Another study found that high doses of L-AA have a growth inhibitory effect and may trigger apoptosis in A549 cells when the exposure was maintained for longer periods of time [70, 71]. However, it has been widely reported that L-AA has a protective effect against ROS-induced oxidative stress [72]. Four different NP concentrations were used: 10, 20, 50 and 100 μg/ml. To determine whether these NPs may cause oxidative stress in A549 cells, all impedance-based NP toxicity experiments were done in the presence of 250 μM L-AA and 1 mM 2-P-AA. This data was compared with similar impedance-based experiments performed without L-AA and 2-P-AA.

The cell viability decreased with increasing concentration of all three Ag NPs in the presence of L-AA and 2-P-AA. All concentrations of AgNWs higher than 10 µg/ml resulted in a significant decrease in viability of cells. Only at the highest concentration did cells show a significant decrease in viability when exposed to AgNP-1. Furthermore, no significant values were found in cells exposed to AgNP-2. The AgNWs are a group of high aspect-ratio NPs that are increasingly being used in electronics. The aspect-ratio refers to the NP's length to width ratio.

According to Li et al. (2021), the toxicity of AgNWs is less dependent on the release of Ag ions than that of AgNPs [73]. This is supported further by Scanlan et al. (2013), who claim that the effects of AgNW are distinctly different from those of ionic Ag [58]. High-aspect-ratio and fibre shaped NPs are of concern because they resemble asbestos and are therefore expected to have similar toxic effects [74]. Recent studies state that the aspect-ratio is indeed very important when it comes to the toxicity of AgNWs. However, studies show that this aspect-ratio dependent toxicity only extends to a certain level before the toxicity diminishes with increased aspect-ratio. Lehmann et al. (2019), has indicated that AgNWs with reduced diameter (higher aspect-ratio) are more likely to be mechanically crumpled and fully internalized in endolysosomes, which diminishes toxicity, while thicker AgNWs puncture the enclosing membrane, releasing Ag ions and lysosomal content to the cytoplasm, initiating oxidative stress [75]. This oxidative stress pathway of cytotoxicity is further supported by the results from this thesis, as the addition of L-AA and 2-P-AA remedies the overall toxicity greatly. However, the AgNWs still display highly toxic effects, indicating that oxidative stress is only a part of the toxic potential it possesses. The ability of AgNWs to puncture lysosomes and release lysosomal content to the cytoplasm may account for a greater portion of the overall toxicity, as lysosomal content release results in autolysis, the destruction of cells by their own enzymes [76].

AgNPs are increasingly used in consumer products such as cosmetics and textiles and as a bactericidal agent, and can be released from these products, increasing the human skin exposure to NPs [77, 78]. Other studies show that AgNPs exhibit genotoxicity and cytotoxicity, as well as causing oxidative stress [79]. The toxicity of AgNPs is largely due to the release of Ag ions, which can disrupt membranes and enhance their permeability, or enhancing the production of ROS [80, 81]. These claims are supported in part by the results of impedance-

based measurements of A549 cells exposed to AgNP-1 and AgNP-2. Although results for AgNP-2 had no statistically significant differences from negative control, both AgNPs showed toxic trends at higher concentrations. The FC of A549 cells exposed to all concentrations of AgNP-1 seemed to be somewhat remedied by the addition of antioxidants. However, the FC of A549 cells exposed to AgNP-2 with added antioxidants showed no clear difference compared to the FC of cells exposed in the absence of antioxidants, suggesting that ROS/oxidative stress played little to no part in the overall toxicity of the NP. Other studies have shown that AgNPs are more likely to enhance ROS generation when the particle size is smaller [82]. Additionally, smaller size AgNPs have been shown to be more toxic than larger ones [83]. This can explain the higher toxicity of the smaller AgNP-1 compared to AgNP-2, as well as the small oxidative effect of AgNP-1 compared to the non-oxidative effect of AgNP-2.

Regarding TiO_2 NPs, it has been shown that this type of NPs are able to reach organs, such as the liver, brain, and lungs after inhalation or ingestion exposure. Moreover, the uptake of TiO_2 NPs in several cell types, such as A549 is high even at low concentrations [84]. Other studies have reported that TiO_2 NPs induce strong oxidative stress that leads to mitochondrial damage and apoptosis [85-87]. According to Liao et al. (2019), the toxicity and levels of ROS generated by the NPs has a positive dose-dependency and a negative size-dependent effect [88]. Other studies have concluded that the oxidative stress caused by TiO_2 NPs leads to DNA and chromosome damage [89]. These findings are supported by impedance-based tests taken in the absence of L-AA and 2-P-AA, which are reported in Table 5.4 and demonstrate the similar dosage dependency and negative size dependency. Additionally, these findings are consistent with results presented in section 5.1.3, which shows an enhanced intrinsic oxidative potential for smaller TiO_2 NPs than for the larger ones. Based on those results, it is likely that the smaller TiO_2 NPs will display higher ROS generation than the larger ones. However, these findings are not widely accepted, as other studies imply that larger aggregates are more harmful, or at least as toxic as smaller TiO2 NPs [61, 90]. In the presence of L-AA and 2-P-AA, none of the TiO_2 NPs used in this study resulted in statistically significant changes of viability/proliferation compared to the negative control. Yet, exposure to the smallest 8 nm TiO_2 NPs resulted in a dose-dependent increase of FC values. This dose dependency was not seen for the larger TiO_2 NPs. When studying the effect that the addition of antioxidants had for the toxicity of the TiO_2 NPs, it is clear that cells exposed to the 8 nm TiO_2 NPs are affected the most; 8 nm TiO_2 elicit

the highest toxic response of the TiO_2 NPs in the absence of antioxidants, but they are the least toxic in the presence of antioxidants. The supplementation of L-AA and 2-P-AA resulted in statistically significant changes in FC at concentrations ≥ 50 μg/ml for cells exposed to 8 nm TiO_2. Cells exposed to 50 nm TiO_2 NPs benefited greatly from this supplementation as well, with FC values increasing from significantly lower to values higher than control. However, the difference between supplemented and unsupplemented groups was not significant for any of the concentrations of 50 nm TiO_2.

According to the results presented in this thesis, the effect of high aspect-ratio resulting in high toxicity does not apply to the TiO_2 NPs, as the TiO_2 nanorods display the lowest toxicity of the TiO_2 NPs. This could be because of the shape of the nanorods. Other studies have shown that similarly shaped TiO_2 NPs are not internalized at the same level as more spherically shaped particles [91]. Gold nanorods have shown the same tendencies, as uptake rates were lower for higher aspect-ratio NPs [92]. It has been proposed that this aspect-ratio dependence on NP uptake is a result of rod-shaped NPs having a higher contact area with cell membrane receptors than spherical NPs. This could reduce the number of binding and internalization sites accessible [93]. Overall, the cytotoxicity of TiO_2 NPs seems to be attenuated by the addition of L-AA and 2-P-AA. This could indicate that ROS overproduction induced by TiO_2 NPs plays a crucial role in the NP-induced toxicity. However, it does not explain why larger doses of TiO_2 NPs results in increased viability/proliferation compared to control, when supplemented with antioxidants. Additionally, TiO_2 nanorods showed among the highest intrinsic oxidative potential (section 5.1.3), but did not seem very cytotoxic when impedance measurements were carried out. One reason that this could happen is based on poor cellular uptake of the TiO_2 nanorods. This will be further discussed in section 6.5.

Several studies claim that CeO_2 NPs have the potential to reduce the viability of cells, cause morphological damage, and induce apoptosis via oxidative stress, and that this effect is both dose and time dependent [94-96]. Additionally, Ma et al. (2021), report that this toxicity is size dependent, but questions whether ROS production is the leading cause of CeO_2 NPs' toxicity, as the supplementation of the antioxidant N-acetyl-L-cysteine to exposed cells resulted only in modest protective effect on NP-induced cytotoxicity [97]. Different studies on CeO_2 NPs toxicity on A549 cells has reported adverse effects [98]. Other studies reported no toxic effect

of CeO_2 NPs at 24 h, but genotoxic effects after 10 days [99]. These reports are contradicted by others, who claim that CeO_2 NPs display ROS scavenging behaviour [100, 101]. This high variability in results stresses the need of additional thorough research to assess the features of CeO_2 NPs.

Here, in the presence of L-AA and 2-P-AA, cells exposed to the two smallest CeO_2 NPs tested (3.5 nm and 10 x 10 nm CeO_2) displayed a concentration dependent decrease in FC with statistically significant differences only for cells exposed to the highest concentration of these NPs, while cells exposed to 50 nm CeO_2 showed more adverse effects. The opposite effect was exhibited by cells exposed to the CeO_2 NPs without the supplementation of L-AA and 2-P-AA. DLS results of CeO_2 NPs in cell culture medium reveals an HDD much larger than the listed sizes for all the NPs. These findings are consistent with other researchers' assessment of the agglomeration kinetics of CeO_2 NPs [102]. This apparent agglomeration could explain why the results are less obvious. Furthermore, the DLS results of 50 nm CeO_2 had a large standard deviation. This size variation may influence the results.

From the FC vs. control of A549 cells exposed to the various concentrations of NPs, one can obtain the EC_{50} value. This value is the concentration of NPs that gives the half-maximal response [103, 104]. It gives a good indication of the toxicity of the NPs. Comparing the EC_{50} values of one NP using different cell lines can also indicate the resistance of the cells to the toxic effect of the NPs. Furthermore, in this thesis, it was used to assess the mitigating effect that the supplementation of antioxidants had on NP toxicity. However, the EC_{50} was only reached for cells exposed to AgNW, with a value of 58.32 µg/ml in the presence of L-AA and 2-P-AA, compared to a value of 34.62 µg/ml in their absence. This indicates that the supplementation of L-AA and 2-P-AA has a considerable beneficial effect on dosage of AgNWs necessary to induce high toxicity.

6.6 Fluorometry

The fluorescence-based assay was used to corroborate results from CV and the impedance-based assay by monitoring ROS production in cells exposed to NMs. Conditions with and without the supplementation of L-AA and 2-P-AA were compared. When using fluorescent

probes to assess ROS generation of NPs, the results have varied considerably [105]. The NPs have been shown to interfere with assays such as these (fluorimetric), and the results can be unreliable.

The possibility that the NPs could absorb light at wavelengths that interfere with the fluorescent dye's excitation and emission is one problem this method encounters. The AgNPs have been shown to possess a size dependent light absorbance, and that larger NPs tend to absorb light closer to the active region of the CellROX dye used in this study [106]. The HDD of the 20 and 50 nm AgNPs in the cell culture medium determined by DLS demonstrated that both AgNPs are sufficiently large to absorb light that could quench the fluorescence emitted by the CellROX dye. Based on the measured HDDs of these NPs, AgNP-2 seems to possess a larger potential for interference with the assay. It is evident from Figures 5.4.3 and 5.4.4 that the larger AgNP-2 concentrations do in fact cause this effect to manifest. Throughout the whole experiment, the fluorescence intensity of cells exposed to the 50 and 100 µg/ml concentrations of AgNP-2 were low, with and without the supplementation of L-AA and 2-P-AA. This effect makes it hard to assess the ROS generation initiated by the NPs. The same effect might occur for AgNP-1, where two competing effects are seen. The fluorescence intensity of cells exposed to the smallest concentration of AgNP-1 was higher than that of the negative control, and groups exposed to higher concentration of the NP. The quenching of the fluorescence signal may not be that noticeable at this low concentration, and the ROS-producing effect of the NPs is more prominent. The AgNWs were deemed unsuitable for this method, as initial tests showed little to no fluorescence. This phenomenon is likely due to the light absorbance by AgNWs, which according to Ramasamy et al. (2012), is dependent on thickness, and is high in the active range of the fluorescent dye used [107].

The fluorescence intensities of cells exposed to the three TiO_2 NPs all tend to decrease with increased concentration of the NPs. These results contrast the results from the label-free impedance-based method, which showed a decrease in toxicity when ROS were scavenged by the supplementation of antioxidants, indicating that the production of ROS does indeed contribute to the overall toxicity of the NPs. Both the 8 nm TiO_2 and TiO_2 nanorods also displayed an intrinsic oxidative potential as shown in section 6.1.3. These contrasting results could be explained by light absorbance as well, as Panda et al. (2018), reports that TiO_2 NPs

with HDD average of 421.1 nm moderately absorbs light with wavelengths of 300 – 800 nm. This property makes the NPs suitable as coating on ITO glasses used as windows to conserve energy, among other uses [108]. However, this finding does limit the use of a fluorescence-based assay for determining the properties of TiO_2 NPs.

The fluorescence measurements using CeO_2 NPs seemed to be consistent with the results gathered using CV and xCELLigence. The cells exposed to 3.5 nm CeO_2 NPs display an increased ROS generation over time compared to control apparent from the resulting fluorescence intensity over time (Figure 5.4.8 A)). This is in line with the moderate oxidative effect the 3.5 nm CeO_2 displays in the absence of cells, as seen in figure 5.1.9. Although this increased fluorescence intensity in cells exposed to 3.5 nm CeO_2 was the highest among the tested NPs, it was considerably lower than that of the positive control. The 50 nm CeO_2 NPs did not show increased ROS generation compared to control, as the negative control always displayed higher fluorescence than the NP-treated groups. This is in line with the CV measurements, which showed no intrinsic oxidative potential of these NPs.

6.7 Transmission electron microscopy imaging

To understand how NPs can be toxic, it is important to know where they might affect the cells. For this purpose, cells were exposed to the nine NPs, fixed and subsequently prepared for TEM analysis. All NPs were readily taken up by the A549 cells, mostly found enclosed in vesicles. In addition, 20 and 50 nm Ag NPs were located in the nucleus of the cells.

For all Ag NPs, fully engulfed agglomerates were observed (Figure 5.5.1). The AgNWs induced substantial structural damage to cells leading to abundant cell death. We could even observe structures that resemble autophagosomes with enclosed AgNWs. However, not many AgNWs could be detected inside the cells. This relationship of high toxicity with low uptake is unclear. However, one explanation might be that the AgNWs dissolved over the 24 h exposure time and during sample preparation; processing of samples for TEM takes several days in which the sample is immersed and incubated in different solutions. It has previously been reported that AgNWs can dissolve rapidly [109]. Alternatively, the high-aspect ratio AgNWs could have inflicted physical damage at the cell membrane level and/or extensive oxidative stress while

in the extracellular milieu. Thus, active internalization by cells may have not been possible since AgNWs exhibited high toxicity shortly after addition to the cell culture. Both 20 and 50 nm Ag NPs were observed inside the nucleus. This could imply that these NPs have the capacity to directly cause genotoxic effects in cells. Genotoxicity could be evaluated by mutations or changes in number and structure of chromosomes [110]. Although these effects would not be noticed at these short periods of exposure (24 h), they could be seen if the exposure time was increased [111, 112].

Fully engulfed agglomerates were also found for all TiO_2 NPs (Figure 5.5.2). The 50 nm TiO_2 aggregates were larger but less densely packed than the other TiO_2 NPs. This observation is consistent with DLS measurements taken after 24 h of exposure (Table 5.2), which demonstrate that the 50 nm TiO_2 NPs had the highest HDD of the three TiO_2 NPs. The DLS measurements also show that over the 24 h, the 50 nm TiO_2 NPs had a tendency of agglomerating, displaying higher values at 24 h than at the start of exposure. Based on the TEM pictures, it is plausible to infer that the 50 nm TiO_2 may have not interacted as much with the cells as the 8 nm TiO_2 NPs, which appeared to be located in smaller clusters. Individual particles or smaller clusters of particles have a better likelihood of interacting with cells more strongly than agglomerated ones because larger particles/agglomerates limit the available surface area for contact [113]. Larger particles or agglomerates might also hinder internalization by inhibiting receptor clustering and endocytosis [114]. TiO_2 nanorods appear to be the least aggregated of the three TiO_2 NPs and were usually observed in small-size agglomerates at around 200 nm. This size is consistent with the DLS measurements of TiO_2 nanorods in cell culture medium, which showed similar diameters. The TiO_2 nanorods were incorporated into the cells at a lower level than the other TiO_2 NPs. This could contribute to explaining why the TiO_2 nanorods displayed a high intrinsic oxidative potential, but low cytotoxic effects.

All CeO_2 NPs were readily taken up by the A549 cells. CeO_2 stamps, in particular, demonstrated considerably higher cellular internalization than all other NPs studied. Furthermore, the size of the cells appeared to expand after uptake of the CeO_2 stamps. However, inferring this from a small sample size can be problematic.

However, because TEM pictures of cells were taken at the end of the exposure, it is difficult to identify how particles are engulfed by the cells. Images with shorter exposure lengths, preferably in real-time, should be better suited to providing this information. High-resolution dark-field microscopy could be implemented for this purpose. Furthermore, because of the small sample size used in this experiment, as well as the qualitative nature of TEM, it is difficult to draw accurate conclusions on changes in cell morphology based only on the micrographs.

6.8 Printing of electrodes

Several issues arose during the printing of the electrodes. One such problem occurred shortly after high temperature curing of the printed silver ink layer. The prints were always a couple of millimetres off when aligned using the alignment markers to print the carbon layer on top, exposing some silver behind the carbon. This would have major implications when the electrodes were utilised, as silvers are more conductive than carbon. After some deliberation, it occurred to us that the problem was that the PET films shrunk during the curing process. Because of this shrinking, the distances between previously printed features were reduced, making subsequent alignment difficult. To address this issue, all PET films were baked in an oven before the first layer was printed. This appeared to fix the problem, as the PET films were irreversibly shrunk by this method.

Another issue that arose during printing was that the conductive carbon ink utilised had a low viscosity and was thus difficult to manage reliably. This caused blotching of the ink, which usually resulted in wider variances in results. A different formulation of carbon ink with higher viscosity and high conductivity should be chosen to further establish this process. Alternatively, a cooling coil wrapped around the ink dispenser should help keep a low temperature and thus giving the user more control over the dispersing ink. This would, however, need to be tested further.

Overall, the in-house printing produced electrodes that were comparable to commercial electrodes in terms of sensitivity for detection of ascorbic acid while maintaining low background signal (noise). These were preliminary results, and we were unable to establish a

totally ideal configuration of conductive inks that would offer more stable high-quality electrodes.

6.9 Future perspectives

The partial discrepancy in toxicity ranking of NPs when comparing results from change in area and peak height in CV suggests that both parameters must be considered for determining the oxidative effect of NPs [115]. In addition, the results of this thesis reveal that the NPs tested do not interfere with CV measurements, and the method could thus be utilised to analyse the oxidative stress exerted by NPs in more complex biological fluids with a wider range of antioxidants, and with longer incubation times. Therefore, the natural continuation of this work would be to further solidify the use of CV as a method in nanotoxicology. This might be accomplished by measuring oxidative stress in various biofluids (e.g., blood, interstitial fluid) of animals and cell culture media conditioned by cells exposed to NPs. Cell lysis might also be conducted on cells exposed to NPs to assess the depletion of intracellular antioxidants like glutathione.

Optimizing the established printing process can help provide more uniform electrodes, which would decrease the costs of each test and increase the throughput. Alternative electrode sizes and configurations as well as different conductive inks, like graphene-based or boron-doped diamond, should be tested to improve detection and resolution of antioxidants in complex samples. Although real-time measurements with CV are not possible since the analyte (i.e., antioxidant) is consumed, pseudo real-time analysis could be achieved in a multi-well format with SPE immersed in the cell culture and sequential sampling of consecutive wells.

7 Conclusions

The aim of this thesis was to establish cyclic voltammetry as a method for evaluating NP toxicity. This method provided results indicating that several of the tested NPs have an intrinsic oxidative potential. CV demonstrated potential as a way of evaluating NP-induced oxidative stress, with little to no interference from the NPs. In particular, AgNWs had the highest oxidative potential, followed by TiO_2 nanorods, 8 nm TiO_2 NPs, and 3.5 nm CeO_2 NPs. These findings were in line with those obtained using impedance-based cell viability measurements of cells exposed to NPs supplemented L-AA and 2-P-AA to determine the role of oxidative stress to the overall toxicity. These findings indicated that the NPs that benefitted the most from the supplementation were AgNWs at the concentration of 100 µg/ml and 8 nm TiO_2 at concentrations ≥ 50 µg/ml.

Overall, Ag NPs showed a size- and shape-dependent oxidative effects, as well as overall toxicity. However, the size-dependency did not result in significant differences between the two spherical Ag NPs, with sizes 20 and 50 nm. The toxicity of Ag NPs appears to be determined by their shape. When evaluated with a fluorescent dye, the 50 nm Ag NPs exhibited a strong quenching of the fluorescent signal. Furthermore, all Ag NPs were readily taken up by cells. The two spherical ones were also observed within the nucleus.

TiO_2 NPs demonstrated size and aspect ratio dependent toxicity and oxidative potential. Notably, when antioxidants were added, none of these NPs exhibited cytotoxic effects. TiO_2 nanorods possess strong oxidative potential, but minimal toxicity. Additionally, the TiO_2 nanorods showed substantially poorer cellular uptake than the other TiO_2 NPs.

CeO_2 NPs displayed size-dependent intrinsic oxidative potential, and the smallest CeO_2 NP showed significant ROS production over time at a concentration of 100 µg/ml. The ROS production was mitigated by supplementation of antioxidants. However, the supplementation of antioxidants did not significantly alter the viability of cells exposed to any of the CeO_2 NPs. All CeO_2 NPs were abundantly taken up by cells, especially the CeO_2 stamps.

The printing of electrodes produced encouraging results, but more work is needed to refine the configuration of conductive inks for a more reliable printing process.

Cited Works

1. Karimi, M., R. Sadeghi, and J. Kokini, *Human exposure to nanoparticles through trophic transfer and the biosafety concerns that nanoparticle-contaminated foods pose to consumers.* Trends in Food Science & Technology, 2018. **75**: p. 129-145.
2. *Commission Recommendation of 18 October 2011 on the definition of nanomaterial Text with EEA relevance*. 2011. p. 38-40.
3. Lespes, G., S. Faucher, and V.I. Slaveykova, *Natural Nanoparticles, Anthropogenic Nanoparticles, Where Is the Frontier?* Frontiers in Environmental Science, 2020. **8**.
4. Sharma, V.K., et al., *Natural inorganic nanoparticles – formation, fate, and toxicity in the environment.* Chemical Society Reviews, 2015. **44**(23): p. 8410-8423.
5. Zhang, Q., et al., *Nanomaterials in medicine and pharmaceuticals: Nanoscale materials developed with less toxicity and more efficacy.* European Journal of Nanomedicine, 2013. **5**: p. 1-19.
6. Huang, Y.-W., M. Cambre, and H.-J. Lee, *The Toxicity of Nanoparticles Depends on Multiple Molecular and Physicochemical Mechanisms.* International Journal of Molecular Sciences, 2017. **18**(12): p. 2702.
7. Tulve, N.S., et al., *Characterization of silver nanoparticles in selected consumer products and its relevance for predicting children's potential exposures.* International Journal of Hygiene and Environmental Health, 2015. **218**(3): p. 345-357.
8. Misra, R., S. Acharya, and S.K. Sahoo, *Cancer nanotechnology: application of nanotechnology in cancer therapy.* Drug Discovery Today, 2010. **15**(19-20): p. 842-850.
9. Choi, C.H., et al., *Mechanism of active targeting in solid tumors with transferrin-containing gold nanoparticles.* Proc Natl Acad Sci U S A, 2010. **107**(3): p. 1235-40.
10. Lesniak, A., et al., *Nanoparticle Adhesion to the Cell Membrane and Its Effect on Nanoparticle Uptake Efficiency.* Journal of the American Chemical Society, 2013. **135**(4): p. 1438-1444.
11. Sung, J.H., et al., *Lung Function Changes in Sprague-Dawley Rats After Prolonged Inhalation Exposure to Silver Nanoparticles.* Inhalation Toxicology, 2008. **20**(6): p. 567-574.
12. Gundert-Remy, U., et al., *Toxicology: a discipline in need of academic anchoring—the point of view of the German Society of Toxicology.* Archives of Toxicology, 2015. **89**(10): p. 1881-1893.
13. McCallion, C., et al., *Graphene in therapeutics delivery: Problems, solutions and future opportunities.* European Journal of Pharmaceutics and Biopharmaceutics, 2016. **104**: p. 235-250.
14. Collins, A.R., et al., *High throughput toxicity screening and intracellular detection of nanomaterials.* WIREs Nanomedicine and Nanobiotechnology, 2017. **9**(1): p. e1413.
15. Graudejus, O., et al., *Bridging the gap between in vivo and in vitro research: Reproducing in vitro the mechanical and electrical environment of cells in vivo.* Frontiers in Cellular Neuroscience, 2018. **12**.
16. Syahir, A., et al., *Label and Label-Free Detection Techniques for Protein Microarrays.* Microarrays (Basel), 2015. **4**(2): p. 228-44.
17. Ong, K.J., et al., *Widespread Nanoparticle-Assay Interference: Implications for Nanotoxicity Testing.* PLoS ONE, 2014. **9**(3): p. e90650.

18. Ostermann, M., et al., *Label-free impedance flow cytometry for nanotoxicity screening.* Scientific Reports, 2020. **10**(1).
19. Cimpan, M.R., et al., *An impedance-based high-throughput method for evaluating the cytotoxicity of nanoparticles.* Journal of Physics: Conference Series, 2013. **429**: p. 012026.
20. Vishwakarma, V., S.S. Samal, and N. Manoharan, *Safety and Risk Associated with Nanoparticles - A Review.* Journal of Minerals and Materials Characterization and Engineering, 2010. **09**(05): p. 455-459.
21. Kim, T.H., et al., *Size-dependent cellular toxicity of silver nanoparticles.* J Biomed Mater Res A, 2012. **100**(4): p. 1033-43.
22. Favi, P.M., et al., *Shape and surface chemistry effects on the cytotoxicity and cellular uptake of metallic nanorods and nanospheres.* Journal of Biomedical Materials Research Part A, 2015. **103**(12): p. 3940-3955.
23. Mohajerani, A., et al., *Nanoparticles in Construction Materials and Other Applications, and Implications of Nanoparticle Use.* Materials (Basel), 2019. **12**(19).
24. Gosens, I., et al., *Impact of agglomeration state of nano- and submicron sized gold particles on pulmonary inflammation.* Particle and Fibre Toxicology, 2010. **7**(1): p. 37.
25. Weiss, M., et al., *Density of surface charge is a more predictive factor of the toxicity of cationic carbon nanoparticles than zeta potential.* Journal of Nanobiotechnology, 2021. **19**(1).
26. Kim, H.-J. and A.E. Nel, *The Role of Phase II Antioxidant Enzymes in Protecting Memory T Cells from Spontaneous Apoptosis in Young and Old Mice.* The Journal of Immunology, 2005. **175**(5): p. 2948-2959.
27. Pizzino, G., et al., *Oxidative Stress: Harms and Benefits for Human Health.* Oxidative Medicine and Cellular Longevity, 2017. **2017**: p. 1-13.
28. Horie, M. and Y. Tabei, *Role of oxidative stress in nanoparticles toxicity.* Free Radical Research, 2020: p. 1-12.
29. Suresh, D., et al., *Total antioxidant capacity – a novel early bio-chemical marker of oxidative stress in HIV infected individuals.* Journal of Biomedical Science, 2009. **16**(1): p. 61.
30. Chevion, S., M.A. Roberts, and M. Chevion, *The use of cyclic voltammetry for the evaluation of antioxidant capacity.* Free Radic Biol Med, 2000. **28**(6): p. 860-70.
31. Espinoza, E.M., et al., *Practical Aspects of Cyclic Voltammetry: How to Estimate Reduction Potentials When Irreversibility Prevails.* Journal of The Electrochemical Society, 2019. **166**(5): p. H3175-H3187.
32. Psotová, J., et al., *DETERMINATION OF TOTAL ANTIOXIDANT CAPACITY IN PLASMA BY CYCLIC VOLTAMMETRY. TWO CASE REPORTS.* Biomedical Papers, 2001. **145**(2): p. 81-83.
33. Chevion, S., et al., *Evaluation of Plasma Low Molecular Weight Antioxidant Capacity by Cyclic Voltammetry.* Free Radical Biology and Medicine, 1997. **22**(3): p. 411-421.
34. Chevion, S., et al., *Antioxidant Capacity of Edible Plants: Extraction Protocol and Direct Evaluation by Cyclic Voltammetry.* Journal of Medicinal Food, 1999. **2**(1): p. 1-10.
35. Elgrishi, N., et al., *A Practical Beginner's Guide to Cyclic Voltammetry.* Journal of Chemical Education, 2018. **95**(2): p. 197-206.
36. Britannica, T., *electrical impedance*, in *Encyclopedia Britannica* E.o. Encyclopaedia, Editor. (2022, June 29.

37. Ngoc Le, H.T., et al., *A Review of Electrical Impedance Characterization of Cells for Label-Free and Real-Time Assays.* BioChip Journal, 2019. **13**(4): p. 295-305.
38. Liu, Q., et al., *Cell-Based Biosensors and Their Application in Biomedicine.* Chemical Reviews, 2014. **114**(12): p. 6423-6461.
39. Schwan, H.P. *Electrical properties of tissues and cell suspensions: mechanisms and models*. in *Proceedings of 16th Annual International Conference of the IEEE Engineering in Medicine and Biology Society*. 1994.
40. Cimpan, M.R., *Standard Operation Procedure (SOP) and background documentation for real-time label-free impedance-based nanotoxicity assessment*.
41. Gu, H., et al., *Side population cells from long-term passage non-small cell lung cancer cells display loss of cancer stem cell-like properties and chemoradioresistance.* Oncology Letters, 2016. **12**(4): p. 2886-2893.
42. Sundareshan, P. and M.J.C. Hendrix, *Growth, morphologic, and invasive characteristics of early and late passages of a human endometrial carcinoma cell line (RL95-2).* In Vitro Cellular & Developmental Biology - Animal, 1992. **28**(7-8): p. 544-552.
43. Corp., I., *IBM SPSS Statistics for Windows*. 2019: Armonk, NY.
44. Clayton, K.N., et al., *Physical characterization of nanoparticle size and surface modification using particle scattering diffusometry.* Biomicrofluidics, 2016. **10**(5): p. 054107.
45. Ćwik, M., et al., *Optical Properties of Submillimeter Silver Nanowires Synthesized Using the Hydrothermal Method.* Materials, 2019. **12**(5): p. 721.
46. Wang, H.-W., et al., *Cyclic Voltammetry in Biological Samples: A Systematic Review of Methods and Techniques Applicable to Clinical Settings.* Signals, 2021. **2**(1): p. 138-158.
47. Maeda, H., et al., *Anodization of Glassy Carbon Electrodes in Oligomers of Ethylene Glycol and Their Monomethyl Ethers as a Tool for the Elimination of Protein Adsorption.* Analytical Sciences, 1997. **13**(5): p. 721-727.
48. García-Miranda Ferrari, A., S.J. Rowley-Neale, and C.E. Banks, *Screen-printed electrodes: Transitioning the laboratory in-to-the field.* Talanta Open, 2021. **3**: p. 100032.
49. Bitew, Z. and M. Amare, *Electrochemical Determination of Ascorbic Acid in Pharmaceutical Tablets using Carbon Paste Electrode.* 2019.
50. Nafisi, S., G. Bagheri Sadeghi, and A. PanahYab, *Interaction of aspirin and vitamin C with bovine serum albumin.* Journal of Photochemistry and Photobiology B: Biology, 2011. **105**(3): p. 198-202.
51. Van Benschoten, J.J., et al., *Cyclic voltammetry experiment.* Journal of Chemical Education, 1983. **60**(9): p. 772.
52. Forster, R.J., *Microelectrodes: new dimensions in electrochemistry.* Chemical Society Reviews, 1994. **23**(4): p. 289.
53. Lee, P.T., D. Lowinsohn, and R.G. Compton, *The use of screen-printed electrodes in a proof of concept electrochemical estimation of homocysteine and glutathione in the presence of cysteine using catechol.* Sensors (Basel), 2014. **14**(6): p. 10395-411.
54. Ayres, J.G., et al., *Evaluating the Toxicity of Airborne Particulate Matter and Nanoparticles by Measuring Oxidative Stress Potential—A Workshop Report and Consensus Statement.* Inhalation Toxicology, 2008. **20**(1): p. 75-99.

55. De Mori, A., et al., *Evaluation of Antibacterial and Cytotoxicity Properties of Silver Nanowires and Their Composites with Carbon Nanotubes for Biomedical Applications.* International Journal of Molecular Sciences, 2020. **21**(7): p. 2303.
56. Delaval, M., et al., *Assessment of the oxidative potential of nanoparticles by the cytochrome c assay: assay improvement and development of a high-throughput method to predict the toxicity of nanoparticles.* Archives of Toxicology, 2017. **91**(1): p. 163-177.
57. Breznan, D., et al., *Acellular oxidative potential assay for screening of amorphous silica nanoparticles.* The Analyst, 2020. **145**(14): p. 4867-4879.
58. Scanlan, L.D., et al., *Silver Nanowire Exposure Results in Internalization and Toxicity to Daphnia magna.* ACS Nano, 2013. **7**(12): p. 10681-10694.
59. Kim, S.H., et al., *Nanoscale Chemical and Electrical Stabilities of Graphene-covered Silver Nanowire Networks for Transparent Conducting Electrodes.* Scientific Reports, 2016. **6**(1): p. 33074.
60. Zhang, L., et al., *Size-dependent cytotoxicity of silver nanoparticles to Azotobacter vinelandii: Growth inhibition, cell injury, oxidative stress and internalization.* PLoS One, 2018. **13**(12): p. e0209020.
61. Murugadoss, S., et al., *Agglomeration of titanium dioxide nanoparticles increases toxicological responses in vitro and in vivo.* Particle and Fibre Toxicology, 2020. **17**(1).
62. Allouni, Z.E., et al., *Agglomeration and sedimentation of TiO2 nanoparticles in cell culture medium.* Colloids Surf B Biointerfaces, 2009. **68**(1): p. 83-7.
63. Meißner, T., A. Potthoff, and V. Richter, *Physico-chemical characterization in the light of toxicological effects.* Inhalation Toxicology, 2009. **21**(sup1): p. 35-39.
64. Westmeier, D., R.H. Stauber, and D. Docter, *The concept of bio-corona in modulating the toxicity of engineered nanomaterials (ENM).* Toxicology and Applied Pharmacology, 2016. **299**: p. 53-57.
65. Maguire, C.M., et al., *Characterisation of particles in solution – a perspective on light scattering and comparative technologies.* Science and Technology of Advanced Materials, 2018. **19**(1): p. 732-745.
66. ECACC, *Fundamental Techniques in Cell Culture* 4th Edition ed. Laboratory Handbook 2018, Darmstadt, Germany: Merck - Sigma Aldrich.
67. Chepda, T., et al., *MONITORING OF ASCORBATE AT A CONSTANT RATE IN CELL CULTURE: EFFECT ON CELL GROWTH.* In Vitro Cellular & Developmental Biology - Animal, 2001. **37**(1): p. 26.
68. Fujisawa, K., et al., *Evaluation of the effects of ascorbic acid on metabolism of human mesenchymal stem cells.* Stem Cell Research & Therapy, 2018. **9**(1).
69. Hata, R.-I. and H. Senoo, *L-ascorbic acid 2-phosphate stimulates collagen accumulation, cell proliferation, and formation of a three-dimensional tissuelike substance by skin fibroblasts.* Journal of Cellular Physiology, 1989. **138**(1): p. 8-16.
70. Takamizawa, S., *Effects of ascorbic acid and ascorbic acid 2-phosphate, a long-acting vitamin C derivative, on the proliferation and differentiation of human osteoblast-like cells.* Cell Biology International, 2004. **28**(4): p. 255-265.
71. Zhai, P., et al., *[Effects of vitamin C on A549 cell proliferation, apoptosis and expressions of Caspase, Survivin].* Zhongguo Fei Ai Za Zhi, 2010. **13**(2): p. 89-93.
72. Fu, Y., et al., *[Nickel exposure to A549 cell damage and L-ascorbic acid interference effect].* Zhonghua Lao Dong Wei Sheng Zhi Ye Bing Za Zhi, 2015. **33**(5): p. 323-6.

73. Li, Y. and W.-X. Wang, *Silver nanowires kinetics and real-time imaging of in situ Ag ion dissolution in Daphnia magna.* Science of The Total Environment, 2021. **782**: p. 146933.
74. Donaldson, K., et al., *Identifying the pulmonary hazard of high aspect ratio nanoparticles to enable their safety-by-design.* Nanomedicine (Lond), 2011. **6**(1): p. 143-56.
75. Lehmann, S.G., et al., *Crumpling of silver nanowires by endolysosomes strongly reduces toxicity.* Proceedings of the National Academy of Sciences, 2019. **116**(30): p. 14893-14898.
76. Aits, S. and M. Jäättelä, *Lysosomal cell death at a glance.* Journal of Cell Science, 2013. **126**(9): p. 1905-1912.
77. Ahamed, M., M.S. Alsalhi, and M.K. Siddiqui, *Silver nanoparticle applications and human health.* Clin Chim Acta, 2010. **411**(23-24): p. 1841-8.
78. Ferdous, Z. and A. Nemmar, *Health Impact of Silver Nanoparticles: A Review of the Biodistribution and Toxicity Following Various Routes of Exposure.* International Journal of Molecular Sciences, 2020. **21**(7): p. 2375.
79. Syafiuddin, A., et al., *A Review of Silver Nanoparticles: Research Trends, Global Consumption, Synthesis, Properties, and Future Challenges.* Journal of the Chinese Chemical Society, 2017. **64**(7): p. 732-756.
80. Yin, I.X., et al., *<p>The Antibacterial Mechanism of Silver Nanoparticles and Its Application in Dentistry</p&gt.* International Journal of Nanomedicine, 2020. **Volume 15**: p. 2555-2562.
81. Ramkumar, V.S., et al., *Biofabrication and characterization of silver nanoparticles using aqueous extract of seaweed Enteromorpha compressa and its biomedical properties.* Biotechnology Reports, 2017. **14**: p. 1-7.
82. Carlson, C., et al., *Unique Cellular Interaction of Silver Nanoparticles: Size-Dependent Generation of Reactive Oxygen Species.* The Journal of Physical Chemistry B, 2008. **112**(43): p. 13608-13619.
83. Park, M.V.D.Z., et al., *The effect of particle size on the cytotoxicity, inflammation, developmental toxicity and genotoxicity of silver nanoparticles.* Biomaterials, 2011. **32**(36): p. 9810-9817.
84. Brandão, F., et al., *Genotoxicity of TiO2 Nanoparticles in Four Different Human Cell Lines (A549, HEPG2, A172 and SH-SY5Y).* Nanomaterials, 2020. **10**(3): p. 412.
85. Huerta-García, E., et al., *Titanium dioxide nanoparticles induce strong oxidative stress and mitochondrial damage in glial cells.* Free Radical Biology and Medicine, 2014. **73**: p. 84-94.
86. Shukla, R.K., et al., *Titanium dioxide nanoparticles induce oxidative stress-mediated apoptosis in human keratinocyte cells.* J Biomed Nanotechnol, 2011. **7**(1): p. 100-1.
87. Márquez-Ramírez, S.G., et al., *Titanium dioxide nanoparticles inhibit proliferation and induce morphological changes and apoptosis in glial cells.* Toxicology, 2012. **302**(2-3): p. 146-56.
88. Liao, F., et al., *The size-dependent genotoxic potentials of titanium dioxide nanoparticles to endothelial cells.* Environ Toxicol, 2019. **34**(11): p. 1199-1207.
89. Chen, T., J. Yan, and Y. Li, *Genotoxicity of titanium dioxide nanoparticles.* J Food Drug Anal, 2014. **22**(1): p. 95-104.

90. Magdolenova, Z., et al., *Impact of agglomeration and different dispersions of titanium dioxide nanoparticles on the human related in vitro cytotoxicity and genotoxicity.* Journal of Environmental Monitoring, 2012. **14**(2): p. 455.
91. Allouni, Z.E., et al., *Role of physicochemical characteristics in the uptake of TiO2 nanoparticles by fibroblasts.* Toxicology in Vitro, 2012. **26**(3): p. 469-479.
92. Chithrani, B.D. and W.C.W. Chan, *Elucidating the Mechanism of Cellular Uptake and Removal of Protein-Coated Gold Nanoparticles of Different Sizes and Shapes.* Nano Letters, 2007. **7**(6): p. 1542-1550.
93. Chithrani, B.D., A.A. Ghazani, and W.C.W. Chan, *Determining the Size and Shape Dependence of Gold Nanoparticle Uptake into Mammalian Cells.* Nano Letters, 2006. **6**(4): p. 662-668.
94. Cheng, G., et al., *Cerium oxide nanoparticles induce cytotoxicity in human hepatoma SMMC-7721 cells via oxidative stress and the activation of MAPK signaling pathways.* Toxicology in Vitro, 2013. **27**(3): p. 1082-1088.
95. Lin, W., et al., *Toxicity of Cerium Oxide Nanoparticles in Human Lung Cancer Cells.* International Journal of Toxicology, 2006. **25**(6): p. 451-457.
96. Nemmar, A., et al., *Cerium Oxide Nanoparticles in Lung Acutely Induce Oxidative Stress, Inflammation, and DNA Damage in Various Organs of Mice.* Oxidative Medicine and Cellular Longevity, 2017. **2017**: p. 1-12.
97. Ma, Y., et al., *Size-Dependent Cytotoxicity and Reactive Oxygen Species of Cerium Oxide Nanoparticles in Human Retinal Pigment Epithelia Cells.* International Journal of Nanomedicine, 2021. **Volume 16**: p. 5333-5341.
98. Gagnon, J., et al., *Integrating silver compounds and nanoparticles into ceria nanocontainers for antimicrobial applications.* Journal of Materials Chemistry B, 2015. **3**(9): p. 1760-1768.
99. De Marzi, L., et al., *Cytotoxicity and Genotoxicity of Ceria Nanoparticles on Different Cell Lines in Vitro.* International Journal of Molecular Sciences, 2013. **14**(2): p. 3065-3077.
100. Pezzini, I., et al., *Cerium oxide nanoparticles: the regenerative redox machine in bioenergetic imbalance.* Nanomedicine (Lond), 2017. **12**(4): p. 403-416.
101. Gagnon, J. and K.M. Fromm, *Toxicity and Protective Effects of Cerium Oxide Nanoparticles (Nanoceria) Depending on Their Preparation Method, Particle Size, Cell Type, and Exposure Route.* European Journal of Inorganic Chemistry, 2015. **2015**(27): p. 4510-4517.
102. Sendra, M., *Behaviour of CeO2 nanoparticles and bulk and their toxicity in freshwater and seawater microalgae*. 2016.
103. Sebaugh, J.L., *Guidelines for accurate EC50/IC50 estimation.* Pharm Stat, 2011. **10**(2): p. 128-34.
104. Jiang, X. and A. Kopp-Schneider, *Summarizing EC50 estimates from multiple dose-response experiments: a comparison of a meta-analysis strategy to a mixed-effects model approach.* Biom J, 2014. **56**(3): p. 493-512.
105. Zhao, J. and M. Riediker, *Detecting the oxidative reactivity of nanoparticles: a new protocol for reducing artifacts.* J Nanopart Res, 2014. **16**(7): p. 2493.
106. Paramelle, D., et al., *A rapid method to estimate the concentration of citrate capped silver nanoparticles from UV-visible light spectra.* The Analyst, 2014. **139**(19): p. 4855.
107. Ramasamy, P., et al., *Effects of TiO2 shells on optical and thermal properties of silver nanowires.* Journal of Materials Chemistry, 2012. **22**(23): p. 11651.

108. Panda, J., U.P. Singh, and R. Sahu, *Synthesis, characterization of TiO2nano particles for enhancement of electron transport application in DSSC with Cu-BPCA Dye.* IOP Conference Series: Materials Science and Engineering, 2018. **410**: p. 012008.
109. Wu, J., et al., *Quantifying the relative contribution of particulate versus dissolved silver to toxicity and uptake kinetics of silver nanowires in lettuce: impact of size and coating.* Nanotoxicology, 2020. **14**(10): p. 1399-1414.
110. Turkez, H., M.E. Arslan, and O. Ozdemir, *Genotoxicity testing: progress and prospects for the next decade.* Expert Opin Drug Metab Toxicol, 2017. **13**(10): p. 1089-1098.
111. Barabadi, H., et al., *A Systematic Review of the Genotoxicity and Antigenotoxicity of Biologically Synthesized Metallic Nanomaterials: Are Green Nanoparticles Safe Enough for Clinical Marketing?* Medicina, 2019. **55**(8): p. 439.
112. Phillips, D.H. and V.M. Arlt, *Genotoxicity: damage to DNA and its consequences.* Exs, 2009. **99**: p. 87-110.
113. Cohen, J.M., J.G. Teeguarden, and P. Demokritou, *An integrated approach for the in vitro dosimetry of engineered nanomaterials.* Particle and Fibre Toxicology, 2014. **11**(1): p. 20.
114. Mazumdar, S., D. Chitkara, and A. Mittal, *Exploration and insights into the cellular internalization and intracellular fate of amphiphilic polymeric nanocarriers.* Acta Pharmaceutica Sinica B, 2021. **11**(4): p. 903-924.
115. Cimpan, E., Hofshagen,O.B., Mondragon,I.R., Cimpan,M.R., *Assessment of nanoparticle-induced oxidative stress using cyclic voltammetry and the convolution technique*, in *«Nano-week» & NanoCommons Final Conference, Cyprus*. 2022, Western Norway University of Applied Sciences.